THE EFFECT OF MECHANICAL STIMULI ON CALCIFICATION RESPONSE IN TISSUE-ENGINEERED BONE IN VITRO USING TYPE I COLLAGEN SCAFFOLDS EVALUATED BY A NON-DESTRUCTIVE OPTICAL MONITORING DEVICE

MR. CHAIYONG KOAYKUL

A THESIS SUBMITTED IN PARTIAL FULFILLMENT
OF THE REQUIREMENTS FOR
THE DEGREE OF MASTER OF ENGINEERING (BIOLOGICAL ENGINEERING)
FACULTY OF ENGINEERING
KING MONGKUT'S UNIVERSITY OF TECHNOLOGY THONBURI
2012

The Effect of Mechanical Stimuli on Calcification Response in Tissue-Engineered Bone In Vitro using Type I Collagen Scaffolds Evaluated by a Non-Destructive Optical Monitoring Device

Mr. Chaiyong Koaykul B.Eng. (Mechanical Engineering)

A Thesis Submitted in Partial Fulfillment
of the Requirements for
the Degree of Master of Engineering (Biological Engineering)
Faculty of Engineering
King Mongkut's University of Technology Thonburi
2012

Thesis Committee

…… (Dr. Peerapong Santiwong, Ph.D.)	Chairman of Thesis Committee
……. (Asst. Prof. Anak Khantachawana, Ph.D.)	Member and Thesis Advisor
……. (Asst. Prof. Kwanchanok Pasuwat, Ph.D.)	Member and Thesis Co-Advisor
……. (Asst. Prof. Diew Koolpiruck, Ph.D.)	Member

Thesis Title	The Effect of Mechanical Stimuli on Calcification Response in Tissue-Engineered Bone In Vitro using Type I Collagen Scaffolds Evaluated by a Non-Destructive Optical Monitoring Device
Thesis Credits	12
Candidate	Mr. Chaiyong Koaykul
Thesis Advisors	Asst. Prof. Dr. Anak Khantachawana Asst. Prof. Dr. Kwanchanok Pasuwat
Program	Master of Engineering
Field of Study	Biological Engineering
Faculty	Engineering
B.E.	2555

Abstract

To investigate the osteogenic response of sinusoidal loading frequencies in vitro, a mechanical load with deformation in the physiological range was applied to a bone-like construct and the change in the degree of calcification was monitored for 42 consecutive days. Tissue-engineered bone was made by seeding pre-osteoblastic cells (MC3T3-E1) into a type I collagen sponge scaffold in osteogenic medium. Sinusoidal mechanical loads with a peak of 0.3% deformation with vibration (Gaussian quasi-white noise with a standard deviation of 0.03% deformation) was applied to the constructs at 0.5, 1.0, 1.5, 2.0 and 2.5 Hz for 3 minutes per day for 42 consecutive days using a piezoelectric mechanical stimulator. A non-destructive optical monitoring device using near-infrared light was used for the detection of the calcification response of the tissue-engineered bone once a day. The degree of calcification was evaluated as calcium content (mg/cm^3) based on the initial calcium calibration curve.

Mechanical loading promoted higher calcification of the osteoblasts cultured in the scaffolds when compared with the calcification of the scaffolds without loading. The degree of calcification started to increase in the stimulated constructs after day 8. On day 42, the calcium content of the control constructs was 1.19-fold higher than its initial measurement (day 0). The calcium content in the stimulated constructs at 0.5, 1.0, 1.5, 2.0 and 2.5 Hz was 1.32, 1.52, 1.90, 2.00 and 1.32-fold, respectively, higher than that of the control construct on day 42. From the results, it was concluded that the sinusoidal loading frequency could function as a potent enhancer of osteogenesis in vitro, suggesting the usefulness of mechanical loading in bone tissue engineering.

Keywords : Bone / Calcification / Infrared / Mechanical Stimuli / Piezoelectric / Tissue Engineering

หัวข้อวิทยานิพนธ์	การศึกษาอิทธิพลของการให้ภาระทางกลแบบต่างๆ ต่อการสร้างกระดูกใหม่ภายนอกร่างกายบนคอลลาเจน Scaffold ชนิดที่ 1 โดยใช้ระบบสังเกตการณ์แบบไม่ทำลาย
หน่วยกิต	12
ผู้เขียน	นายชัยยง โกยกุล
อาจารย์ที่ปรึกษา	ผศ. ดร.อนรรฆ ขันธะชวนะ
	ผศ. ดร.ขวัญชนก พสุวัต
หลักสูตร	วิศวกรรมศาสตรมหาบัณฑิต
สาขาวิชา	วิศวกรรมชีวภาพ
คณะ	วิศวกรรมศาสตร์
พ.ศ.	2555

บทคัดย่อ

เพื่อตรวจสอบการตอบสนองการเกิดกระดูกใหม่ภายนอกร่างกายต่อการกระตุ้นทางกลด้วยความถี่ต่าง ๆ ในรูปแบบไซน์ งานวิจัยนี้จึงได้ทดลองใช้แรงทางกลที่เกิดจากการเคลื่อนที่ทางกายภาพในการกระตุ้นกระดูกใหม่ที่สร้างจากหลักวิศวกรรมเนื้อเยื่อ และตรวจสอบการเปลี่ยนแปลงของอัตราการเกิดกระดูกใหม่อย่างต่อเนื่องเป็นเวลา 42 วัน ทั้งนี้สร้างกระดูกใหม่จากหลักวิศวกรรมเนื้อเยื่อโดยการฉีดเซลล์ก่อนสร้างกระดูก (Pre-osteoblast, MC3T3-E1) ลงไปในโครงร่างสังเคราะห์สามมิติซึ่งทำมาจากคอลลาเจนชนิดที่ 1 และเลี้ยงในอาหารเลี้ยงเซลล์ชนิดเหนี่ยวนำการสร้างกระดูก จากนั้นจึงทดสอบใส่แรงทางกลในรูปแบบไซน์ด้วยระยะการเคลื่อนที่สูงสุด 0.3 % ของความเครียดและการสั่นแบบเก๊าส์ควอไซไวท์ (Gaussian quasi-white) ที่ระยะการเคลื่อนที่ 0.03 % ของส่วนเบี่ยงเบนมาตรฐาน ต่อกระดูกที่สร้างขึ้น ณ ความถี่ 0.5, 1.0, 1.5, 2.0 และ 2.5 เฮิรตซ์ เป็นเวลา 3 นาทีต่อวัน เป็นเวลา 42 วันต่อเนื่อง โดยใช้เครื่องกระตุ้นทางกลเพียโซอิเล็กทริก และใช้เครื่องตรวจสอบโดยแสงอินฟราเรดแบบไม่ทำลายำหรับการวัดการเกิดกระดูกใหม่ของกระดูกที่สร้างจากหลักวิศวกรรมเนื้อเยื่อวันละหนึ่งครั้งเป็นเวลา 42 วันต่อเนื่อง โดยอัตราการเกิดกระดูกใหม่ประเมินจากปริมาณความหนาแน่นของแคลเซียม (มิลลิกรัม/ลูกบาศก์เซนติเมตร) ซึ่งได้จากฐานข้อมูลของกราฟสอบเทียบมาตรฐาน

แรงทางกลสนับสนุนการเกิดกระดูกใหม่ของเซลล์สร้างกระดูกที่เลี้ยงในโครงร่างสังเคราะห์สามมิติเมื่อเปรียบเทียบกับกระดูกที่สร้างขึ้นโดยไม่ได้รับแรงกระตุ้น กระดูกที่สร้างขึ้นโดยได้รับแรง

กระตุ้นจะเริ่มการสร้างกระดูกใหม่ตั้งแต่วันที่ 8 ของการเลี้ยงเซลล์ และในวันที่ 42 ของการเลี้ยงเซลล์ กระดูกที่สร้างโดยไม่ได้รับการกระตุ้นมีปริมาณความหนาแน่นแคลเซียมเพิ่มขึ้นเท่ากับ 1.19 เท่าเมื่อเทียบกับวันที่เริ่มเลี้ยง (วันที่ 0) ส่วนปริมาณความหนาแน่นแคลเซียมของกระดูกที่สร้างขึ้นโดยได้รับการกระตุ้น ณ ความถี่ 0.5, 1.0, 1.5, 2.0 และ 2.5 เฮิรตซ์ มีปริมาณเพิ่มขึ้นเท่ากับ 1.32, 1.52, 1.90, 2.00 และ 1.32 เท่าตามลำดับ เมื่อเปรียบเทียบกับกระดูกที่สร้างขึ้นโดยไม่ได้รับการกระตุ้นในวันที่ 42 ของการเลี้ยง จากผลการทดสองสรุปได้ว่าความถี่ของแรงกระตุ้นทางกลในรูปแบบไซน์นั้นมีความสามารถที่จะเสริมการเกิดกระดูกใหม่ภายนอกร่างกายได้ ซึ่งสามารถนำมาประยุกต์ใช้ในการเสริมการสร้างกระดูกใหม่ด้วยหลักวิศวกรรมเนื้อเยื่อกระดูกได้

คำสำคัญ : กระดูก / กระตุ้นทางกล / การเกิดกระดูกใหม่ / เพียโซอิเล็กทริก / วิศวกรรมเนื้อเยื่อกระดูก / อินฟราเรด

ACKNOWLEDGMENTS

I would like to express a great deal of gratitude to my major advisor, Asst. Prof. Dr. Anak Khantachawana, and my co-advisor, Asst. Prof. Dr. Kwanchanok Viravaidya-Pasuwat for their helpful guidance, persistence and encouragement throughout all my graduate studies. Especially for their kindly help and willpower, which kept me passing thought hard times and never let me down.

I would like to thank my chairman and committee members, Dr. Peerapong Santiwong, and Asst. Prof. Dr. Diew Koolpiruck for guidance and kindness in their thesis examination.

I wish to express my sincere thanks to i-Tissue Laboratory, Faculty of Medicine, Chulalongkorn University and Faculty of Dentistry, Mahidol University for support technique, materials and equipment.

Furthermore, I would like to express my sincere thanks to Assoc. Prof. Dr. Shigeo Tanaka, Kanazawa University for his kindly help and valuable suggestions.

I am very thankful to all of the members in SMART Lab (Smart Materials and Advanced Manufacturing Research Team Laboratory), the Mammalian cell culture laboratory, Department of Mechanical Engineering, Department of Control System and Instrumentation Engineering, Faculty of Engineering, King Mongkut's University of Technology Thonburi (KMUTT) for their kindness, support and assistance towards me, in particular with laboratory equipment.

I would like to acknowledge the higher education research promotion and National Research University (NRU) project of Thailand by the Office of the Higher Education Commission, and also the National Research Council of Thailand (NRCT), Toray Science Foundation (TSF, Japan), National Metal and Materials Technology Center (MTEC) byway of the National Science and Technology Development Agency (NSTDA) (Project Number: MT-B-52-BMD-13-179-G) for their financial support.

And last but not least, I am grateful to my family for their support, entire care and love. The usefulness of this dissertation I dedicate to my mother, my father and all the teachers who have taught me since my childhood.

CONTENTS

PAGE

PAGE

LIST OF TABLES

LIST OF FIGURES

PAGE

PAGE

LIST OF TECHNICAL VOCABULARY AND ABBREVIATIONS

3D	=	Three-dimensional
^{o}	=	Degree
^{o} C	=	Degree Celsius
ø	=	Diameter
Au	=	Gold
B	=	Billion
BD	=	Bulk density
C	=	Carbon
Ca	=	Calcium
CC	=	Calcium content
Cl	=	Chlorine
cm	=	Centimeter
cm^3	=	Milliliter
Cu	=	Copper
dm^3	=	Liter
DNA	=	Deoxyribonucleic Acid
E	=	Electric field
ECM	=	Extracellular matrix
EDS	=	Energy Dispersive Spectroscopy
H	=	Hydrogen
HA	=	Hydroxyapatite
Hz	=	Hertz
I	=	Intensity from a photo detector
I_0	=	Intensity from LEDs
K	=	Potassium
kHz	=	Kilohertz
kV	=	Kilovolt
LED	=	Light-emitting diode
M	=	Million
mg	=	Milligram
ml	=	Milliliter
mm	=	Millimeter
mmol	=	Millimole
mol	=	Mole
MSC	=	Mesenchymal stem cell
Na	=	Sodium
nm	=	Nanometer
O	=	Oxygen
P	=	Phosphorus
Pa	=	Pascal
PD	=	Photo detector
pH	=	Potential of Hydrogen ion
P_s	=	Polarization
PZT	=	Lead zirconate titanate
R	=	Radius
R^2	=	Coefficient of determination
SDS	=	Sodium dodecyl sulfate
SE	=	Standard error of the mean

sec	=	Second
SEM	=	Scanning Electron Microscope
Si	=	Silicon
SD	=	Standard deviation
T_c	=	Curie temperature
U	=	Unit
USA	=	United States of America
V	=	Volt
α	=	Alpha
α-MEM	=	Minimum Essential Medium Eagle - Alpha modification
β	=	Beta
μg	=	Microgram
μm	=	Micrometer

CHAPTER 1 INTRODUCTION

Bones are rigid parts and they are major components of the endoskeleton in a human body. Bones have many functions that are vital to human life. Nowadays, many people face various problems pertaining to bones, rather by accident, osteoporosis or surgical operation. The trend of this problem is rapidly increasing. But the materials used currently for healing can cause many problems after surgical treatment. Bone tissue engineering is used for creating tissue-engineered bone. This kind of material not only has perfect biocompatibility and good mechanical properties, but the material is also suitable for bone replacement. However, the calcification in a bone cell culture takes too long a period of time and the quantity of reinforcement is still low. This research focuses on mechanical stimulation for the promotion of calcification in the cultured period of tissue-engineered bone.

1.1 Bones

Bones are physiologically dynamic tissues whose primary functions are to transmit the force of muscular contraction from one part of the body to another during movement, provide for physical protection of soft tissues and organs, and also functions as a storage feature for systemic mineral homeostasis in the body [1].

1.1.1Bone Morphology

The long bones (e.g., femur and tibia) are used as a classical model for the macroscopic structure of bone (Figure 1.1). The typical adult long bone comprises of a central cylindrical shaft (diaphysis), and two wider rounded ends (epiphysis). Conical regions (metaphysis) link the diaphysis with each epiphysis. Most bone ends are wider than their central part because the bone ends have joints which are covered by articular cartilage for loading transmission to other parts [2].

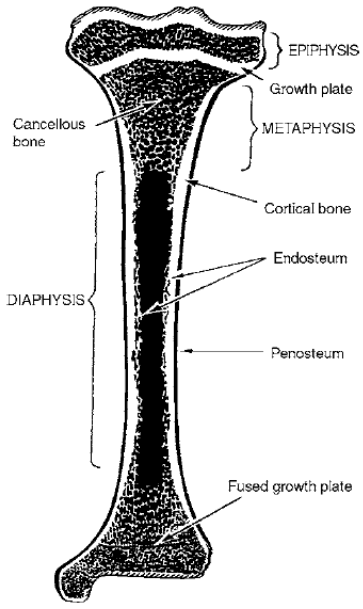

Figure 1.1 Schematic diagram of a human tibia [3].

The diaphysis is mostly made of cortical or compact bone, the epiphysis and metaphysis main contain cancellous, trabecular or spongy bone with a thin shell of the cortical bone (Figure 1.2). The cortical bone is a solid mass and dense with many microscopic channels. Approximately 80% of the bone mass in an adult human is cortical bone. The remaining 20% of the skeletal mass is cancellous bone which is found in the inner parts of bones (Figure 1.3). Moreover, cortical and cancellous bones differ in their architecture, development, function, proximity to the bone marrow, blood supply and turnover time, as shown in Table 1.1 [4, 5].

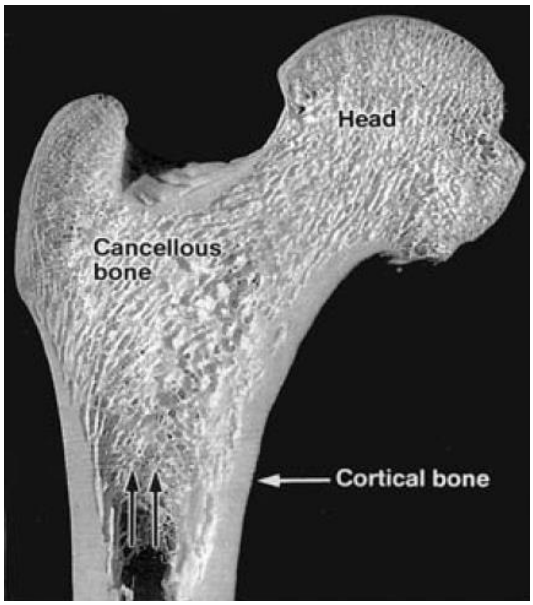

Figure 1.2 Bone X-ray section of dried epiphysis of a human femur [3].

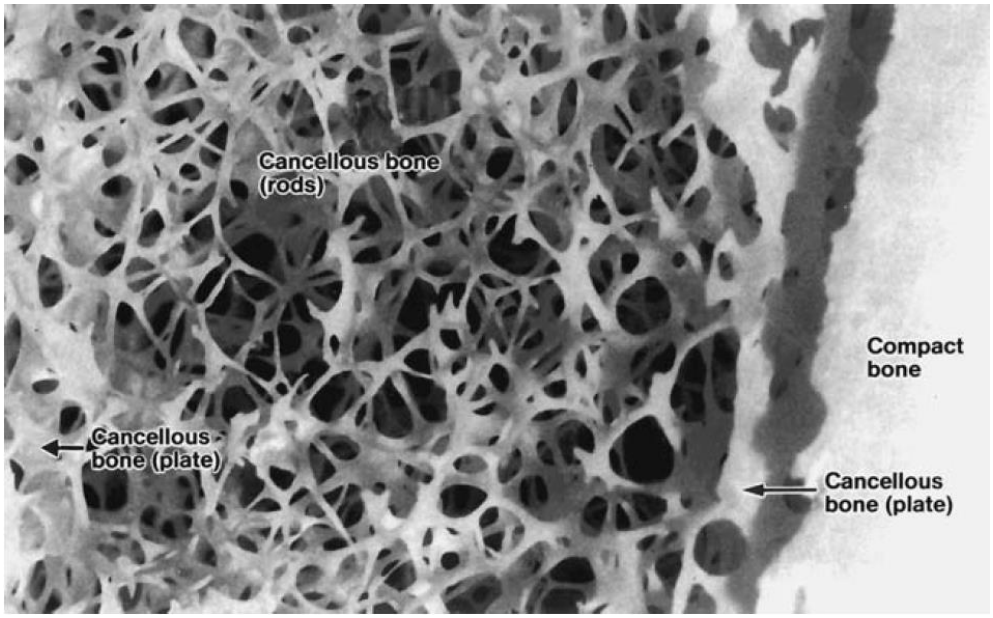

Figure 1.3 Thick ground section of a proximal tibia [3].

Table 1.1 Differential properties between cortical and cancellous bone [5]

	Cortical	Cancellous
- Bone mass	80 %	20 %
- Bone surface	33 %	67 %
- Surface/volume ratio (mm^2/mm^3)	20	2.5
- Soft tissue	10 %	75 %
- Porosity	Low	High
- Marrow	Fatty	Hematopoietic
- Developmental	Intramembranous ossification	Endochondral ossification
- Turnover	Slow	Fast
- Function	Mainly biomechanical	Mainly mineral homeostasis

1.1.2 Basic Bone Composition

Bone tissue is made up of water, organic and inorganic compounds. Regarding weight basis, bone is approximately 60% inorganic compound, 30% organic compound and 10% water. As for its volume basis, these ratios are about 40%, 35%, and 25%, respectively [6]. The organic phase of bone consists principally of type I collagen (90% by weight), some other collagen types (III and VI), and a variety of non-collagenous proteins such as osteocalcin, osteonectin (ON) and bone sialoprotein (BSP) [7]. The inorganic phase of bone is a ceramic mineral crystal which is an impure form of calcium phosphate, mostly referred to as hydroxyapatite ($Ca_{10}(PO_4)_6(OH)_2$) [8].

1.2 Statement of Bone Problems

Nowadays, there are a large number of patients who have been victimized by bone disease, as well as accidents, osteoporosis, and so on. One of the most common bone diseases is osteoporosis (Figure 1.4). The current definition of osteoporosis created at the Consensus Development Conference in 1991 [9], was given credibility by a World Health Organization (WHO) study group in 1994 [10]. It defines osteoporosis as "a disease characterized by low bone mass and micro-architectural deterioration of bone tissue leading to enhanced bone fragility and a consequent increase in fracture risk." This indisposition is characterized by reduced bone density, alteration in the micro-architecture of bone tissue, reduced bone strength and an increased risk of bone fracture. The standard sites of osteoporotic fractures are the hip, the spine and the wrist. Over 1.3 million fractures occur annually in the United States of America and approximately 70 % of osteoporosis patients are over 45 years of age [11].

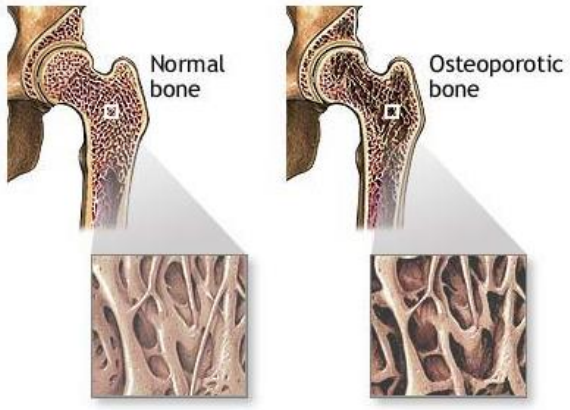

Figure 1.4 Bone density comparisons between normal bone and osteoporotic bone [11].

The monetary cost associated with osteoporotic fractures is tremendous. The total cost for medical and hospital expenses, possibly nursing-home care and lost productivity reached 16.9 billion U.S. dollars in 2005 (Figure 1.5). In the year 2000, there were estimated to be 620,000 new fractures at the hip and 620,000 clinical spine fractures in men and women aged 50 years or more in Europe. In many countries, people are living longer and the proportion of the elderly in the population is increasing, especially those aged 85 years or over. Global demographic changes are expected to increase the frequency of hip fractures nearly 4-fold by the year 2050 [12].

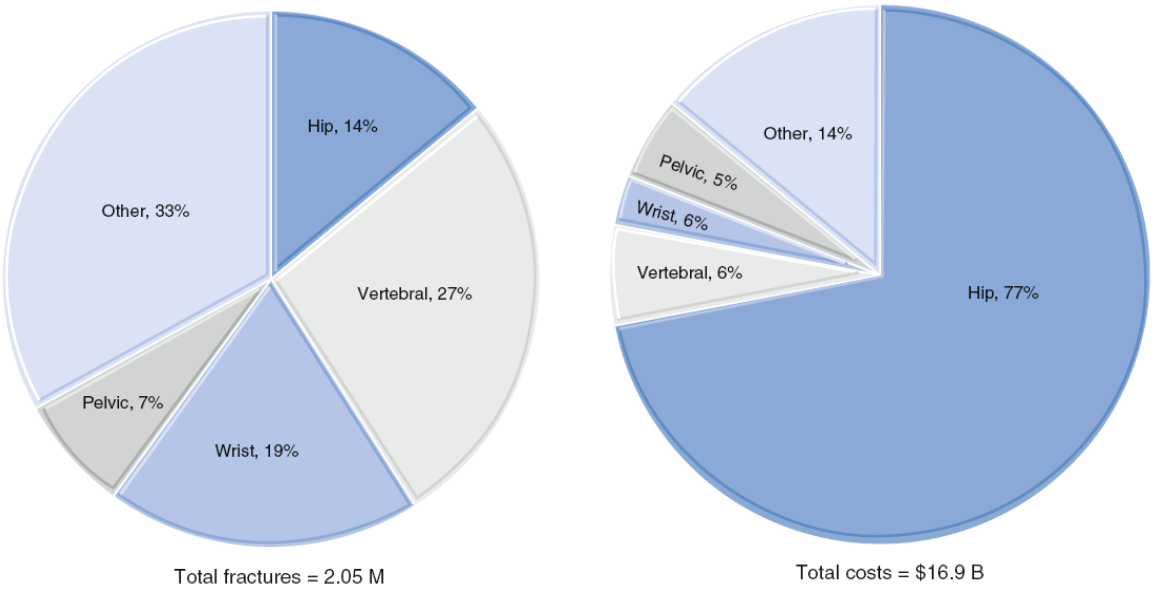

Figure 1.5 Information of osteoporosis patients in the United States of America (2005),
(A) numbers of bone fracture distribution by types,
(B) cost distribution by type of bone fractures [12].

1.3 Current Strategies for Bone Repair

Current treatments are found with autologous bone grafts (autograft), autogenous bone grafts (allograft), metals and ceramics [13, 14]. With autologous bone graft, a bone is taken from another part of the patient's own body, it has been the gold standard of bone replacement for many years because it provides bone cells as well as essential chemical factors needed for bone healing and regeneration [14]. It is generally taken in the form of cancellous bone from the patient's iliac crest, but cortical bone can be used as well [15]. Although, it presents relatively good percentages of success, the spectrum of cases in which it can be used is restricted, mostly owing to the limited number of the autografts that can be acquired, and due to donor site unhealthiness [14-16].

Allograft is a bone which is taken from somebody else's body. Although it can be an alternative, the rate of graft incorporation is lower than autograft. Allograft bone presents the possibility of immune system rejection and pathogen transmission from donor to patient, and infections can happen in the recipient's body after the transplantation [15, 17].

Figure 1.6 Human allograft for use in spinal fusion applications [18].

As an option to these two bone grafts, there are metals and ceramics. However, both of them have several disadvantages. Regarding metals, for example; though supplying immediate mechanical support at the site of the defect, it presents poor integration with bone and tissue at the implantation site, and can fail because of infection, wearing, and difference of modulus of elasticity between implant materials and bone tissue. Moreover, ceramics have very a high modulus of elasticity and are brittle, and it should not be used in locations of significant torsion, bending, normal stress or shear stress areas [13].

With these troubles, researchers have looked for alternative materials to current treatment modalities. Tissue engineering theory represents a field of biological engineering research where promising progress has been constructed. It is based on the principle of restoring

function, replacing damaged or diseased tissues through the application of engineering and biological theories. In terms of its suitability to bone tissue, the objective is to create a bone healing response in the anatomic area, the tissue constructed is integrated structurally with the surrounding bone tissue and it has the biomechanical properties necessary to be durable and effective. Furthermore, the bone regeneration and repairing by tissue engineering occurs during the ordered sequence of cellular events that are affected by several biological and mechanical factors [18-21].

1.4 Objectives

1. To fabricate a non-destructive optical monitoring device for evaluating calcification of tissue-engineered bone in vitro.
2. Study the effect of mechanical stimuli (sinusoidal loading) to calcification response in tissue-engineered bone in vitro to know the best condition of mechanical stimuli for increasing the rate of new bone fabrication.

1.5 Expected Benefits

1. A non-destructive optical monitoring device for evaluating calcification of tissue-engineered bone in vitro.
2. Mechanical stimulator using a piezoelectric actuator for producing mechanical force to tissue-engineered bone.
3. Best condition of mechanical stimuli (sinusoidal loading) for increasing the rate of new bone fabrication in tissue-engineered bone techniques.

CHAPTER 2 LITERATURE REVIEWS

2.1 Bone Formation Process (Osteogensis) [22-24]

Bone contains a distinctive population of cells, including osteoprogenitor cells, osteoblasts, osteocytes, and osteoclasts (Figure 2.1).

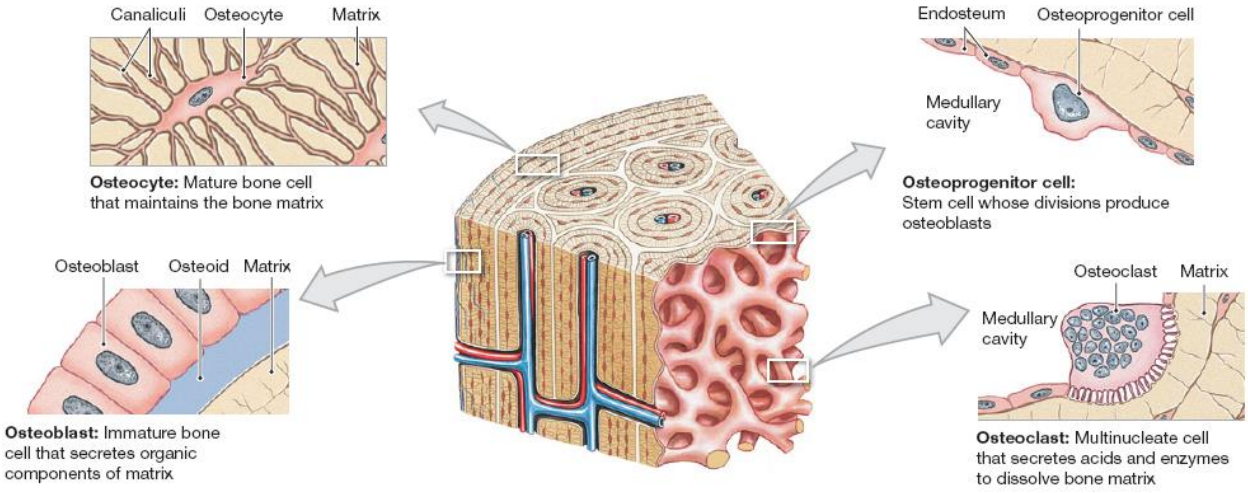

Figure 2.1 Histological structure of the typical bone [22].

Osteocytes are mature bone cells. They maintain and monitor the protein and mineral content of the surrounding bone matrix. The minerals in the matrix are continually recycled. Osteocytes direct both the release of calcium from bone to blood and the deposition of calcium salts in the surrounding bone matrix. Osteocytes capture small chambers, called lacunae which are sandwiched between layers of calcified bone matrix. These bone matrix layers are known as lamellae. Channels called canaliculi spread out through the bone matrix from one lacuna to another lacuna, they are close to free surfaces and near blood vessels. The canaliculi, which are composed of fine cytoplasmic processes and ground substances, connect to the osteocytes. These junctions join these processes and provide a route for the diffusion of nutrients and waste products from one osteocyte to another over gap junctions.

Osteoblasts are cuboidal in shape and found in a single layer on the surfaces of a bone. These cells secrete organic components to the bone matrix. Osteoblasts are responsible for the production of new bone, a process called osteogenesis. It is thought that osteoblasts may respond to a variety of different stimuli, including mechanical and hormonal, to initiate osteogenesis. If osteoblasts become surrounded by bone matrix, they will differentiate into osteocytes.

Osteoprogenitor cells differentiate from mesenchymal stem cells (MSCs). These cells are found in numerous locations, including the innermost layer of the periosteum and in the endosteum lining the medullary cavities. Moreover, they can divide to produce daughter cells that differentiate into osteoblasts.

Osteoclasts are large and multinucleate cells, they are found at sites where bone is being eliminated. These cells are derived from the same stem cells that produce monocytes and neutrophils. They secrete acid solutions through the exocytosis of lysosomes. The acid solutions dissolve the bone matrix, releasing amino acids and stored calcium and phosphate. This erosion process, called osteolysis, is for increasing the calcium and phosphate concentrations in bodily fluids.

During embryonic development, either mesenchyme or cartilage is replaced by bone. This process of replacing other tissues with bone is called ossification. The process of calcification refers to the deposition of calcium salts in the bone tissue. Any tissue can be calcified, but only ossification results in bone formation.

Intramembranous ossification starts when mesenchymal stem cells (MSCs) which accumulate and differentiate into osteoblasts within embryonic or fibrous connective tissue. Intramembranous ossification begins approximately during the eighth week of embryonic development. The steps in the process of intramembranous ossification are shown in Figure 2.2 and summarized as follows:

1. Ossification centers form in the thickened regions of mesenchymal stem cells (MSCs); beginning at the eighth week of development, some cells in the thickened, condensed mesenchymal stem cells divide, and committed cells that result then differentiate into osteoprogenitor cells. Some osteoprogenitor cells turn into osteoblasts and secrete semisolid organic components of the bone matrix called osteoids. Multiple ossification centers develop with the thickened mesenchymal stem cells as the number of osteoblasts increases.
2. The osteoid undergoes calcification; osteoid formation is rapidly followed by the beginning of the process of calcification, calcium salts are deposited on the osteoid which then crystallizes (solidifies). Both the organic matrix formation and calcification happens at the same time at several sites with the condensed mesenchymal stem cells. When calcification traps osteoblasts with lacunae in the matrix, the trapped cells become osteocytes.
3. Woven bone and its surrounding periosteum formation; the newly formed bone tissue is immature and not well formed, a type called woven bone, or primary bone. This woven bone is finally replaced by lamellar bone, or secondary bone. Mesenchymal stem cells which still surround the woven bone start to thicken and ultimately organize to form the periosteum. The bone keeps growing, and new osteoblasts are entrapped in the expanding bone. Moreover, osteoblasts are continually produced as mesenchymal stem cells grow and develop. Newly formed blood vessels also spread during this time.
4. Lamellar bone replaces woven bone as cortical bone and spongy bone forms; lamellar bone replaces the spongy bone of woven bone. On the internal and external surfaces, spaces between the spongy bones are filled, and then the spongy bone becomes cortical bone.

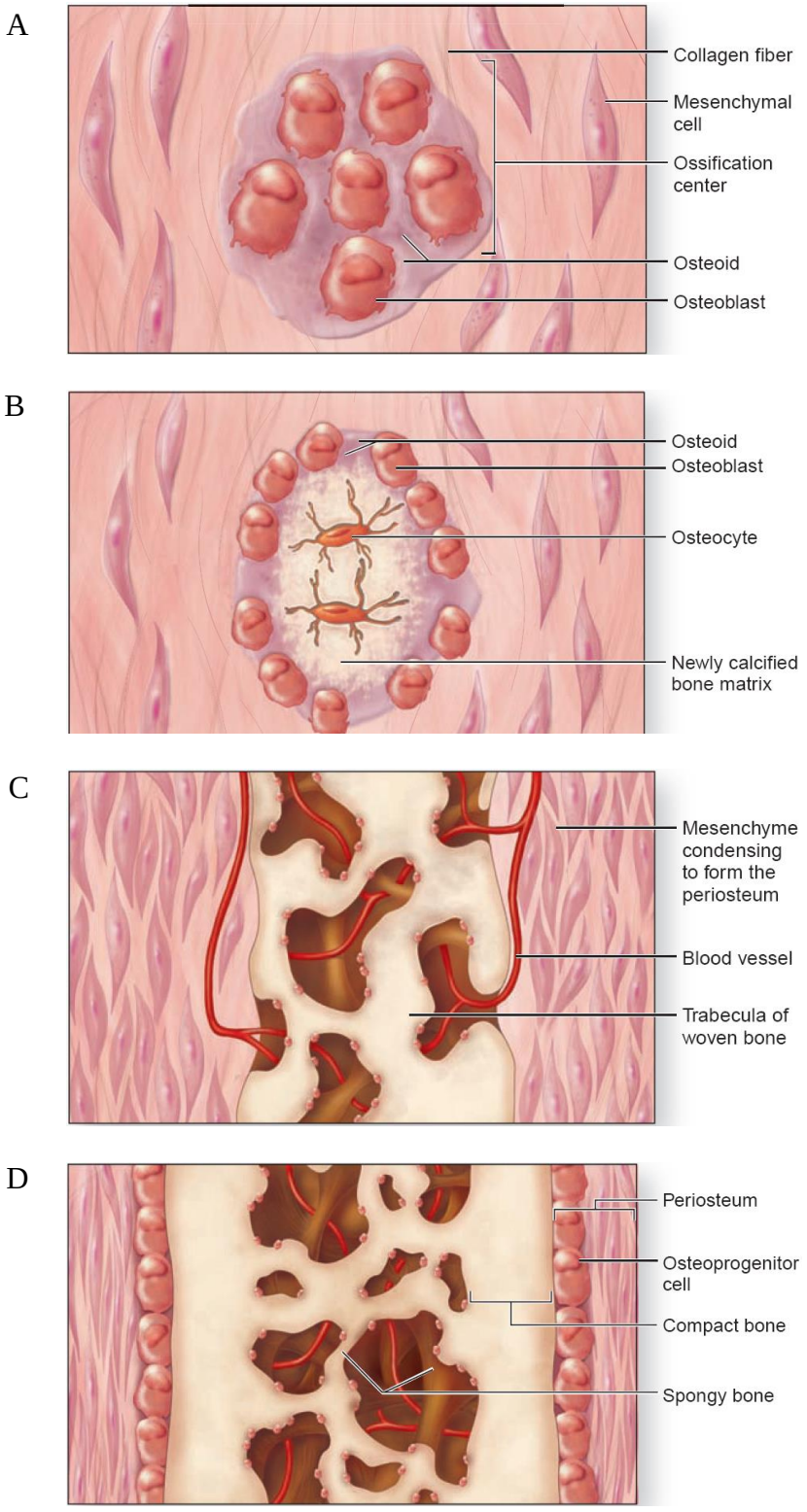

Figure 2.2 Intramembranous ossification. (A) Ossification centers form with thickened regions of mesenchymal stem cells. (B) Osteoid undergoes calcification. (C) Woven bone and surrounding periosteum. (D) Lamellar bone replaces woven bone as spongy and compact bone [23].

2.2 Bone Tissue Engineering

Tissue engineering is a new field that is swiftly rising in significance in many areas in the domain of biomedical engineering. It is an interdisciplinary field that incorporates principles of engineering and life sciences for the development of tissue or organ replacement. The fields of mechanical and chemical engineering, chemistry, materials science, medicine, cellular and molecular biology may all be applied to tissue engineering, demonstrating the multidisciplinary approach that must be taken to solve the problem of tissue or organ replacement [16, 25].

Tissue engineering is a term originally used to describe construction in the laboratory of a device containing viable cells and biological mediators in a synthetic or biological matrix that could be implanted into the patients for tissue regeneration. Recently, the definition has widened to include any attempt to regenerate tissues in the body, either accomplished in the laboratory or directly in the patient, by adding suitable biological mediators and matrices. Tissues are contained cells, soluble molecules and an insoluble extracellular matrix (ECM) that act as cell functional regulators. Therefore, a requirement for tissue regeneration is composed of three necessary components as follows [20]:

1. **Viable cells:** It is necessary to increase the number of cells that construct the tissues as well as reconstruct the structure to support the cells. In an adult, tissues which are composed of labile cells (e.g., epithelial tissue) and stable cells (e.g., connective tissue including bone) can be regenerated.
2. **Scaffolds:** These materials are to be used for the fabrication of a three-dimensional matrix which can serve as a scaffold for cell attachment and proliferation. Moreover, scaffolds can be formed as drug delivery carriers to control a site and a time specific release in order to produce growth factors. These materials included synthetic and natural calcium phosphate, synthetic polymers (e.g., polylactic acid and polyglycolide), and natural polymers (e.g., collagen, fibrin and chitosan).
3. **Growth factors**: These are required to promote cell proliferation and differentiation including polypeptides and steroid hormones.

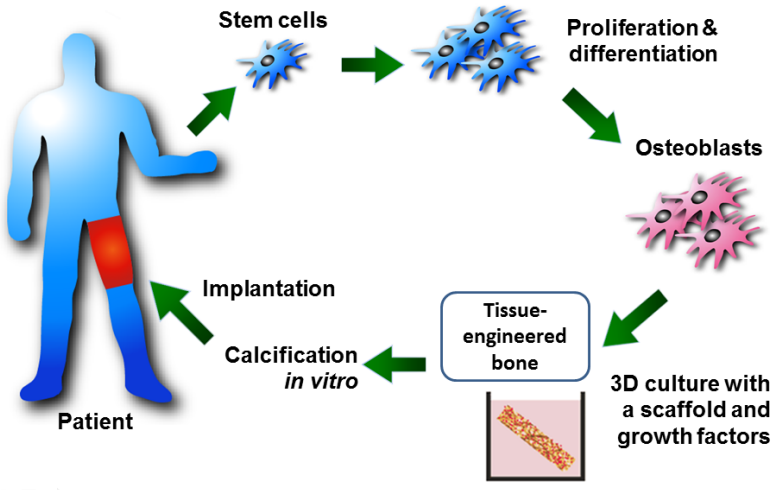

Figure 2.3 Schematic of tissue-engineered bone regeneration by in vitro method.

Osteoblasts are the bone cells that function to form the bone. Mature osteoblasts are generously polarized with a golgi body (typical of highly secretory cells). The main secretory product of osteoblasts is type I collagen, but osteoblasts make other non-collagenous proteins containing osteopontin (ON), osteocalcin, and bone sialoprotein (BSP). Osteoblasts organize the bone by facilitating mineralization, but the mechanism by which this happens is not well understood. One possibility is that the vesicles that bud off of the bone cells create a micro environment where Calcium (Ca^{2+}) and Phosphate (PO_4^{3-}) are concentrated in ratios allowing for optimized micro crystallization. These crystals arrange on secreted collagen and form a nucleation site that facilitates subsequent mineralization and hydroxyapatite (HA, $Ca_{10}(PO_4)_6(OH)_2$) formation. Another possibility is that it is started by some constituents of the collagen molecules in a behavior that is not needed for the vesicles. It is also possible that matrix vesicle-dependent and -independent mineralization happens simultaneously. In any event, osteoblasts are significant in mineralization because they produce vesicles and also secrete collagen molecules [1, 26].

Osteoblasts arise from mesenchymal stem cells (MSCs) (Figure 2.4) that can develop into adipocytes, myocytes, and chondrocytes. The differentiation pathway is taken by the progenitor cell which is regulated by specific transcription factors. For example, Runx2 (Cbfa1) transcription factor enables progenitor cell differentiation into osteoblasts, the MyoD transcription factor enables MSCs differentiation into myocytes, Sox5/6/9 transcription factor enables MSCs differentiation into chondrocytes, and PPARγ transcription factor enables MSCs differentiation into adipocytes. The pluripotent progenitor cells are obligated to the osteoblastic lineage and proceed during three stages of developmental differentiation, which are proliferation, matrix maturation and mineralization. Although these stages and the genes expression during these stages have been identified in vitro, they are excepted to reflect in vivo maturation of osteoblasts as shown in Figure 2.5 [27].

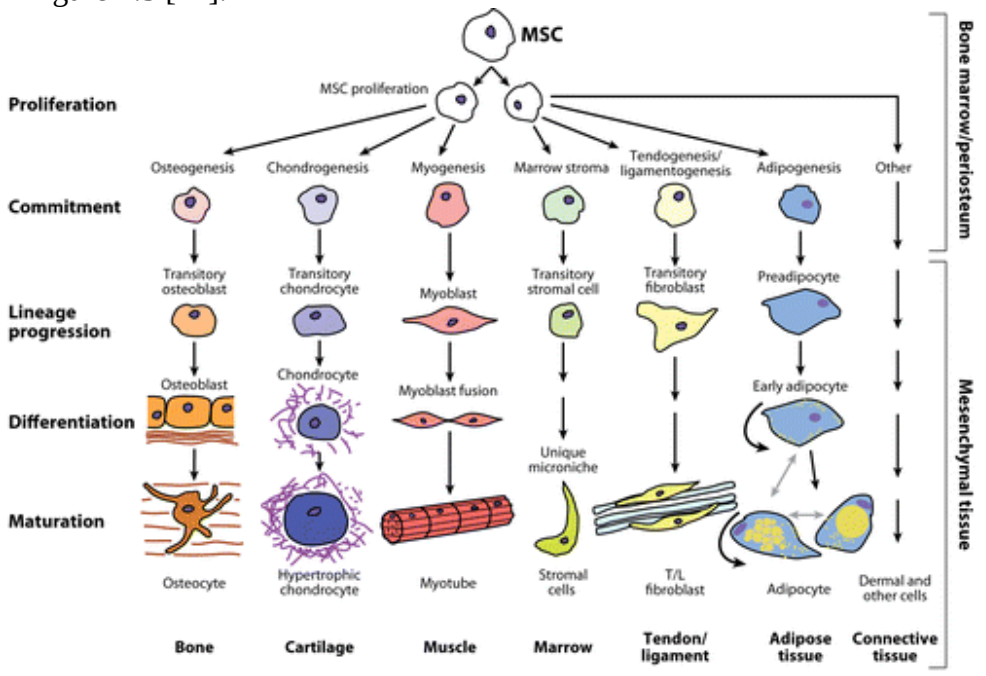

Figure 2.4 The mesengenic process, MSCs have the potential to differentiate into a variety of mesenchymal tissues, such as bone, cartilage, muscle, tendon and fat [28].

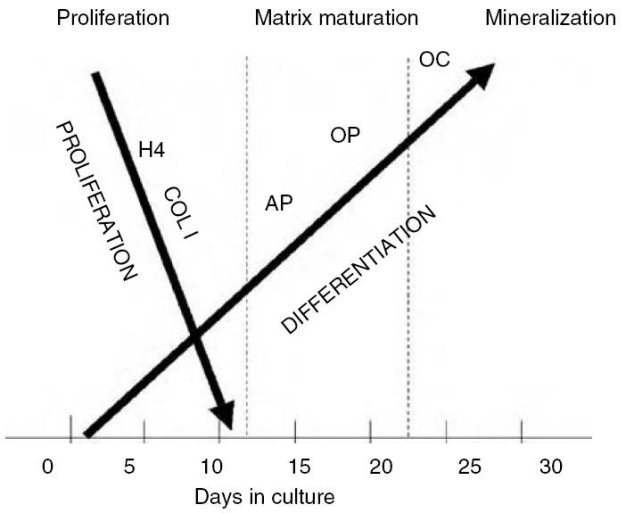

Figure 2.5 Temporary expression of genes characteristic of osteoblastic differentiation. Osteoblastic cells in culture through stages of proliferation, maturation, and mineralization. Type I collagen (COL I) and histone H4 protein peak while the proliferative phase and decline thereafter. Alkaline phosphatase (ALP) peaks during the matrix maturation phase, while osteopontin (OP) and osteocalcin (OC) peak in late maturation or early mineralization phases [27].

In general, histone H4 protein and type I collagen peak during the proliferation phase and decline after alkaline phosphatase (ALP) peaks during the bone formation phase and declines afterward, while osteopontin and osteocalcin (OC) peak during the mineralization phase (Figure 2.5). It is important to report that this differentiation sequence may actually be more complicated. The fact that osteoblasts express phenotypically distinctive genes as they differentiate in vitro has important assumptions for bone tissue engineering. For example, one can inspect the effect of several materials on osteoblastic differentiation and recognize biomaterials that support osteoblastic differentiation in the body. As well, one can recognize biophysical and molecular signals that stimulate bone cell differentiation. These biomaterials and chemical or physical signals could be utilized in bone tissue engineering applications [27].

Although osteoblasts are possibly the most widely studied bone cells, the most plentiful bone cell is the osteocyte. At least 90% of all bone cells are osteocytes [3]. However, they are comparatively difficult to isolate and culture in vitro, so these cells are the least examined of the bone cells. Osteocytes arise from osteoblasts which have become trapped in the mineralized bone matrix. While osteoblasts differentiate into osteocytes, they develop long dendritic like processes that live in small canuliculi. The processes of characteristic osteocytes join with the processes of other osteocytes, as well as with osteoblasts, and communicate via gap junctions, producing a communicative network of cells in the bone matrix that is perfectly located to merge and increase extracellular signals [19].

The regulation of osteoblastic proliferation and differentiation has undergone broad investigation, but little is known concerning the regulation of the transition from osteoblasts to osteocytes (the terminal step in osteoblastic differentiation). However, current studies

have shown that MC3T3-E1 cells (preosteoblastic cells) can differentiate into osteoblasts and osteocytes, there are stellate with interconnected processes, when cultured in a three-dimensional scaffold. These cells do not fail to occur when the cells are cultured on polystyrene material (PMMA) or polymethyl-methacrylate material (acrylic) [29].

2.3 Type I Collagen Scaffolds

Scaffolds form an essential part of bone tissue engineering. Scaffolds provide support to the regenerating tissue and can also be used to transport bioactive molecules to accelerate the healing process. The desirable properties for scaffolds to be used for bone tissue engineering are that the materials should be biocompatible, biodegradable, have a degradation rate that matches the rate of new bone formation, and have suitable mechanical properties and an appropriate porosity to allow for cell ingrowth and bone tissue formation [30].

Collagen is a group of fibrous protein, which is the most plentiful protein in the human body. It is a major component of bone, skin, ligaments, and tendons. Collagen, particularly type I collagen, possesses the unique physical, chemical, mechanical, and biological properties that are appropriate for tissue regeneration. This protein has been widely studied in the past two decades as a biomaterial for medical implant material development. Of particular attention surrounding the various medical uses of collagen is the repair of injured weight-bearing cartilaginous tissues for instance the menisci of a knee joint, so an engineered collagen matrix template is often used to support and guide bone regeneration [20, 25].

CollaCote is a product from the Zimmer dental company (USA). It is a three-dimensional porous matrix (19 mm in width x 38 mm long) and made from type I bovine collagen. Matrix morphology was analyzed using a scanning electron microscope (SEM) as shown in figure 2.6. The pore sizes of the porous matrix, determined from the SEM images, are 89 ± 28 μm [31].

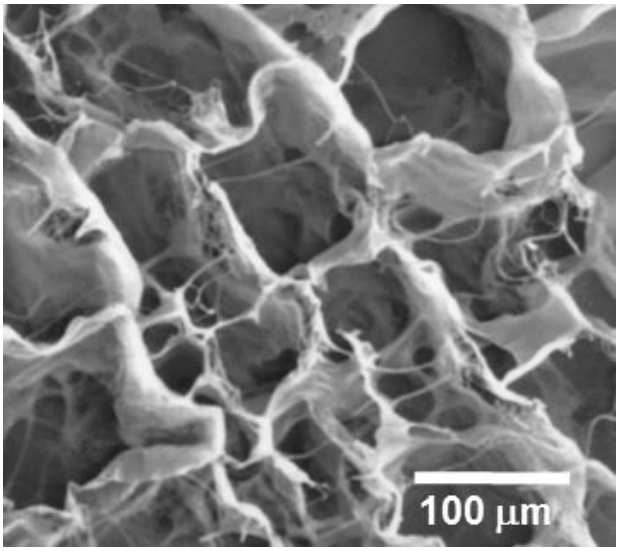

Figure 2.6 SEM observation of the type I collagen scaffold (CollaCote) [31].

2.4 MC3T3-E1 Cells

MC3T3-E1 cells are in the preosteoblastic cell line. They were isolated from newborn mouse (*Mus musculus*) calvaria. Morphology of the MC3T3-E1 cell is fibroblast, and the growth property is adherence to a cultured surface (Figure 2.7). MC3T3-E1 cells (passage number less than 18) exhibit a high level of osteoblast differentiation after growth in 50 μg/ml L-ascorbic acid, 10^{-2} mol/dm^3 β-glycerophosphate, and 10^{-8} mol/dm^3 dexamethasone. This cell line provides good models for studying in vitro osteoblastic differentiation, especially extracellular matrix (ECM) signaling. The base culture medium for this cell line is Alpha Minimum Essential Medium (α-MEM) with 10 % fetal bovine serum (FBS), ribonucleosides, deoxyribonucleosides, 2 mmol/dm^3 of L-glutamine and 1 mmol/dm^3 sodium pyruvate, and with no ascorbic acid [32].

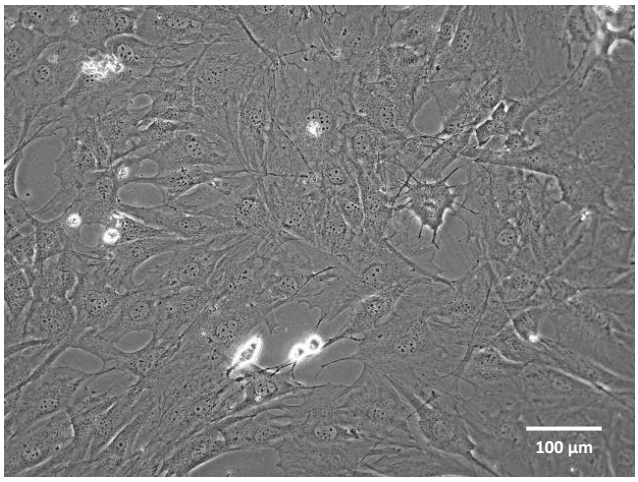

Figure 2.7 Morphology of MC3T3-E1 cells on two-dimensional culture under an optical microscope [33].

2.5 Mechanical Stimulation

Static bone cell in vitro cultures have been ordinarily studied for many decades. These methods have provided sufficient nutrients and oxygen to the bone cells using incubation in a temperature controlled and Carbon dioxide environment with a bicarbonate buffer. In order to make larger tissue-engineered bones (constructs), which have a higher number of cells and larger sizes of constructs, many restrictions or limitations arise, such as problems with nutrients and waste products that need to diffuse between the outside and the center of the construct. If the cells can't get needed nutrients and release waste products between them and the environment, those cell will die. This regularly allows for the fabrication of a tissue-engineered bone that has cell viability and proliferation on the edge of the scaffold, but with a cell seeded scaffold at a center area that is dead. The mechanical stimulation can develop the conditions and also environment for a cultured engineered construct which can induce the diffusion limitations of decreased nutrients and waste products. The biochemical environment in a stimulator can be controlled by allowing the transport of nutrients to cells and removal of degradation products away from cells. Other factors such as pH, growth factors and signal molecules available to the construct can also be delivered [34].

The differences of mechanical stimulation for bone tissue engineering applications are enhancement in mass transportation and utilization of physiologically significant loads to the tissues, which enables tissue constructs to be conditioned in agreement with the implantation environment and hydroxyapatite production to be accelerated in vitro, thus reducing production time. This is especially pertinent to bone tissue engineering where mechanical loading is a major requirement for the bone regenerative application [35].

In vivo investigations have mimicked and shown that the mechanical strain profile on the human skeleton is made up of a number of elements. Long bones such as the tibia and femur are not absolutely straight but curvilinear in nature. So the mechanical application of force induces both localized compressive and tensile force [36]. The nature of the applied mechanical loading is significant for affecting any possible response, for example, dynamic loading of approximately 1000 – 3000 microstrain in vivo is known to induce bone formation [37-39]. The major parameters which define the effectiveness of a particular loading region in stimulation of an osteogenic response are strain magnitude, strain rate and frequency [38, 40, 41]. The period of mechanical loading duration is known to have an effect of cell viability and calcification, but increased periods of loading are known to have a decreasing osteogenesis effect upon load induction, as the calcification response becomes saturated [37, 41].

In the case of bone fracture repairing, the magnitude and type of loading (tensile and compressive) can control which type of tissue will be formed from stem cell sources. In the case of high magnitude strain profiles (5-15% deformation), they have been known to induce fibrocartilage or connective tissue, but in case of low magnitude strain profiles (0.15-0.3% deformation), they have been made to induce the intramembranous ossification (bone formation) [42].

Stochastic resonance (SR) is a phenomenon whereby noise added to a system changes the behavior system. This resonance, in which vibration increases the nonlinear system response to a weak signal, has been monitored in several biological sensory systems. Tanaka et al. [43] has extended experiments to investigate the effect of stochastic resonance on the calcification response. They suggested that the mechanical sensation of osteoblasts can be enhanced with the addition of low-amplitude, broad-frequency vibration noise. Due to the Calcium channels and other ion channels present fundamental functions in bone cells respond to external forces. It has been reported that the ion channels exhibit stochastic resonance, suggesting the molecular mechanism for stochastic resonance in the bone tissue. Therefore, stochastic resonance could be used for increasing the osteogenesis effects in bone tissue engineering applications.

2.6 Piezoelectric Actuator

The piezoelectric effect is found in crystal structures which have an asymmetry structure reference to positive and negative ions of the crystal lattice. Therefore, the requirement for the event of the piezoelectric effect is the existence of polar axes in the crystal structure. The meaning of polar is an electrical dipole moment in the axis directions made by the distribution of an electrical charge in the chemical bond. For a better perceptive, the crystal structure of α-quartz is considered (Figure 2.8) [44].

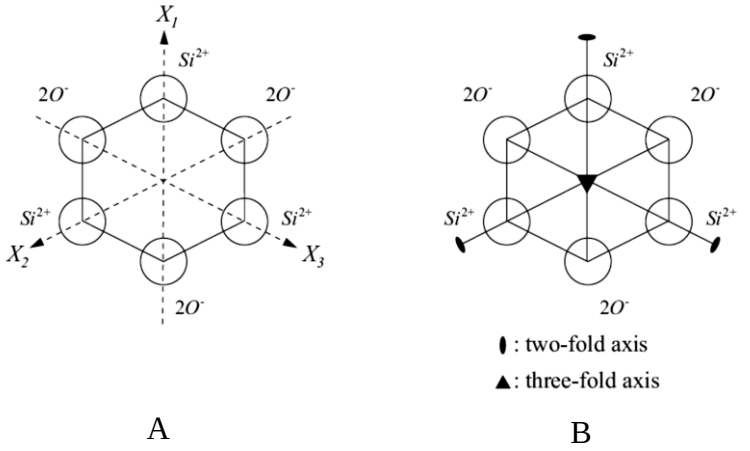

Figure 2.8 Simplified crystal structure of α-quartz. (A) An arrangement of Si- and O-ions with the main crystal axes, (B) two and three-fold axes [44].

Figure 2.8B shows a crystal structure which is composed of Si-ions (positive charged ions) and O-ions (negative charged ions). It has three of two-fold polar rotations in the X_1, X_2 and X_3 axis of plane and a three-fold rotation Z axis of the perpendicular plane. Normally, the electrical charge in this crystal is neutral. If there is a structural deformation in the direction of the polar X_1-axis, an additional electrical polarization (P) presents along this axis. The electrical polarization is affected by the displacement of positive and negative ions in the crystal structure against each other (Figure 2.9A) resulting in a change of electrical charge on the crystal surface that is perpendicular to the X_1 axis and outside of the polarization voltage. This effect is called the direct longitudinal piezoelectric effect. An exposure to tensile and compressive stresses carried out perpendicularly to the X_1-axis results in an additional electrical polarization with the opposite sign in the X_1-axis direction (Figure 2.9B). This behavior is called the direct transversal piezoelectric effect. Both these effects are reversible, e.g., a contraction or expansion of the crystal structure presents under the influence of the electric fields. This effect is called an inverse piezoelectric effect [44-46].

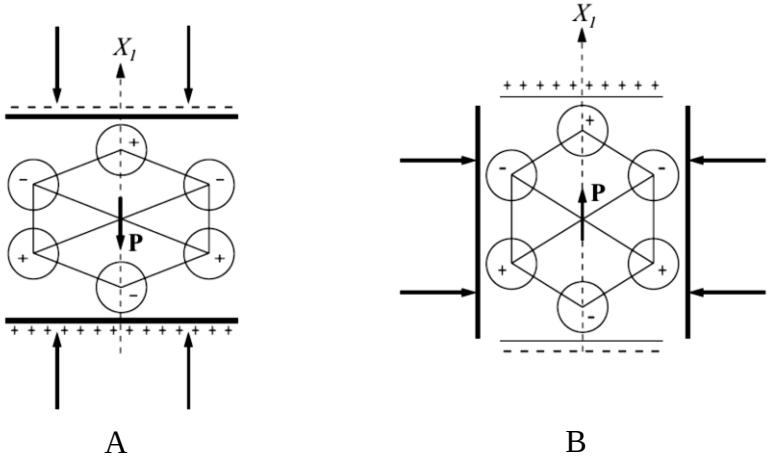

Figure 2.9 Direct piezoelectric effects within a crystal structure. (A) Longitudinal piezoelectric effect, (B) transversal piezoelectric effect [44].

Lead zirconate titanate or PZT is found in the Perovskit structure of ferroelectric crystals of the ABO_3 kind. In the Perovskit structure, A represents a double positive charged ion (lead), B presents a four-fold positive charged ion (titanium, zirconium) and O presents a double negative charged oxygen ion. Above a certain temperature (Curie temperature, T_c), the elementary cell of PZT provides a cubic structure (Figure 2.10A). In this crystal structure, there is no piezoelectric effect because it is existing in the symmetry center.

Below the Curie temperature, the cubic structure changes to a tetragonal structure spontaneously because of energetic reasons. The oxygen ion in the tetragonal structure is shifted in the direction of the crystallographic c-axis, along with a displacement of the positive ion which moves to the opposite direction. This results in an expansion of the crystal structure towards the c-axis, while a contraction towards the two a-axes occurs at the same time (Figure 2.10B). This deformation, induced by the transformation of the paraelectric phase to the ferroelectric phase, is called spontaneous deformation [44, 47].

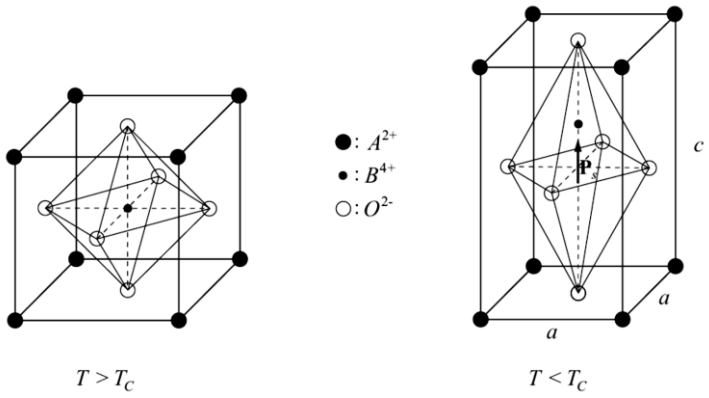

Figure 2.10 Perovskit structures of ferroelectric crystals of the ABO_3 kind.
(A) Cubic structure above the Curie temperature,
(B) tetragonal structure below the Curie temperature [44].

Spontaneous deformation results in the creation of a dipole moment from the center of the tetragonal structure (asymmetry crystal). The amount of the dipole moment depends on the volume of the unit cell, which is called polarization (P_s). As a result, the transformation of the cubic structure to the tetragonal structure allows three directions for the spontaneous expansion and six directions for the spontaneous polarization, respectively [48].

Applying the electric field causes additional deformation and polarization effects, which are generated by the force impact on the centers of charge with the deformed tetragonal structure. This is called the inverse piezoelectric effect. Causes to the elementary structure by an external mechanical load bring about a mechanical stress in which the centers of charge of the elementary structure are displaced. This effect causes an additional polarization and deformation, this is called a direct piezoelectric effect [44].

The compressive or expansive deformation is combined with either a transverse compression or expansion perpendicular to the electric field direction (transverse piezoelectric effect). These facts are illustrated as figure 2.11.

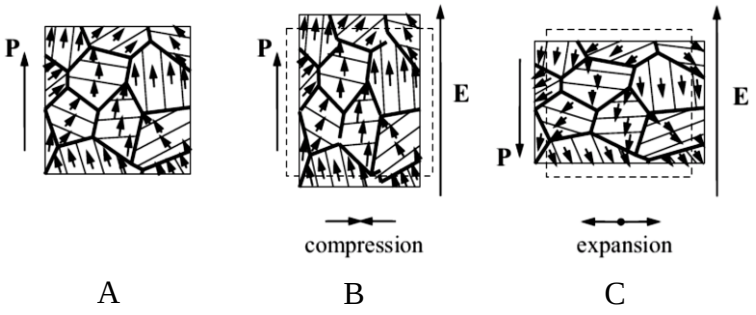

Figure 2.11 Transverse strain behaviors of PZT structure. (A) Polarized state, (B) electric field aligned parallel, (C) electric field aligned antiparallel to the remnant polarization [46].

The typical of PZT structure can be used for the realization of a monomorph structure as shown in figure 2.12.

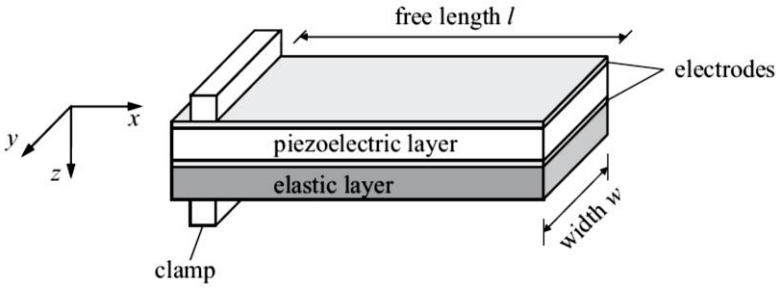

Figure 2.12 Layer sequence of a monomorph [44].

A monomorph structure is composed of one piezoelectric and one elastic layer (Passive layer). The movement of the piezoelectric component caused by its expansion or compression is limited by the elastic layer.

From the result in figure 2.13, an internal dipole moment of piezoelectric layer appears to be distorting the monomorph. Total deformation in the z-direction is much larger than the deflection in the x- and y-directions. Because of the mechanical deformation of the piezoelectric layer into a bending deflection, it is possible to generate large deformations in the z-direction and the actuator is driven by the electric voltages in the 24-250V range [44, 46].

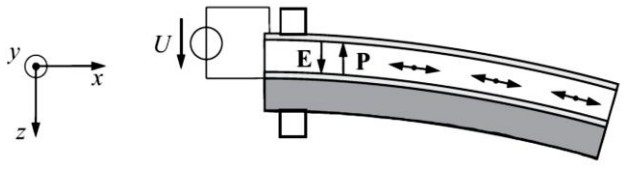

Figure 2.13 Behavior of a monomorph subjected by an electrical voltage [44]

In order to increase the bending deformation of the piezoelectric beam actuator, the elastic layers (passive layer) can be replaced by a second active piezoelectric layer. This piezoelectric beam actuator structure is called a bimorph.

If the polarization (P) directions in the crystal structure of both piezoelectric layers are the same, and if they are driven by the electrical parallel connection, then this structure is a called parallel bimorph. However, if the polarization directions in the crystal structure of both layers are arranged oppositely, and if they are driven by an electrical series connection, then this structure is called a serial bimorph (Figure 2.14) [44, 46]

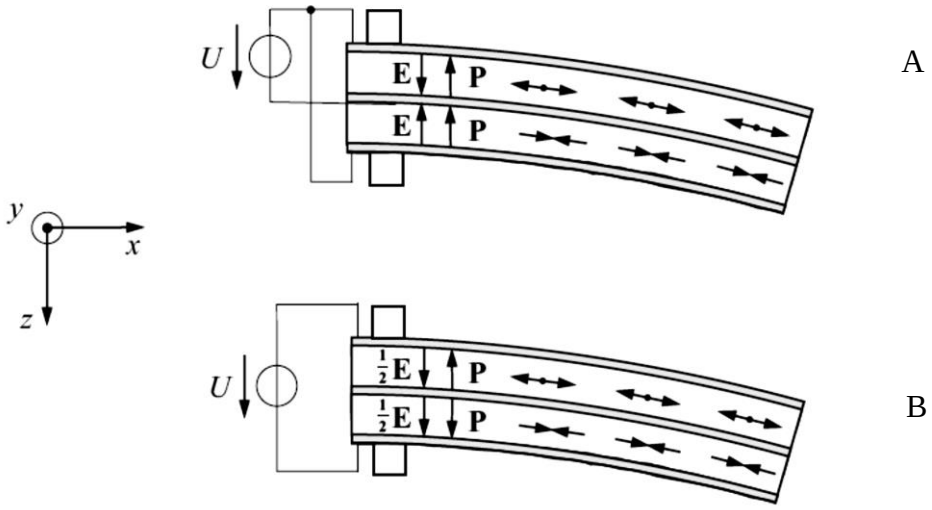

Figure 2.14 Behavior of a bimorph subjected by an electrical voltage. (A) Parallel bimorph, (B) serial bimorph [44].

In summary, the piezoelectric actuator is superior to other power sources for movement such as the servo motor, step motor or hydraulic actuator in terms of size, driving speed, frequency response and control of microscopic displacement. Most importantly, the electric fields and heat radiation from the piezoelectric actuator, which affects cultured cells, are negligible because this actuator use only minimal electric power consumption [46-49].

2.7 Near-Infrared Diffuse Reflectance Spectroscopy

In analytical chemistry, infrared (IR) spectroscopy is mostly used for the analysis of organic components. The qualitative assessment of organic components is presented for the identification of unknown compounds, or for the determination of the chemical structure of compounds. Moreover, infrared spectroscopy analysis can be used for expressing the quantity of the chemical components. Infrared spectroscopy is known as vibration spectroscopy, because of the spectra result from transitions between the vibrational energy levels of a covalent bond of a molecule. The infrared spectrum, which ranges from 1 μm to 1000 μm, is part of the electromagnetic spectrum and is surrounded by

the visible and microwave regions (Figure 2.15). The infrared region can be further subdivided into the near infrared, the mid infrared and the far infrared regions [50].

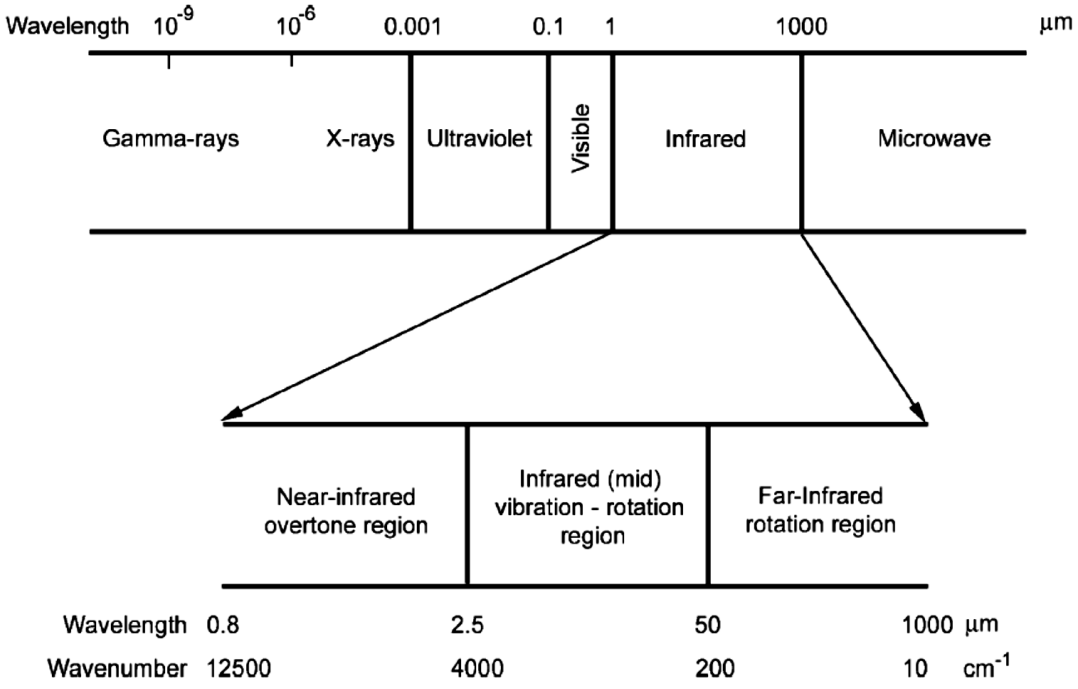

Figure 2.15 Infrared region of the electromagnetic spectrum [50].

Regarding external reflectance, the light energy which infiltrates to the sample is reflected in all directions and this principle is called diffuse reflectance. The diffuse reflectance (infrared) technique is commonly called DRIFT. The DRIFT can reflect the electromagnetic radiation to the sample and collect the energy reflected back over a large angle (Figure 2.16) [51].

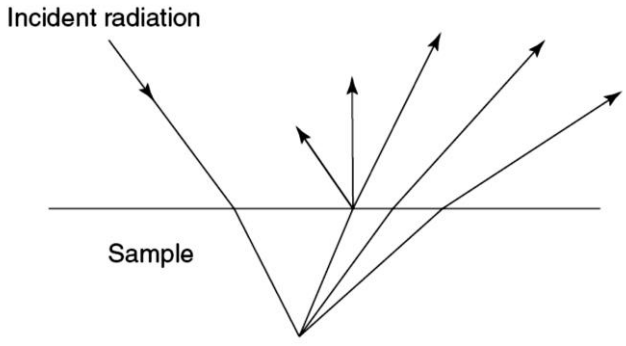

Figure 2.16 Illustration of diffuse reflectance [51].

Kubelka and Munk developed a theory to express the diffuse reflectance procedure for samples which associate the concentration of samples to the scattered radiation intensity. The Kubelka–Munk's equation is as follows:

$$\frac{(1-R)^2}{2R} = \frac{c}{k} \tag{2.1}$$

where R is the absolute reflectance of the layer, c is the concentration of the sample and k is the molar absorption coefficient. An optional relationship between the concentration and the reflected intensity is widely used in near-infrared diffuse reflectance spectroscopy, namely:

$$\log\left(\frac{1}{R}\right) = k'c \tag{2.2}$$

where k′ is a constant.

Near infrared (NIR) spectroscopy is used widely in biomedical applications [52]. Near infrared light can penetrate the type I collagen porous scaffold or tissue-engineered bone easily, so that diffuse reflectance light carries the information of hydroxyapatite crystals inside the tissue-engineered bone [53]. With its safety for cell viability and its deep penetration, near-infrared light is often used in the application of non-invasive biomedical sensing technologies such as pulse oxygen meters [54], blood glucose meters [55],blood pressure measurement [56] and bone densitometry [57].

CHAPTER 3 MATERIALS & METHODS

3.1 Materials and Equipment

All materials and equipment used throughout this study are shown in table 3.1.

Table 3.1 List of materials and equipment

Materials and equipment	Company	Country
35 mm culture dish (153066)	NUNC	Denmark
6½-digit USB multimeter (NI USB-4065, 22-bit)	National instrument	USA
6-well plate (140675, Denmark)	NUNC	Denmark
96-well plate (167008)	NUNC	Denmark
Alpha-modified eagle medium (α-MEM, SH30265.01)	Hyclone	USA
Calcium carbonate, powder ($CaCO_3$, 239216-100G)	Sigma-Aldrich	USA
Calcium chloride dehydrate ($CaCl_2 \cdot 2H_2O$, 127-500G)	Ajax finechem	Australia
Centrifuge tube 15 ml (366036)	NUNC	Denmark
Computer (A8JP model)	ASUS	Taiwan
Dexamethasone (D4902-25MG)	Sigma-Aldrich	USA
Dimethyl Sulfoxide (DMSO, 0231-500ML)	Amresco	USA
Di-Sodium Hydrogen orthophosohate anhydrous (Na_2HPO_4, 621-500G)	Ajax finechem	Australia
Ethanolamine (E0135-100ML, Sigma, USA)	Sigma-Aldrich	USA
Fetal bovine serum (FBS, 10270)	GIBCO	USA
Glutaraldehyde solution (3802-75ML)	Sigma-Aldrich	USA
Hemacytometer	BOEGO	Germany
High speed amplifier (HA400)	PINTEK	Taiwan
High speed near infrared light-emitting diodes (LEDs) at 850 nm (TSHG6200)	Vishay	USA
High speed silicon PIN Photo detector (PD) at 830 - 930 nm (VEMD2000X01)	Vishay	USA
HOECHST 33258 powder (H1398)	Invitrogen	USA
Hydrochloric acid (HCl, 9535-69)	J.T. Baker	Thailand
LabVIEW® software (version 8.6)	National instrument	USA

Table 3.1 List of materials and equipment (continued)

Materials and equipment	Company	Country
L-Ascorbic acid (A4544-25G)	Sigma-Aldrich	USA
Laser displacement sensor controller (LK-G5001)	Keyence	Japan
Laser displacement sensor head (LK-H022)	Keyence	Japan
Low power quad operational amplifiers (LM324)	National semiconductor	USA
Multifunction data acquisition (DAQ, USB-6221 BNC, 16-bit)	National instrument	USA
O-cresolphythalein complex substrate (OCPC, P5631-5G)	Sigma-Aldrich	USA
Penicillin/Streptomycin solution (15140)	GIBCO	USA
Piezoelectric actuators (LPD3713X)	Nihon ceratec	Japan
Potassium chloride (KCl, 383-1KG)	Ajax finechem	Australia
Potassium dihydrogen orthophosphate (KH_2PO_4, 391-500G)	Ajax finechem	Australia
Power supply (HR501)	T.P.K. Electric	Thailand
Silicon rubber glue (748)	Dow Corning	USA
Sodium chloride (NaCl, K39486504)	Merck	Germany
Sodium Dodecyl Sulfate (SDS, SB0485)	Bio basic	Canada
SSC buffer 20x concentrate (S6639-1L)	Sigma-Aldrich	USA
T-75 culture flask (156499)	NUNC	Denmark
Trypan blue stain 0.4% (15250-061)	GIBCO	USA
Trypsin/EDTA 0.25% (25200, GIBCO, USA)	GIBCO	USA
Type I collagen scaffold (CollaCote)	Zimmer dental	USA
β-glycerophosphate (G9422-100G)	Sigma-Aldrich	USA

3.2 Non-Destructive Optical Monitoring Device

A non-destructive optical monitoring device was fabricated for evaluating the calcification response of tissue-engineered bone in vitro. This device consists of four light-emitting diodes (LEDs) and a photo detector (PD) surrounded by the LEDs underneath a culture chamber (Figure 3.1). The LEDs emit near-infrared light to a tissue-engineered bone increasing its intensity linearly at 850 nm, so that diffuse reflectance light carries the information of calcification inside the tissue-engineered bone to a photo detector (PD). The slope of the relationship between intensity from the LED (I_0) and intensity from the PD (I) was used as a parameter to evaluate the calcification.

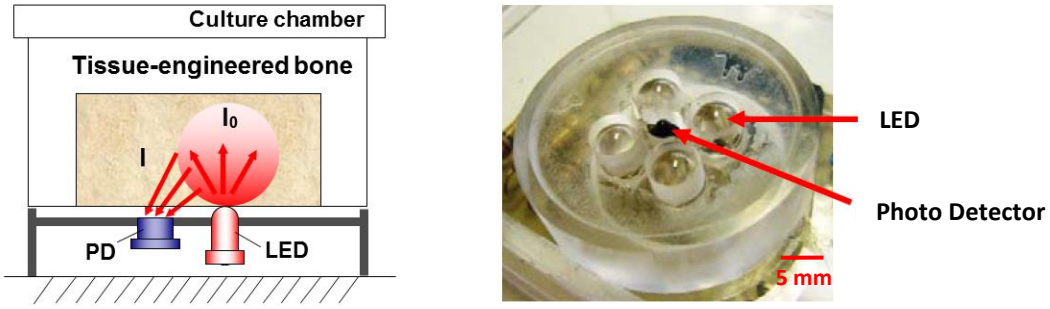

A B

Figure 3.1 Optical monitoring device for the calcification or the tissue-engineered bone. (A) Tissue-engineered bone on a culture chamber is irradiated with near infrared light (850 nm) from LEDs at an intensity of I_0, the diffuse reflective light from the tissue is detected by a PD at an intensity of I. (B) Optical unit consisted of four LEDs and a one of PD.

The intensity of light emission of the LED was controlled by a computer through a multifunction data acquisition (DAQ) with applied currents from 0 to 40 mA, which was amplified by an operational amplifier. The detected signal by the PD was transferred to the computer via a digit USB multimeter and the computer was operated by a program written by LabVIEW® (Figure 3.2).

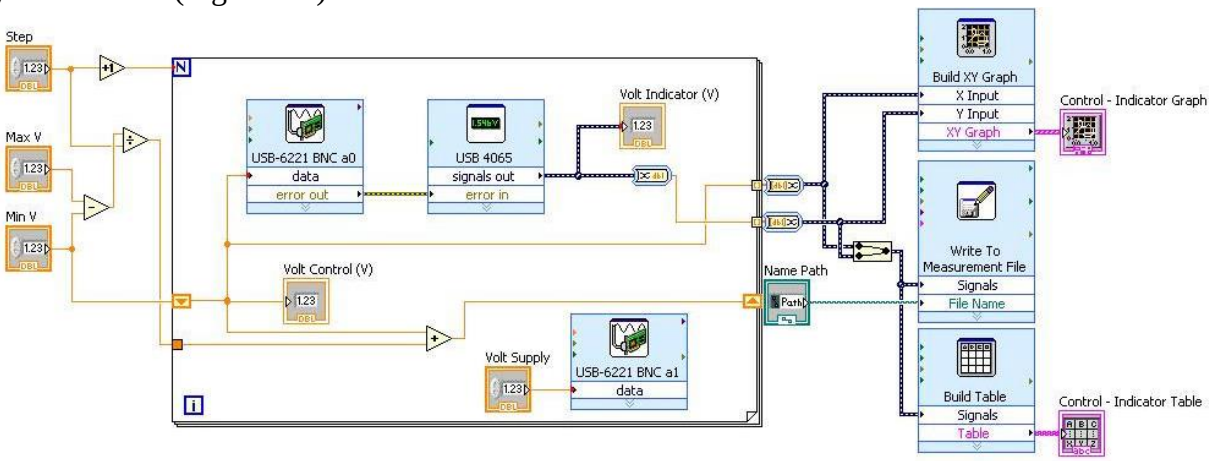

Figure 3.2 Front panels design in the LabVIEW program for controlling the intensity of LEDs and detecting intensity of a photo detector.

In order to reduce the size of the non-destructive optical monitoring device, a printed circuit board (PCB) was designed and used for a circuit board (Figure 3.3).

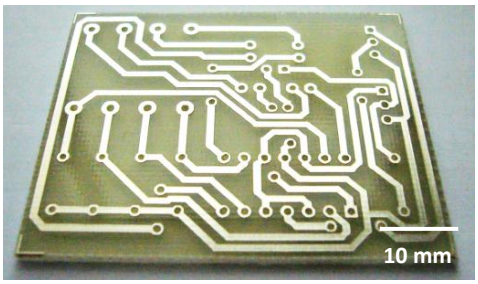

Figure 3.3 A printed circuit board (PCB).

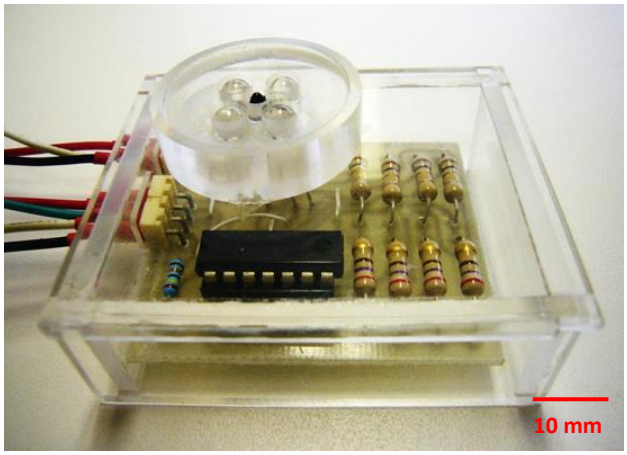

Figure 3.4 A non-destructive optical monitoring device.

3.3 Deposition of Hydroxyapatite (HA) for Scaffold

In order to calibrate the non-destructive optical monitoring device, type I collagen scaffolds were deposited with a varying amount of hydroxyapatite. The degree of calcification of tissue-engineered bone was defined and treated as an equivalent value to bulk density and calcium content of a hydroxyapatite-deposited scaffold.

Type I collagen scaffolds were cut in a dimension of 16 mm (Width) x 19 mm (Length) x 2 mm (Thickness) with a razor blade (Figure 3.5A). The scaffolds were soaked in a 0.5 mol/dm^3 $CaCl_2$ solution for 15 minutes followed by a 0.5 mol/dm^3 Na_2HPO_4 solution for 15 min each. The scaffolds were thoroughly rinsed in Milli-Q water between immersions and alternate immersions in $CaCl_2$ and Na_2HPO_4 solutions and repeated with varying cycle depositions. After this hydroxyapatite deposition, the scaffolds were rinsed in Milli-Q water five times and then rinsed in the culture medium (α-MEM) five times (Figure 3.5B).

A B

Figure 3.5 Type I collagen scaffold (CollaCote). (A) A scaffold in the dimension of 16 mm (Width) x 19 mm (Length) x 2 mm (Thickness).
(B) A hydroxyapatite-deposited scaffold after rinsing in a culture medium.

3.4 Calcium Evaluation on Scaffold by Colorimetric Quantitative Method

Colorimetric quantitative method, which is a conventional method, was performed to quantify the calcium content of hydroxyapatite-deposited scaffolds and tissue-engineered bone. In the principle of this method, O-cresolphythalein complexion (OCPC), which integrates with alkaline earth element, produces a purplish red color. Calcium content of the sample can be determined by measuring the absorbance of a sample solution at 570 nm. The concentration of the purplish red color produced by OCPC is an indication of the calcium content in the sample.

The wet scaffold samples were transferred to a 35 mm culture dish and kept in a desiccator for 24 hours. The samples were then dried using a freeze dryer (FD4.0, Heto, Denmark) at -50^{o} C, 0 Pa for 6 hours. Dry samples (Figure 3.6) were dissolved in a 1 mol/dm^3 HCl solution, minced into small pieces (Figure 3.7), and incubated at 4° C for 4 hours. The frozen samples were homogenized using a plastic stick to get further solubility. The sample solutions were centrifuged and separated into supernatant and scaffold debris. Calcium content in the supernatant was mixed with an ethanolamine buffer solution and OCPC substrate, and then the mixed solution was transferred to a 96-well plate (Figure 3.8) and quantified the calcium content using a photo spectrometer (infinite 200, TECAN, Austria). A standard curve was also prepared in a 1 mol/dm^3 HCl solution with varying amounts of $CaCO_3$ solution.

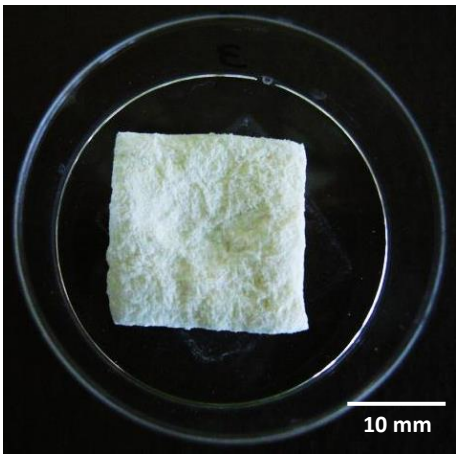

Figure 3.6 A dried hydroxyapatite-deposited scaffold

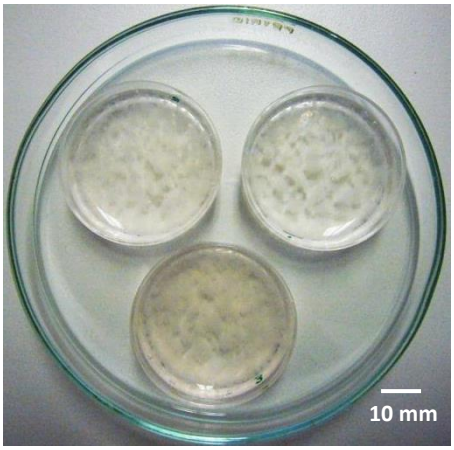

Figure 3.7 Small pieces of scaffold samples in a HCl solution.

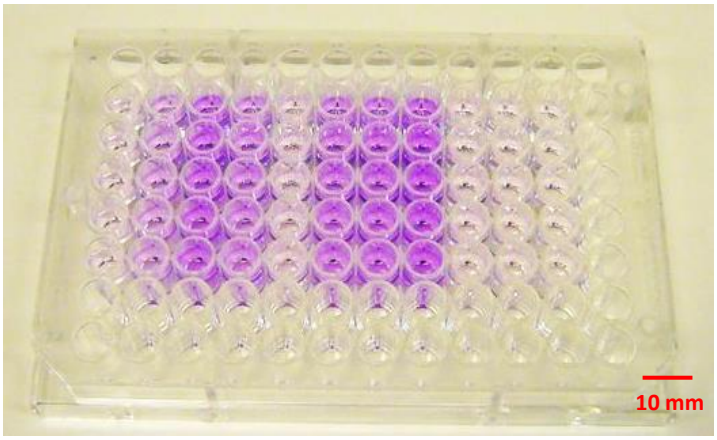

Figure 3.8 The purplish red solutions mixed with sample solutions, an ethanolamine buffer solution and OCPC substrate in a 96-well plate.

3.5 Mechanical Stimulator

The mechanical stimulator was fabricated for stimulating the calcification response of three-dimensional tissue cultures. Aluminum material was used as the base of the mechanical stimulator (Figure 3.9) for a fixed position between a 6-well plate (culture chamber) and moving plungers. Fixed plungers and moving plungers were made from polymethyl-methacrylate (PMMA, Acrylic). Moving plungers were linked to piezoelectric actuators, so that the displacement from the piezoelectric bending transferred the force and movement to the moving plunger and tissue culture directly (Figure 3.10). Positions of the piezoelectric actuators were fixed with Aluminum poles and these poles were at a fixed position using an Aluminum base (Figure 3.11).

Strain waveforms from bending profiles of the piezoelectric actuators were controlled by the computer which was operated by a program written by LabVIEW® program. A voltage-signal was amplified by a high speed amplifier with a frequency response of 600 kHz via a multifunction data acquisition. The displacement at the center of the piezoelectric actuator was measured by a laser displacement sensor with a frequency response of 392 kHz and resolution of 0.02 μm.

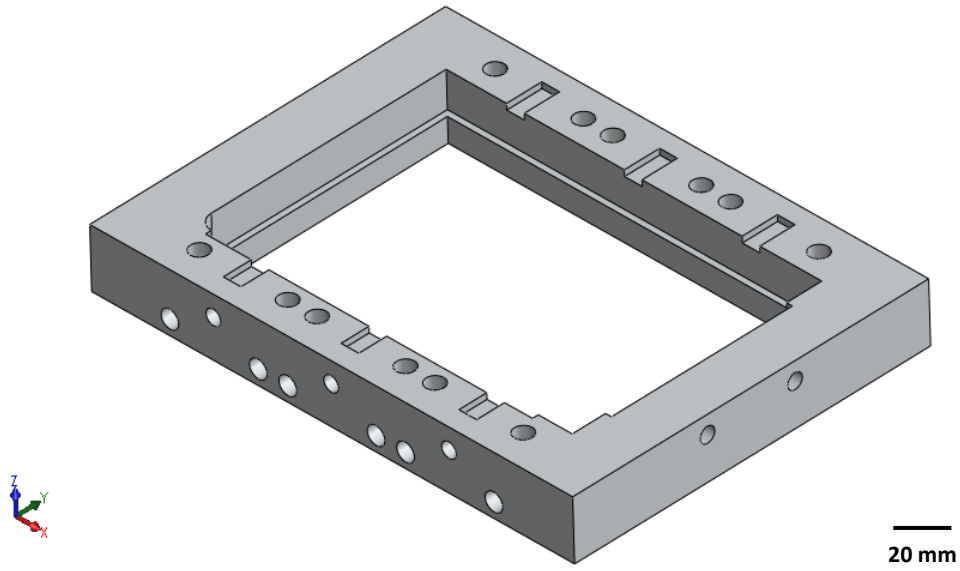

Figure 3.9 The Aluminum base of a mechanical stimulator.

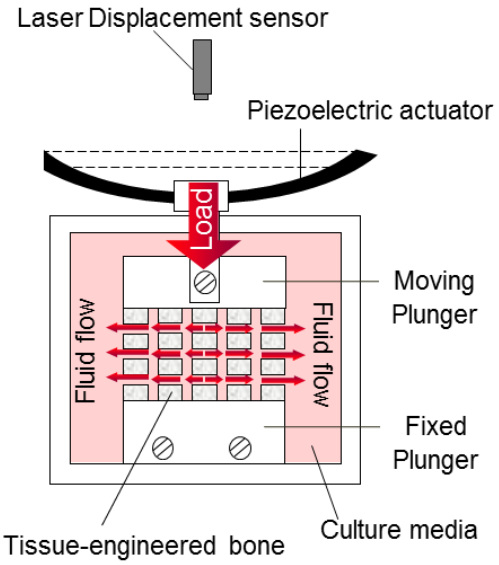

Figure 3.10 Schematic diagram showing the components and motion of the mechanical stimulator.

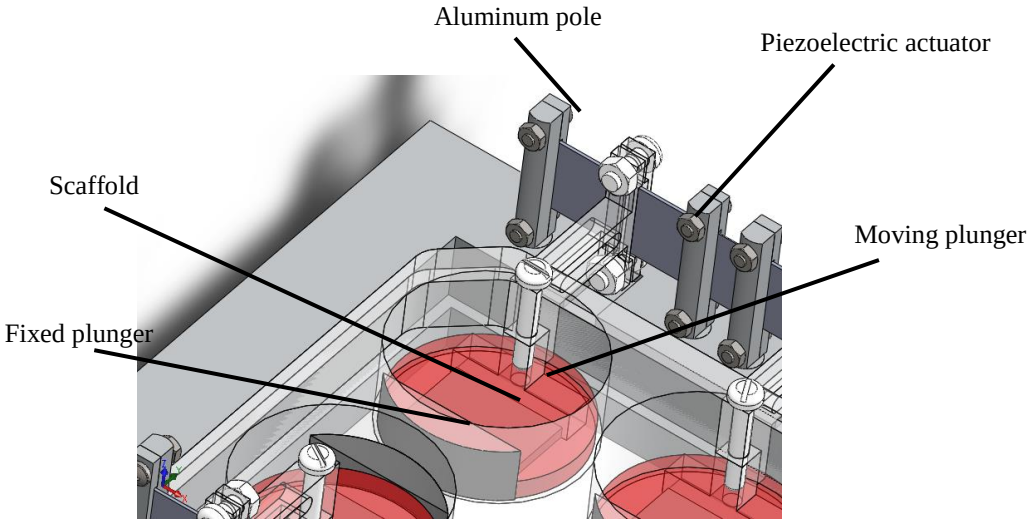

Figure 3.11 Design of a mechanical stimulator.

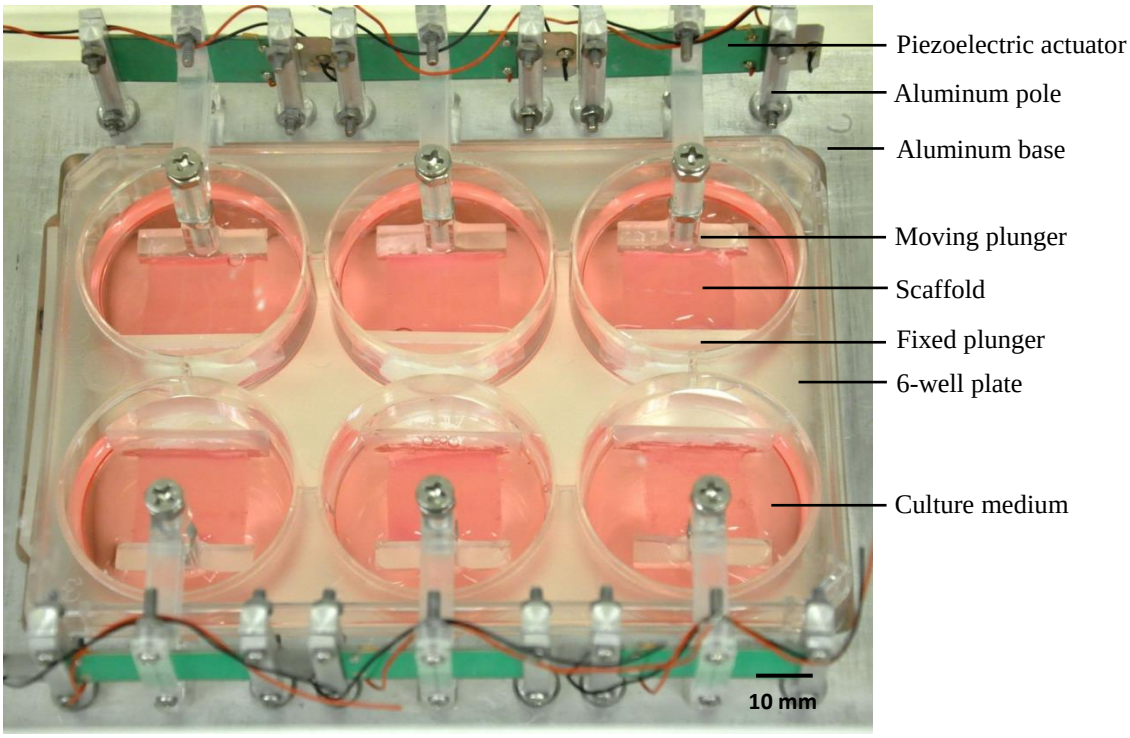

Figure 3.12 A mechanical stimulator with type I collagen scaffolds in culture medium.

3.6 Evaluation of Mechanical Stimuli on Calcification Response of Tissue-Engineered Bone

MC3T3-E1 cells at a passage number of 10 were pre-cultured and maintained in Alpha-modified eagle medium (α-MEM) supplemented with 10% fetal bovine serum (FBS) and 1% antibiotics (0.05 U/ml penicillin and 0.05 μg/ml streptomycin). Type I collagen scaffolds were cut in dimension of 16 mm (Width) x 19 mm (Length) x 2 mm (Thickness) with a razor blade, then the scaffolds were attached to fixed plungers and moving plungers of the mechanical stimulator with Silicon rubber glue (Figure 3.13).

The mechanical stimulator was sterilized by with ethylene oxide gas, then 1.0 x 10^6 of MC3T3-E1 cells at a passage number of 14 (Figure 3.14) were seeded onto the top surface of a scaffold. Eighteen samples were prepared, fifteen samples were stimulated by mechanical stimulation (three samples per one condition), and another fifteen were employed as non-stimulated controls. The tissue-engineered bone was cultured in an osteogenic medium, which was α-MEM containing 10% fetal bovine serum (FBS), 1% antibiotics (0.05 U/ml penicillin and 0.05 μg/ml streptomycin), 50 μg/ml L-ascorbic acid, 10^{-8} mol/dm^3 dexamethasone, and 10^{-2} mol/dm^3 β-glycerophosphate. The tissue-engineered bone was cultured in a CO_2 incubator (3517, Shel lab, USA) at 37 ^oC with 5% CO_2 and the culture medium was changed every 2 days.

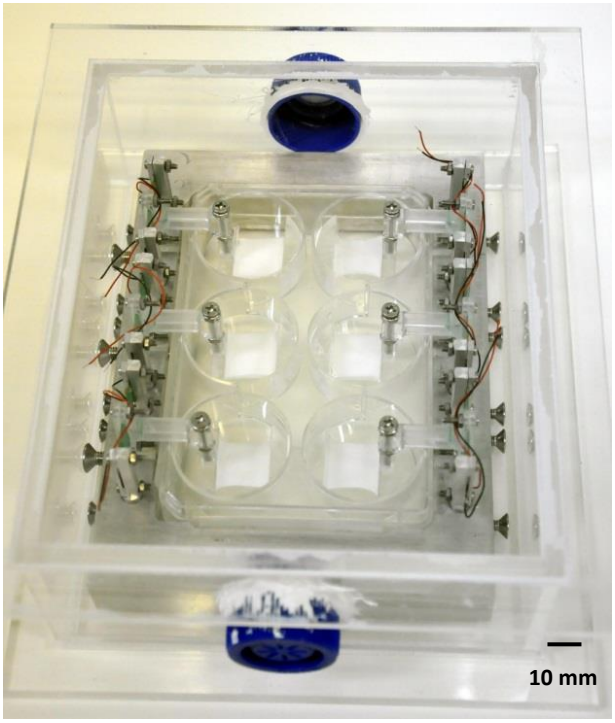

Figure 3.13 The mechanical stimulator was attached with type I collagen scaffolds and sterilized with ethylene oxide gas

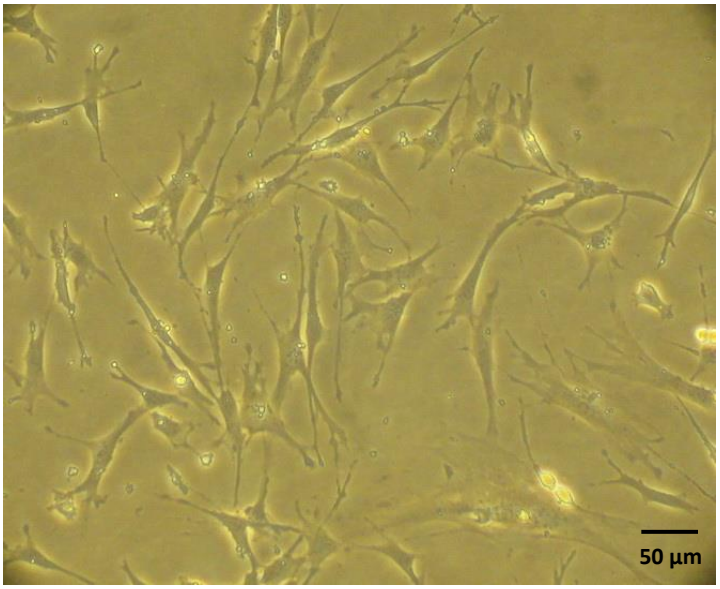

Figure 3.14 Optical microscope observation of MC3T3-E1 cells in two-dimensional culture.

Sinusoidal mechanical loads with a peak of 0.3% deformation with vibration (Gaussian quasi-white noise with a standard deviation of 0.03% deformation and frequency components up to 50 Hz) was applied to the constructs at 0.5, 1.0, 1.5, 2.0 and 2.5 Hz for 3 minutes per day for 42 consecutive days using a mechanical stimulator. A non-destructive optical monitoring device was used for the detection of the calcification response of the tissue-engineered bone once a day.

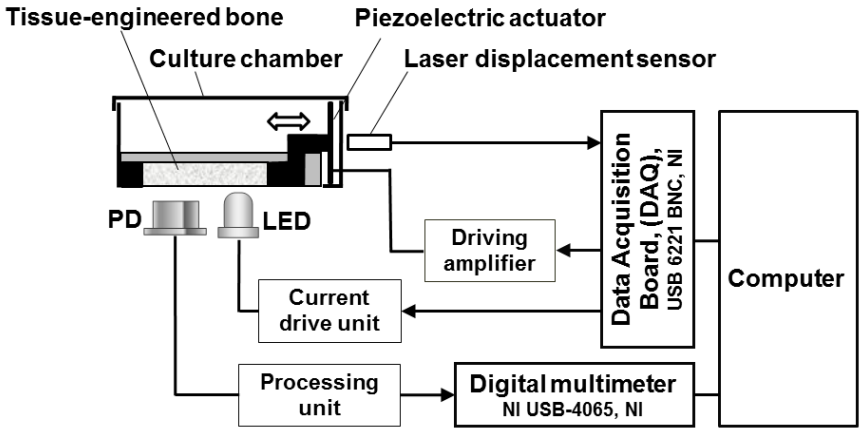

Figure 3.15 Schematic of experimental system.

Figure 3.15 shows the experimental system that consists of two parts, first is a mechanical stimulation part. The movement of piezoelectric actuators was controlled by a computer via a data acquisition board (DAQ) and a high speed driving amplifier. A laser displacement sensor was used for verification of the piezoelectric movement, the moving signal was sent to a computer via a data acquisition board (DAQ). The second part was optical monitoring for calcification. The intensity of LEDs was controlled by a computer via a data acquisition board (DAQ) and a current drive unit. Intensity of reflectance light from a tissue-engineered bone was measured using a photo detector, and the intensity signal was sent to a computer via a processing unit and a digital multimeter with high resolution.

3.7 Cell Viability Test by DNA Assay

The quantity of DNA in bone cells grown on tissue-engineered bone was determined using fluorescence measurement with fluorescent bisbenzimide (Hoechst 33258) dye. The dye is weakly fluorescent itself in a solution which binds specifically to the A-T base pairs in dsDNA of bone cells.

On day 42, tissue-engineered bones were transferred to a 35 mm culture dish and kept in a desiccator for 24 hours. The samples were then dried using a freeze dryer (FD4.0, Heto, Denmark) at -50^{o}C, 0 Pa for 6 hours. Dry samples were dissolved in an SDS lysis buffer solution, and minced into small pieces, then incubated at 37 °C for 1 hour. The incubated sample was homogenized using a plastic stick to get further solubility. The cell lysis solution (Figure 3.16) was transferred to a 96-well plate and mixed with a Hoechst 33258 solution, then quantified the amount of DNA with fluorescence microplate readers (infinite 200, TECAN, Austria) at fluorescent intensity of solution at 355 nm (Excitation) and 460 nm (Emission).

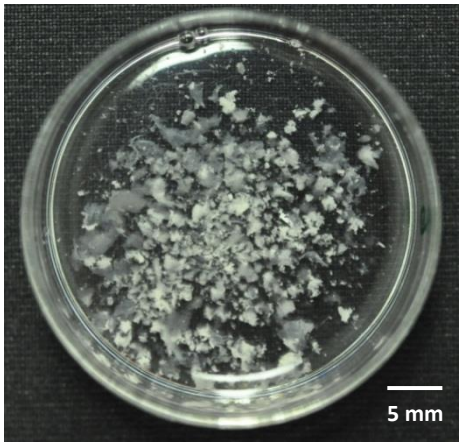

Figure 3.16 A cell lysis solution from a tissue-engineered bone in an SDS lysis buffer solution

3.8 Scanning Electron Microscope (SEM) and Energy Dispersive Spectroscopy (EDS) Analysis

To observe the distribution of the osteoblasts seeded in the scaffold and the hydroxyapatite crystals, on day 42 the tissue-engineered bones were fixed with 2.5% glutaraldehyde in a 0.1 M phosphate buffer solution at 4˚ C for 2 hours. The samples were rinsed twice in a phosphate buffer solution and once in distilled water, then dehydrated in a series of graded ethyl alcohols. The samples in 100% alcohol were dried using a critical point dryer (CPD 020, Balzers union, Liechtenstein). The dried samples were frozen using liquid nitrogen and fractured, the fractured sample was coated with gold by a sputter coater (SCD040, Balzers union, Liechtenstein) (Figure 3.17). Scanning electron microscopy (SEM) and Energy Dispersive Spectroscopy (EDS) (JSM-6400, JEOL, Japan) was performed for the fractured plane, top plane, and bottom plane of the samples at 15 kV.

Figure 3.17 The dried samples were coated with gold for SEM observation and EDS analysis.

3.9 Verification of Hydroxyapatite Crystals

In order to identify the Calcium crystalline phases, the dried sample of tissue-engineered bone was analyzed with X-ray diffraction (D8Discover, BRUKER AXS, Germany) using 1.54 angstrom Cu K α radiation generated at 40 kV and 40 mA. The Specimen was detected at two theta angle of 20 – 60^{o} with a step size of 0.02^{o} and a step time of 0.4 second. Diffraction peaks were identified using a hydroxyapatite standard JCPDS file (reference number 74-0565).

CHAPTER 4 RESULTS & DISCUSSION

4.1 Calibration of Non-Destructive Optical Monitoring Device

In order to simulate the culturing condition of tissue-engineered bone in a mechanical stimulator, type I collagen scaffolds, which were deposited with varying amounts of hydroxyapatite, were dissolved in a culture medium (α-MEM) on a 6-well plate (Figure 4.1). A non-destructive optical monitoring device was used for getting the information of calcification inside the scaffold using the slope of the relationship between intensity from the LEDs (I_0) and intensity from a photo detector (I) as shown in table 4.1.

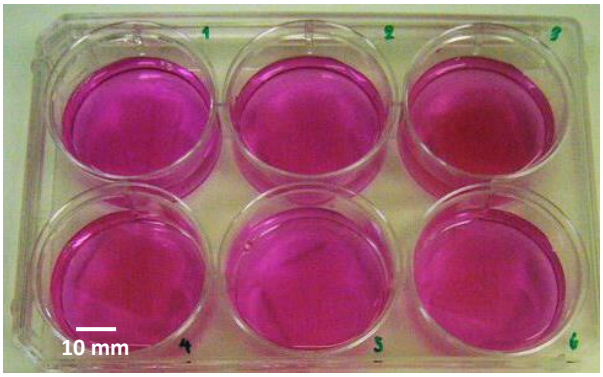

Figure 4.1 Hydroxyapatite-deposited scaffolds were dissolved in a culture medium on a 6-well plate.

Table 4.1 The slope of the relationship between intensity from LEDs (I_0) and intensity from a photo detector (I) of the scaffolds.

Time	The I_0 – I slope of scaffold					
	Number 1	**Number 2**	**Number 3**	**Number 4**	**Number 5**	**Number 6**
1	0.1767	0.2064	0.2200	0.2757	0.3058	0.3548
2	0.1761	0.2066	0.2241	0.2805	0.3098	0.3623
3	0.1769	0.2081	0.2199	0.2682	0.3182	0.3477
4	0.1781	0.2078	0.2213	0.2706	0.3023	0.3623
5	0.1788	0.2043	0.2219	0.2788	0.3039	0.3577
Average	**0.1773**	**0.2066**	**0.2214**	**0.2748**	**0.3080**	**0.3570**
SD	0.0011	0.0015	0.0017	0.0053	0.0064	0.0061
SE	**0.0005**	**0.0024**	**0.0008**	**0.0007**	**0.0028**	**0.0027**

where number 1 is a scaffold without hydroxyapatite deposition, number 2 is a hydroxyapatite-deposited scaffold by 0.2 mol/dm^3 $CaCl_2/Na_2HPO_4$ solutions for 2 cycles, number 3 is a hydroxyapatite-deposited scaffold by 0.2 mol/dm^3 $CaCl_2/Na_2HPO_4$ solutions for 3 cycles, number 4 is a hydroxyapatite-deposited scaffold by 0.2 mol/dm^3 $CaCl_2/Na_2HPO_4$ solutions for 4 cycles, number 5 is a hydroxyapatite-deposited scaffold by 0.5 mol/dm^3 $CaCl_2/Na_2HPO_4$ solutions for 3 cycles, and number 6 is a hydroxyapatite-deposited scaffold by 0.5 mol/dm^3 $CaCl_2/Na_2HPO_4$ solutions for 4 cycles.

The wet scaffolds were dried with a desiccator and a freeze drier, and then weighed using a precision balance for measuring the density of the scaffolds by their dry weight divided by the bulk volume of scaffold, the result is shown in table 4.2.

Table 4.2 The bulk densities of scaffold.

Scaffolds	**Number 1**	**Number 2**	**Number 3**	**Number 4**	**Number 5**	**Number 6**
Bulk Volume (cm^3)	0.722	0.722	0.722	0.722	0.722	0.722
Scaffold (mg)	15.2	16.9	17.0	24.0	25.8	33.6
Density (mg/cm^3)	**21.1**	**23.4**	**23.5**	**33.2**	**35.7**	**46.5**

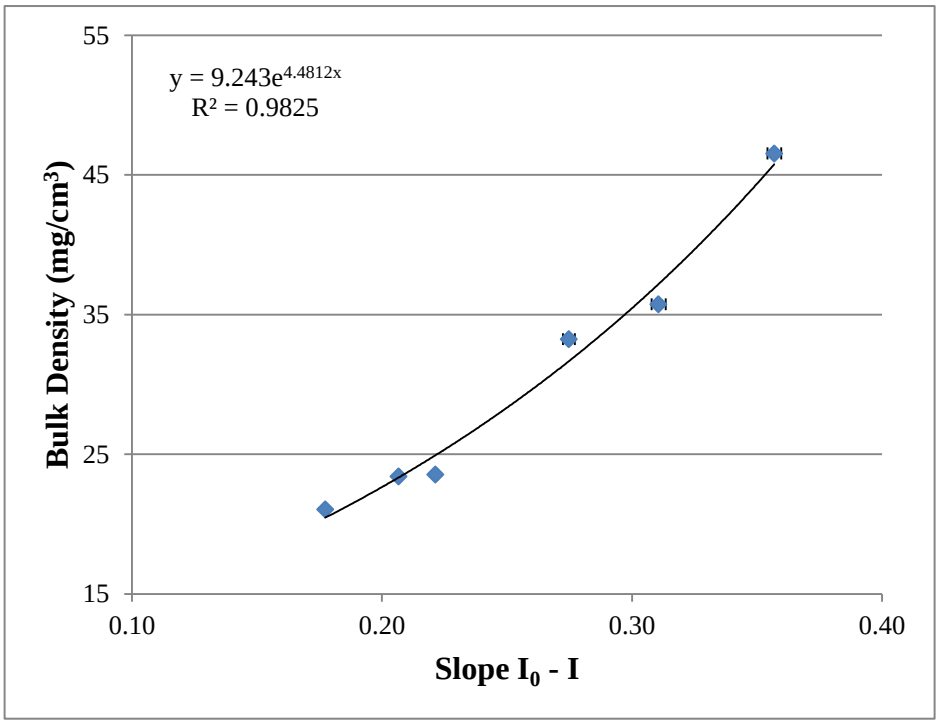

Figure 4.2 Relationship between the slopes of I_0-I curve and the bulk densities of the scaffold. Data represents the mean ± SE for five time measurements.

The slope of the I_0-I curve of the scaffolds correlated positively and exponentially with the bulk density of the scaffolds with a high correlation coefficient (r^2) of 0.9825 (Figure 4.2). Based on these relationships, the following regression curves were obtained and were utilized as calibration curves of a type I collagen scaffold for this optical device as:

$$BD = 9.243e^{4.4812S} \quad (4.1)$$

where BD is bulk density of the scaffold (mg/cm^3) and S is the slope of the I_0-I curve.

After measuring the bulk density, dried scaffolds were measured for their Calcium content by the colorimetric quantitative method (conventional method), the result is shown in table 4.3.

Table 4.3 The Calcium contents of scaffold.

Scaffolds	**Number 1**	**Number 2**	**Number 3**	**Number 4**	**Number 5**	**Number 6**
Bulk Volume (cm^3)	0.722	0.722	0.722	0.722	0.722	0.722
Calcium (mg)	0.88	1.60	1.90	2.97	4.41	7.37
Calcium Content (mg/cm^3)	**1.22**	**2.21**	**2.62**	**4.11**	**6.10**	**10.2**
SE	0.0002	0.0008	0.0008	0.0005	0.0009	0.0008

Table 4.2 and table 4.3 shows that hydroxyapatite-deposited scaffolds which were deposited with higher concentrations of $CaCl_2/Na_2HPO_4$ solutions and numbers of cycles had more bulk density and Calcium content than scaffolds which were deposited with a lower concentration and number of cycles, because hydroxyapatite crystals can be produced by chemical reaction between a $CaCl_2$ solution and a Na_2HPO_4 solution. Therefore, a higher concentration of solution can produce a larger number of hydroxyapatite crystals than lower concentrations of solutions. Moreover, higher numbers of deposited cycles can produce more hydroxyapatite crystals in scaffolds since hydroxyapatite deposition per cycle is limited, so a repeated cycle is necessary for a higher amount of hydroxyapatite deposition.

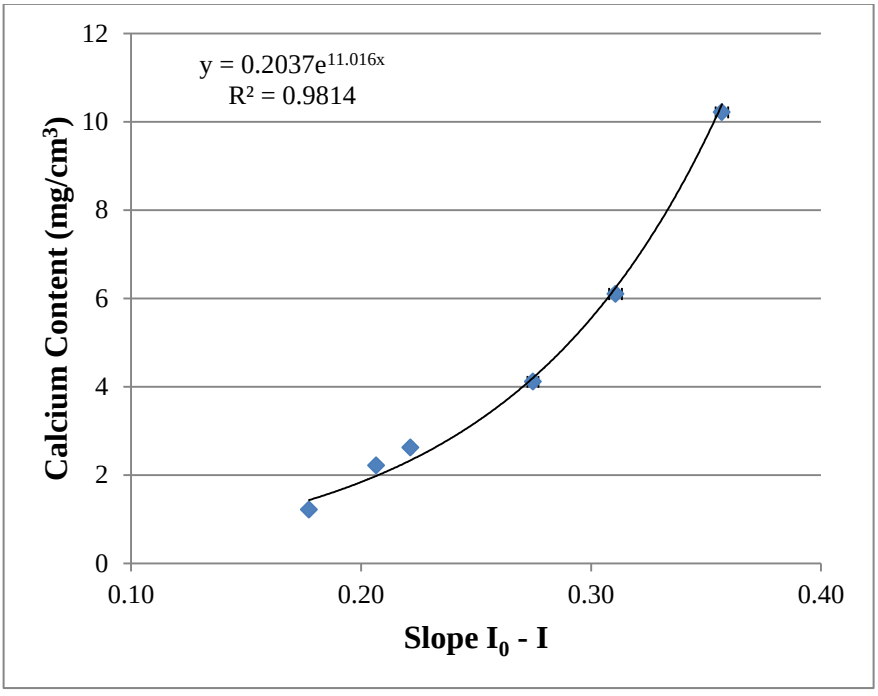

Figure 4.3 Relationship between the slopes of I_0-I curve and the Calcium contents of the scaffold. Data represents the mean ± SE for five time measurements.

The slope of the I_0-I curve of the scaffolds correlated positively and exponentially with the Calcium content of the scaffolds with a high correlation coefficient (r^2) of 0.9814 (Figure 4.3). Based on these relationships, the following regression curves were obtained and were utilized as calibration curves of a type I collagen scaffold for this optical device as:

$$CC = 0.2037e^{11.016S} \quad (4.2)$$

Where CC is the Calcium content of the scaffold (mg/cm^3) and S is the slope of the I_0-I curve.

Figure 4.2 and 4.3 shows the exponential relationships between the slope of the I_0-I curve and the bulk density or Calcium content, respectively. Therefore the relationships accorded with Kubelka–Munk's equation.

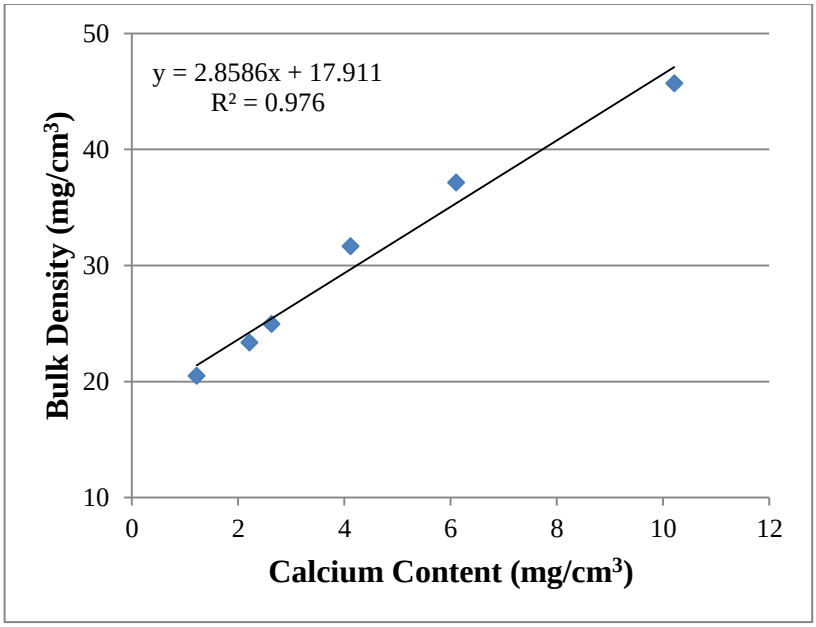

Figure 4.4 Relationship between the bulk density of the scaffold predicted by the optical system and Calcium content measured by the colorimetric quantitative method.

Figure 4.4 shows that the Calcium content of the scaffolds measured by the colorimetric quantitative method correlated linearly with the bulk density of the bone predicted by the non-destructive optical monitoring device with a high correlation coefficient (r^2) of 0.976, suggesting the reliability of the optical monitoring device.

In the past, only destructive ways such as the colorimetric quantitative method, histochemistry by Alzarin red, Fourier transform infrared (FTIR), von Kossa staining method, flame atomic absorption spectrometry, and X-ray diffraction were available and employed to evaluate the calcification response in vitro. With these destructive methods, in order to investigate accurate changes in calcification response over the long-term in the culture period, many samples of tissue-engineered bone and time for investigation must be prepared. In contrast, with a non-destructive method such has been used only for two-

dimensional culture studies, mineralized nodules on the surface of a culture plate are counted by with microscopic digital image analyzer. However, this method is not appropriate for the detection of calcification in a three-dimensional cell culture because visible light cannot penetrate a three-dimensional matrix because of the reflection and scattering on the top surface of the scaffold. As a result, a non-destructive optical monitoring device not only gives a more time- and work-saving investigation, but also suggests the potency of this system for long term monitoring.

4.2 Calcification Response of Tissue-Engineered Bone under Mechanical Stimulation

Sinusoidal mechanical loading was applied to the tissue-engineered bones at 0.5, 1.0, 1.5, 2.0 and 2.5 Hz for 3 minutes per day for 42 consecutive days using a mechanical stimulator. A non-destructive optical monitoring device was used for the detection of the calcification response of the tissue-engineered bone once a day. The results of bulk density and Calcium content observation using an optical monitoring device are shown in figure 4.5 and 4.6, respectively.

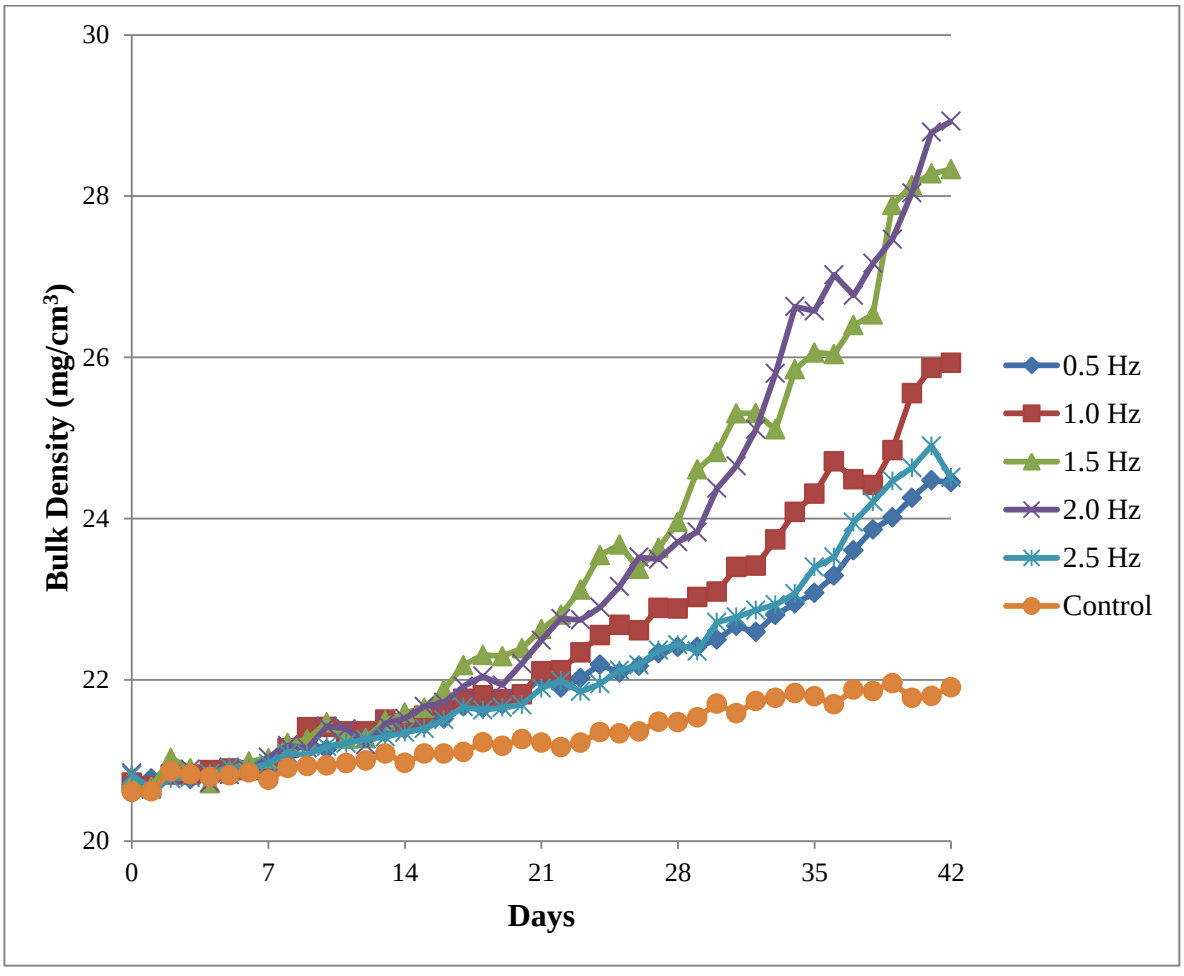

Figure 4.5 Change in the bulk density of tissue-engineered bones over time in culture.

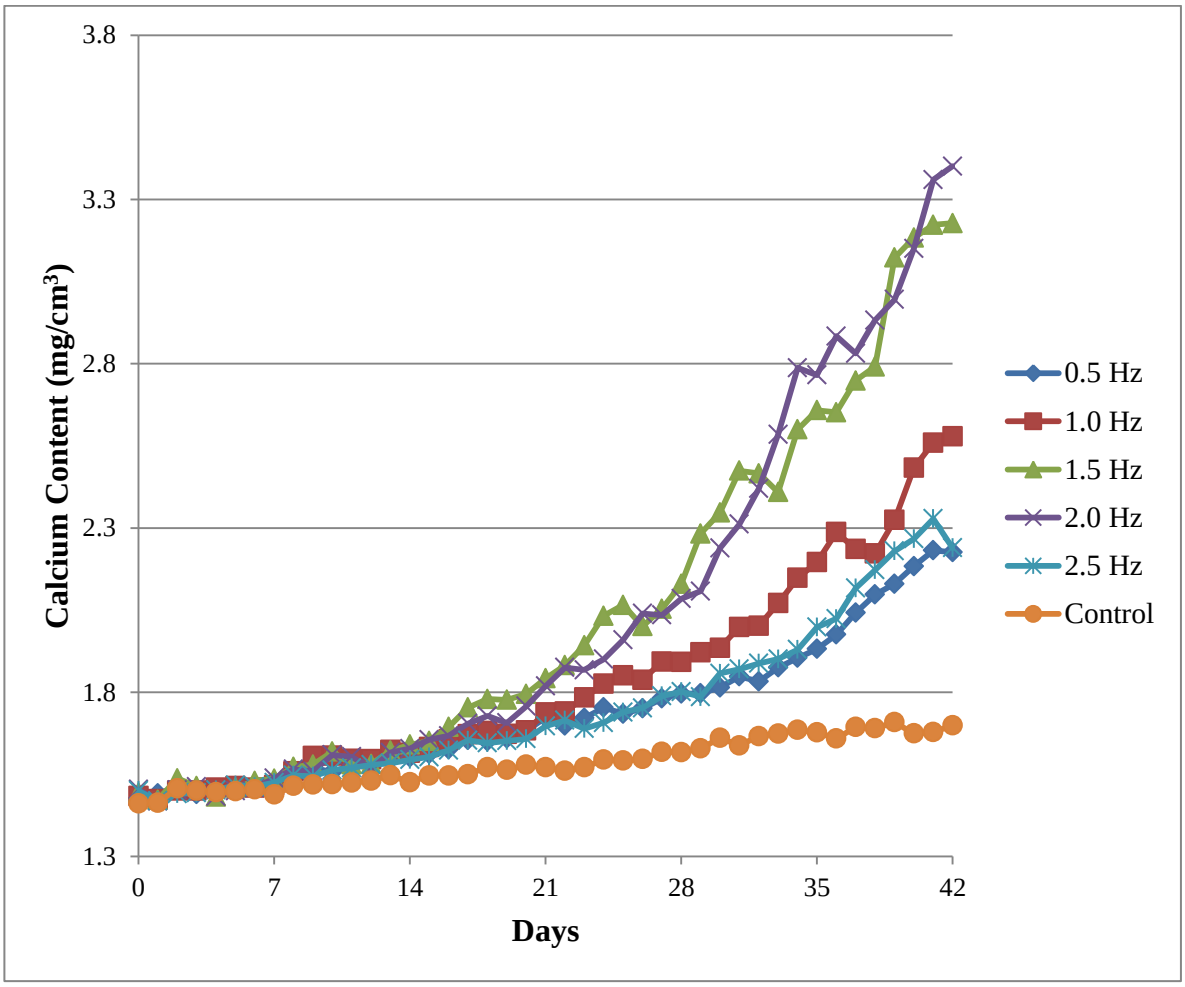

Figure 4.6 Change in the Calcium content of tissue-engineered bones over time in culture.

On day 42 of non-stimulated constructs (control), the Calcium content was 1.19-fold higher than its initial measurement on day 0. This means that bone cells which are cultured in an osteogenic differentiation medium without stimulate loading have a little of hydroxyapatite formation and production to the bone matrix. On the other hand, the degree of calcification started to increase in the stimulated constructs after day 8. On day 42, the calcium content in the stimulated constructs at 0.5, 1.0, 1.5, 2.0 and 2.5 Hz was 1.32, 1.52, 1.90, 2.00 and 1.32-fold, respectively, higher than that of the control constructs.

Application of a mechanical load to a tissue-engineered bone results in the stimulation of bone cells by two types of mechanical stimuli: construct strain and fluid flow from the culture medium. These stimuli mimic the mechanical environment under mechanical loading. Bone cells are exposed to fluid flow through canaliculi and lacunae in the bone matrix that are strained by the loading. This event is called strain-induced fluid flow (SIFF). When fluid flows in this construct, fluid shear stress occurs and acts on the bone cells. Fluid shear stress has been reported to have a strong effect on osteoblastic activation in vitro. Therefore, it could be considered that fluid shear plays an important role in the promotion of calcification by mechanical loading cooperating with construct strain.

As a result, a mechanical stimulation with higher frequency occurs with increased fluid flow and fluid shear stress in a tissue-engineered bone. In the case of stimulation at 0.5 and 1.0 Hz, fluid shear stress which was happens is low and not sufficient to activate an osteogenic response. However, fluid shear stress which occurs from stimulated condition at 1.5 and 2.0 Hz is suitable for osteoblastic activation of the osteogenesis process. Therefore, the bulk density and Calcium content in these conditions are the highest in this experiment. Nevertheless, the bulk density and Calcium content of stimulated constructs at 2.5 Hz are low. It might be that fluid shear stress is very high and not proper for ossification.

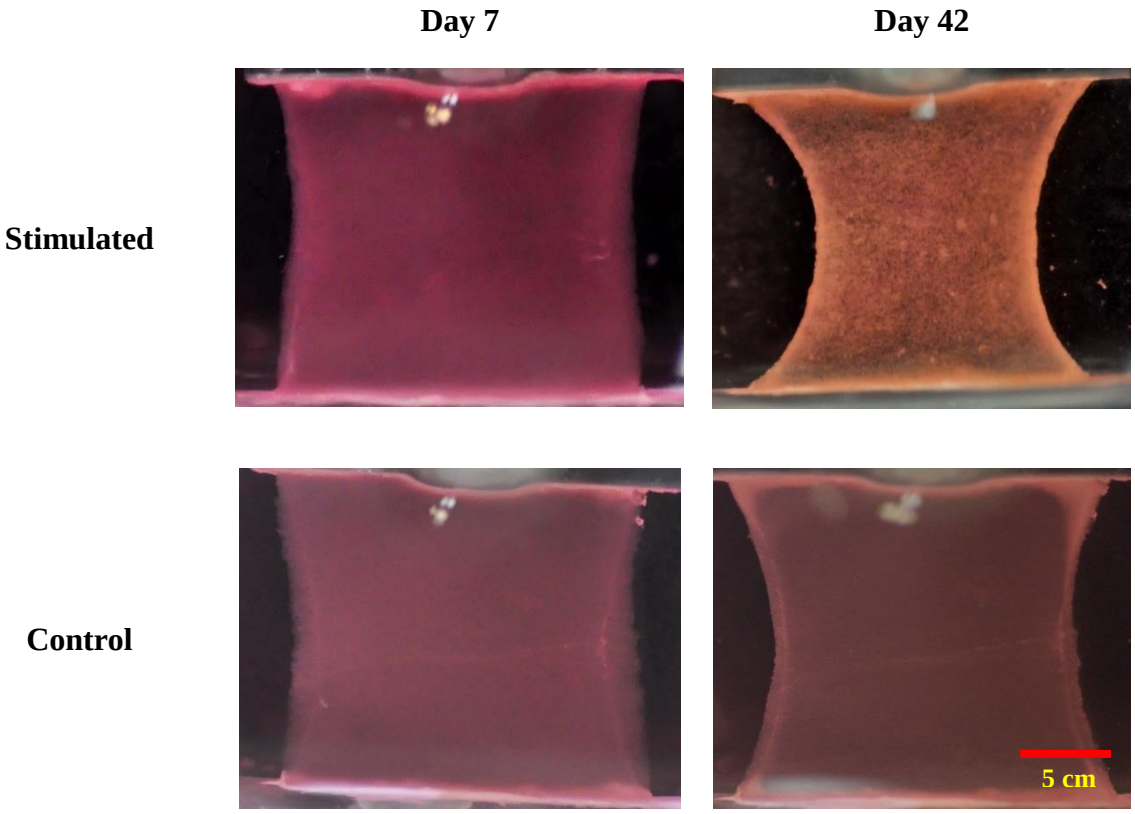

Figure 4.7 Close-up photographic images of the top view of constructs on days 7 and 42, showing the change in the appearance of the control and stimulated tissue-engineered bones over time in culture.

Figure 4.7 shows typical close-up photographic images of the tissue-engineered bones on days 7 and 42. On day 7, there was no significant difference between the control and stimulated constructs and there was no obvious calcified area in any construct. On day 42, the stimulated construct was spotted with white turbid areas that represent calcification. In contrast, the control construct also had white turbid areas at the edge only. It proved that fluid flow from mechanical stimulation not only activates the osteogenesis process but also transfers nutrients and waste products which affect the cell viability at the center of the construct.

4.3 Validation of Non-Destructive Optical Monitoring Device

On day 42, Tissue-engineered bones were measured for their Calcium content using the colorimetric quantitative method (conventional method). The Calcium content by colorimetric quantitative method was compared with the Calcium content predicted by a non-destructive optical monitoring device, the error of Calcium content was calculated with the following equation (Figure 4.8):

$$\frac{|CC\ from\ Colorimetric\ method - CC\ from\ optical\ monitoring\ device|}{CC\ from\ Colorimetric\ method} \times 100\% \qquad (4.3)$$

Where CC represents Calcium content of the tissue-engineered bone.

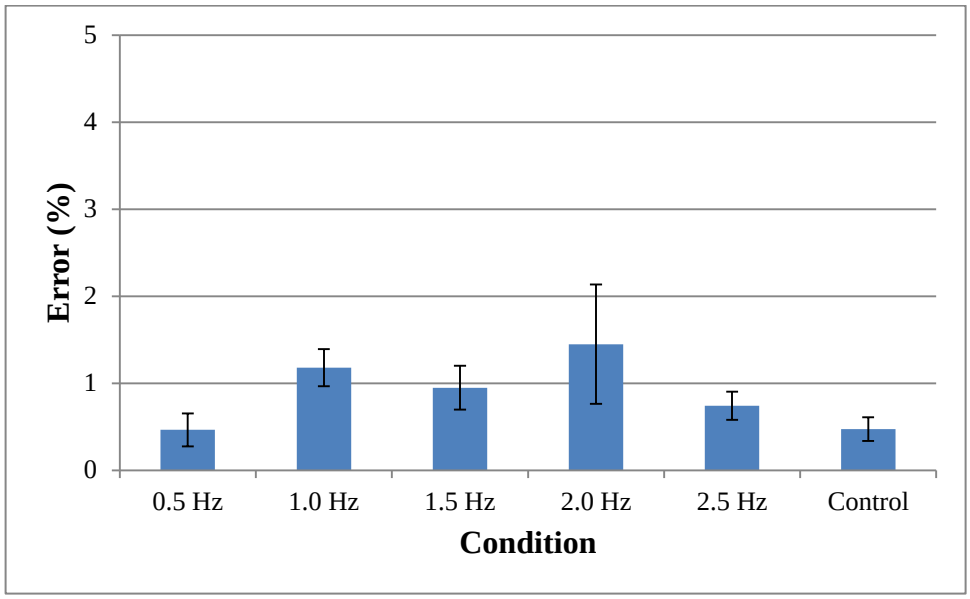

Figure 4.8 The percent error of Calcium content of tissue-engineered bone. Data represents the mean ± SE for three time measurements.

From figure 4.8, the percent error from optical measurement in every condition of tissue culture is less than 5 %. It indicates a superior reliability of the non-destructive optical monitoring device.

4.4 Cell Viability by DNA Assay

Cell viability in tissue-engineered bone was presented by the number of DNA. On day 42, the tissue-engineered bones were measured for the number of DNA by fluorescence measurement (Figure 4.9). MC3T3-E1 cells can proliferation from 1 x 10^6 cells on day 0 under all culturing conditions. The control construct had a higher number of DNA than the stimulated construct, and the stimulated construct at 2.5 Hz had the lowest number of DNA. So mechanical loading in higher frequency which has a high velocity of fluid flow and fluid shear stress, indicated affects to cell proliferation.

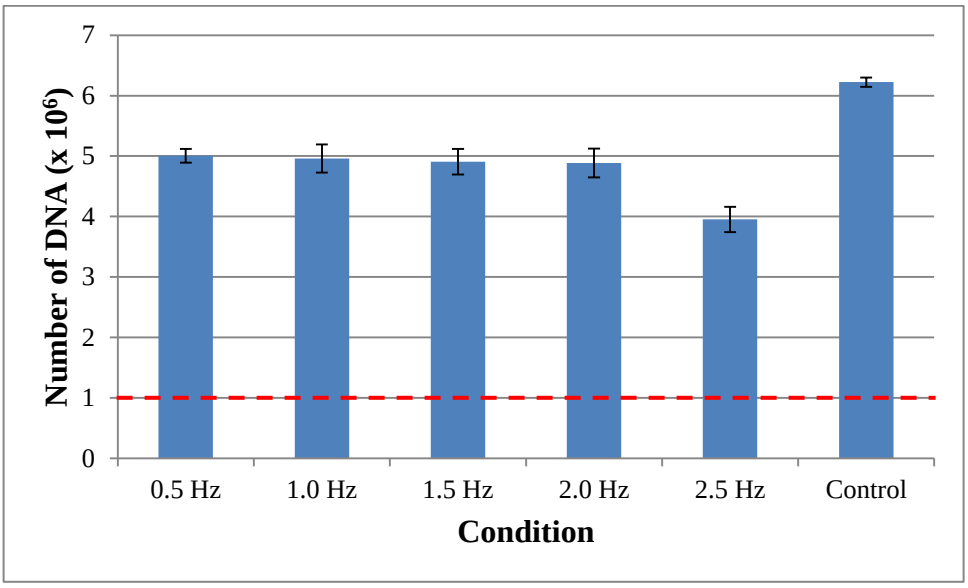

Figure 4.9 The number of DNA from tissue-engineered bone on day 42, dash line represents the initial number of MC3T3-E1 cells on day 0. Data represents the mean ± SE for three time measurements.

4.5 Scanning Electron Microscope (SEM) and Energy Dispersive Spectroscopy (EDS) Analysis

On day 42, the tissue-engineered bones were prepared for SEM observation and EDS analysis. The top surface of tissue-engineered bone (Figure 4.10 – 4.11) had a higher amount of cell density than the bottom surface (Figure 4.12 – 4.13) and middle region (Figure 4.14 – 4.16). The tissue-engineered bones were made by placing MC3T3-E1 cells that were suspended in a culture medium onto the upper surface of type I collagen scaffolds. The cells drop down into the deeper side of the scaffolds by gravity, but mostly cells were trapped by the fibril network of collagen in the upper region of the scaffolds, resulting in a higher cell density.

Figure 4.10 – 4.16 show the heterogeneous calcification in many regions which are likely to be caused by site-dependent differences in microstructure of the scaffolds and the local cell density, both of which modulate the magnitude of fluid shear stress applied to the bone cells which would affect the osteogenesis process. Therefore, improvements in the cell seeding method are required to guarantee the homogeneous distribution of calcification in a tissue-engineered bone.

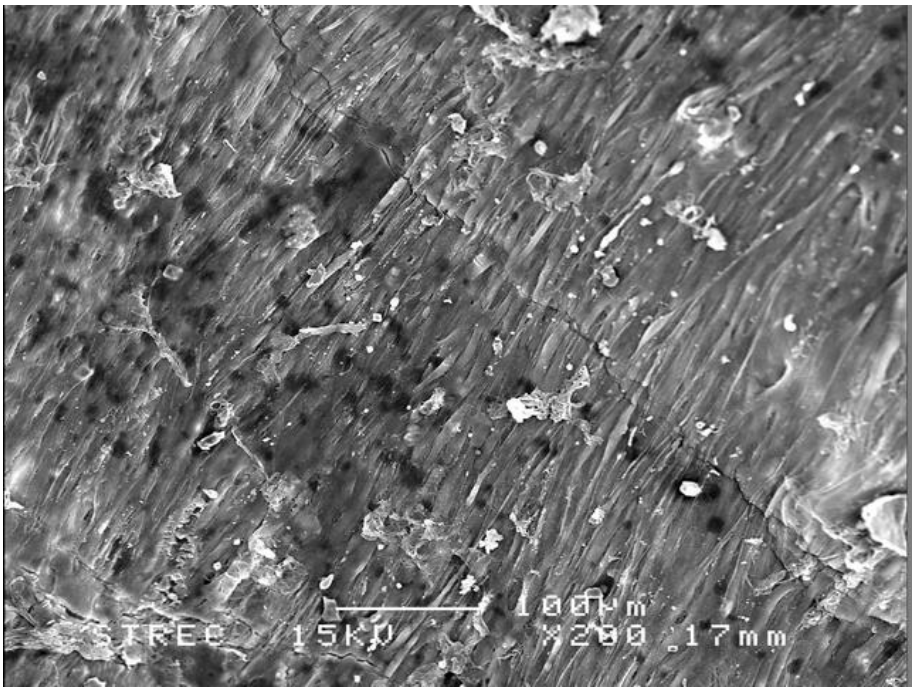

Figure 4.10 SEM observation of bone cells on the top surface of the stimulated construct.

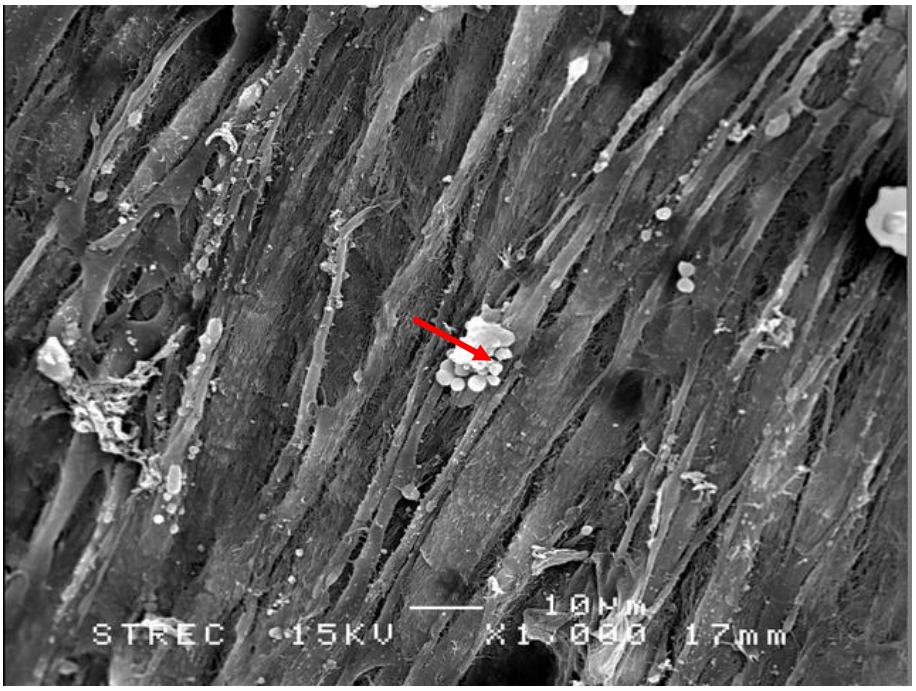

Figure 4.11 SEM observation of bone cells on the top surface of the stimulated construct, the arrow points to the Calcium crystals.

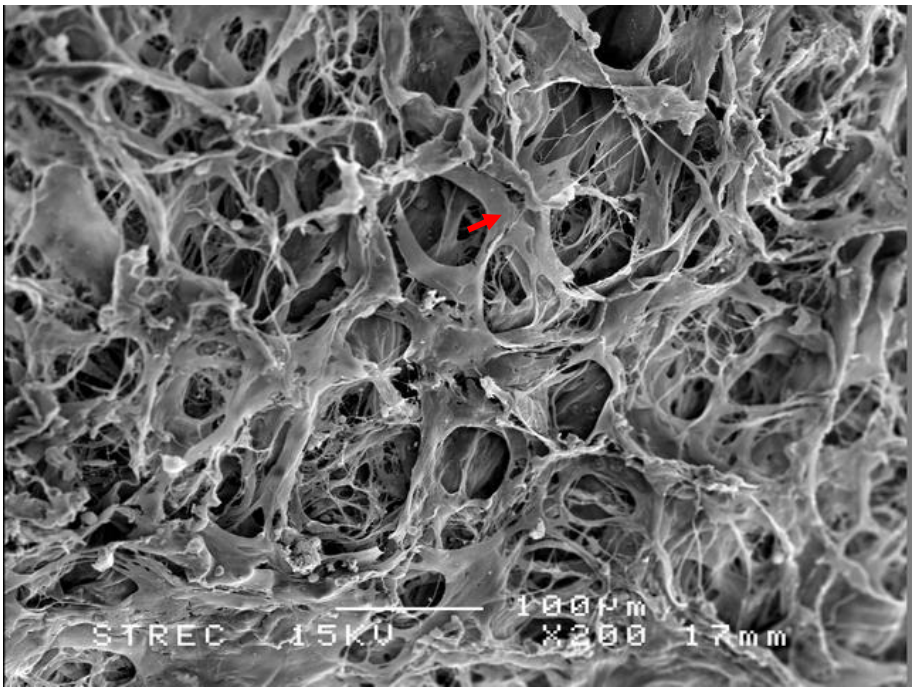

Figure 4.12 SEM observation of bone cells on the bottom surface of the stimulated construct, the arrow points to the osteoblast.

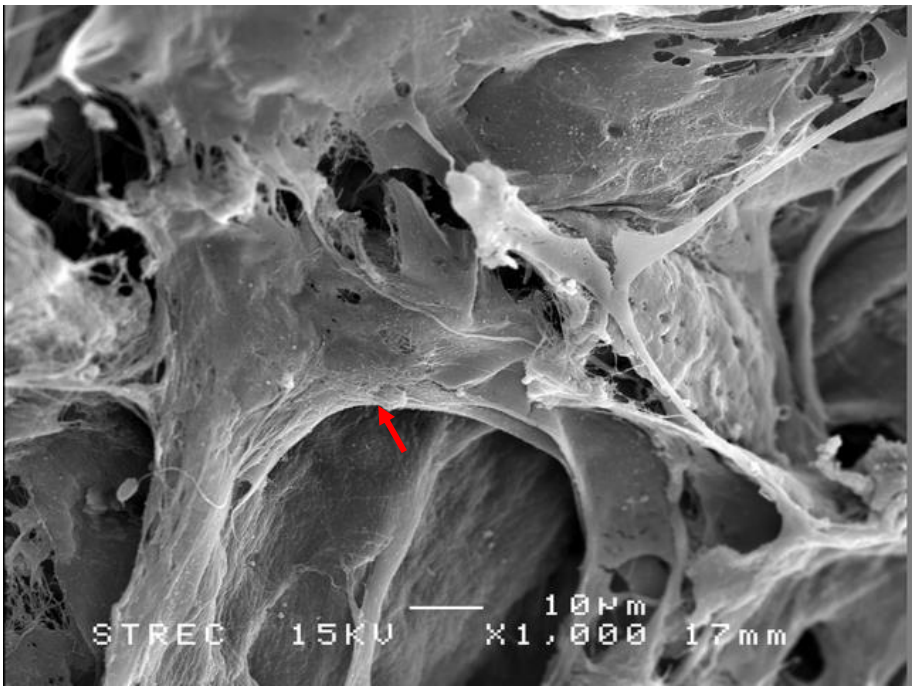

Figure 4.13 SEM observation of bone cells on the bottom surface of the stimulated construct, the arrow points to the osteoblast.

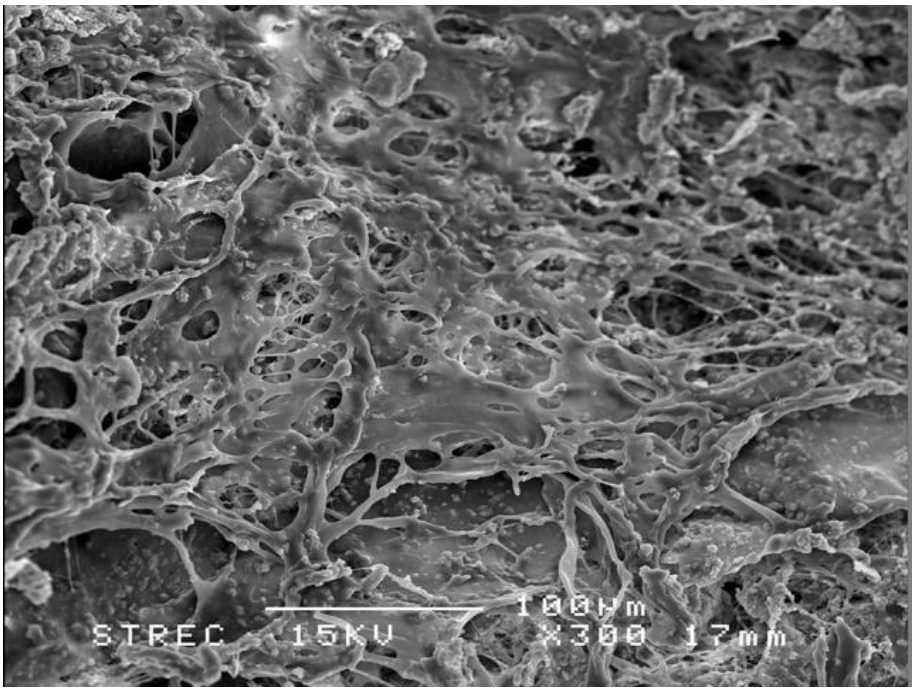

Figure 4.14 SEM observation of bone cells in the middle region of the stimulated construct.

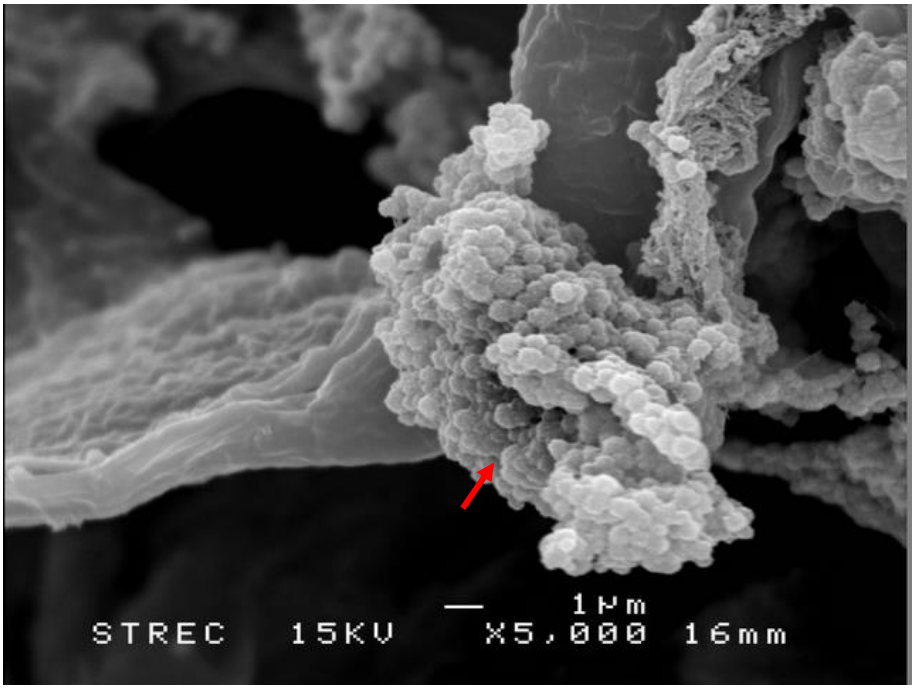

Figure 4.15 SEM observation of bone cells in the middle region of the stimulated construct, the arrow points to the Calcium crystals attached to an osteoblast.

Figure 4.16 SEM observation of bone cells with calcium crystals in the middle region of the stimulated construct.

Energy Dispersive Spectroscopy (EDS) was used for quantifying the elements of the selected area from an SEM image. On the type I collagen scaffold without MC3T3-E1 cells (Figure 4.17), there is no energy of Calcium peak in an EDS spectrum (Figure 4.18). On the tissue-engineered bone in a Calcium crystal area, has energy of Calcium peaks in EDS spectrums (Figure 4.20, 4.22, 4.24), but in an MC3T3-E1 cell area, no energy of Calcium peak is in the EDS spectrum (Figure 4.25) are indicated. From these results, crystals which are shown in SEM images, are proven by EDS spectrums to be Calcium crystals.

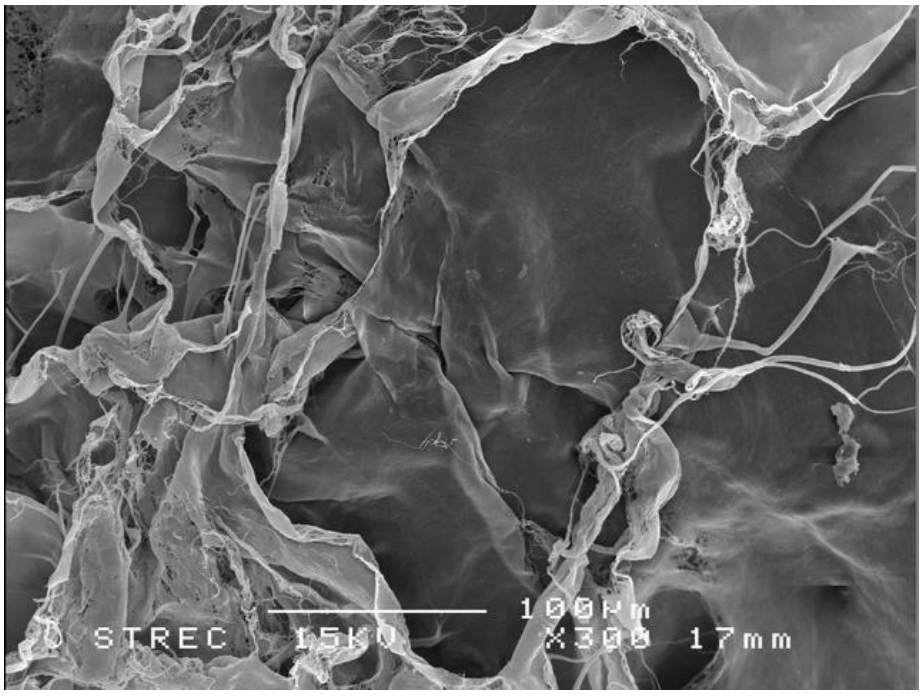

Figure 4.17 SEM observation of type I collagen scaffold without cells.

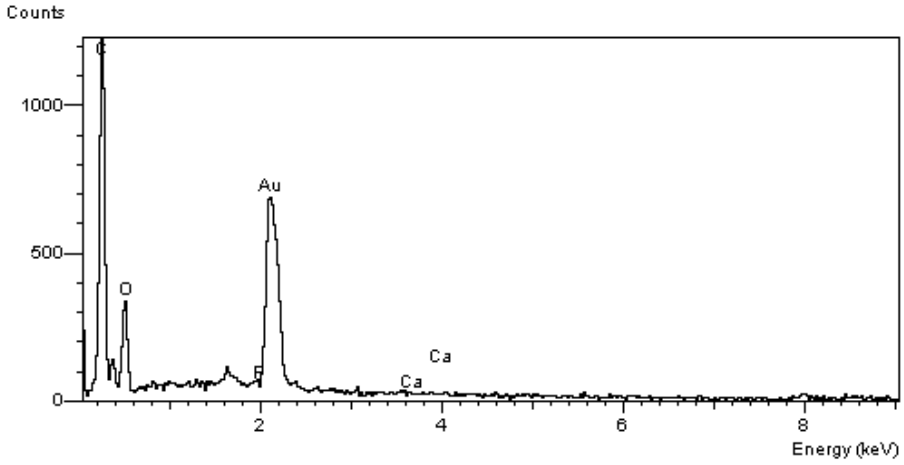

Figure 4.18 EDS spectrum of SEM image from figure 4.17.

Figure 4.19 SEM observation of bone cells with Calcium crystals in the middle region of the stimulated construct.

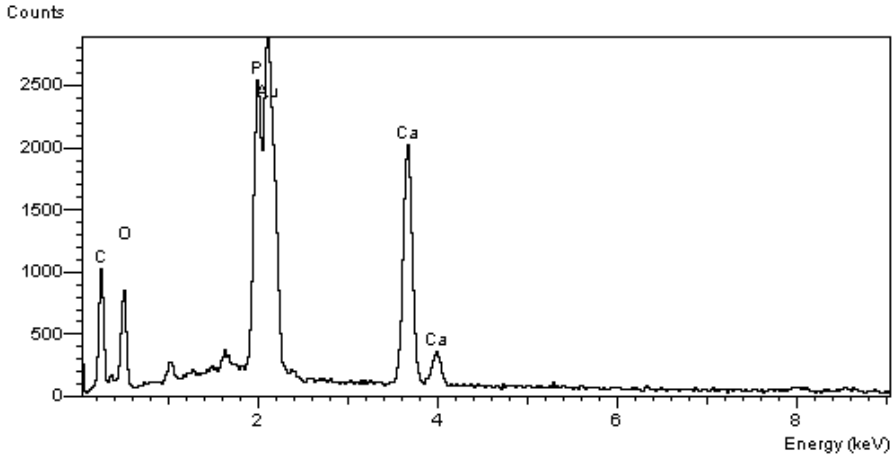

Figure 4.20 EDS spectrum of SEM image from figure 4.19 (circle area)

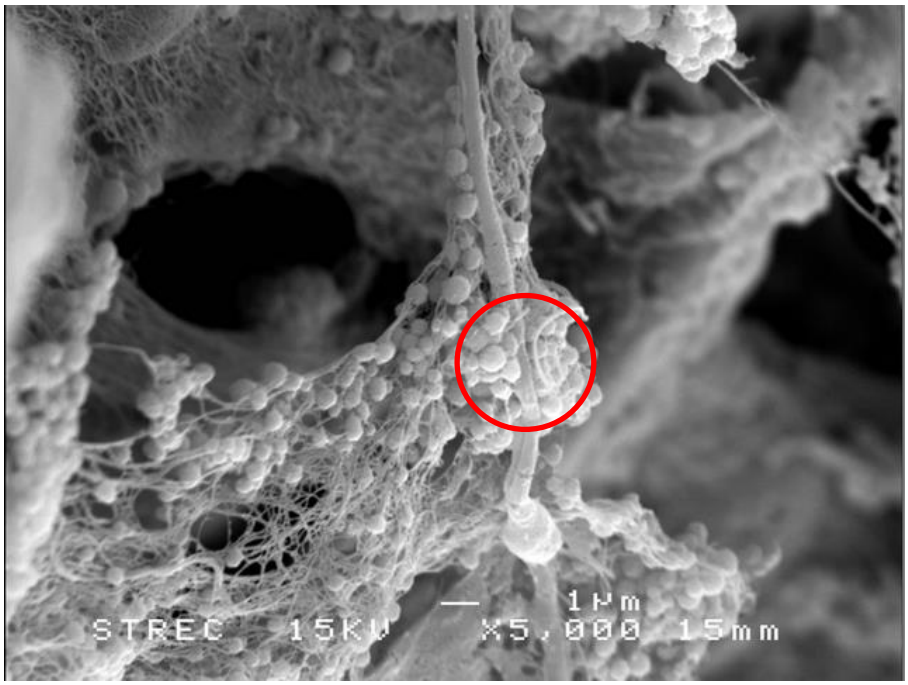

Figure 4.21 SEM observation of bone cells with Calcium crystals in the middle region of the stimulated construct.

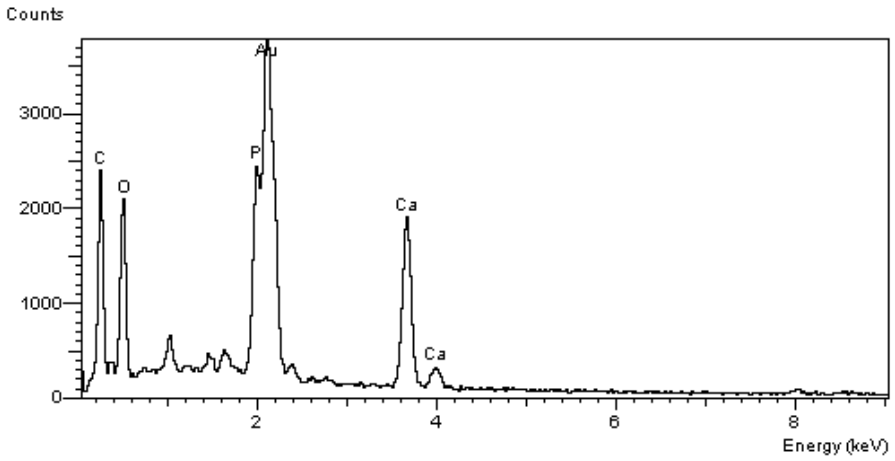

Figure 4.22 EDS spectrum of SEM image from figure 4.21 (circle area)

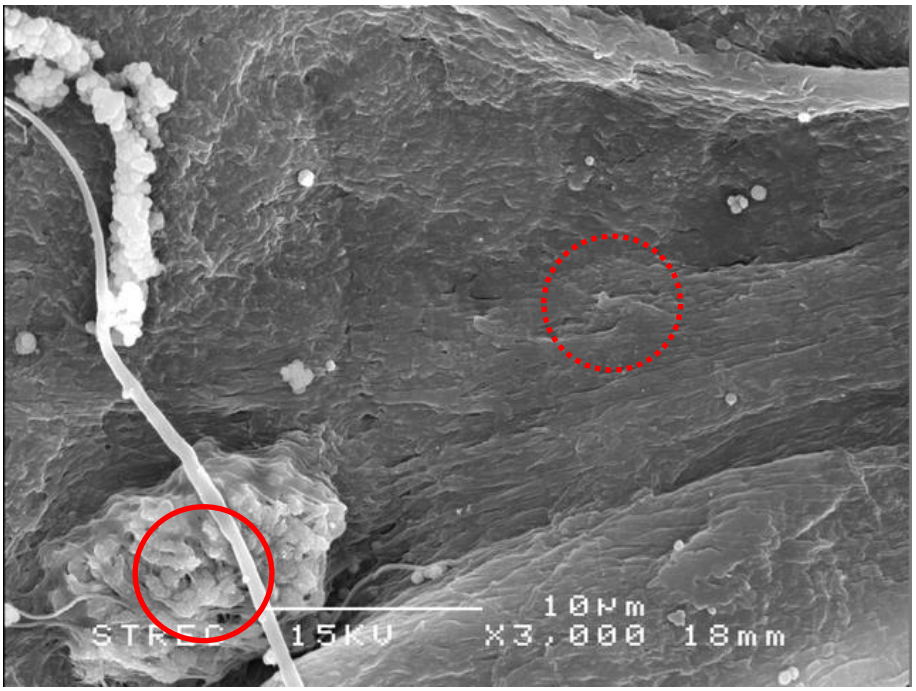

Figure 4.23 SEM observation of bone cells with Calcium crystals in the middle region of the stimulated construct.

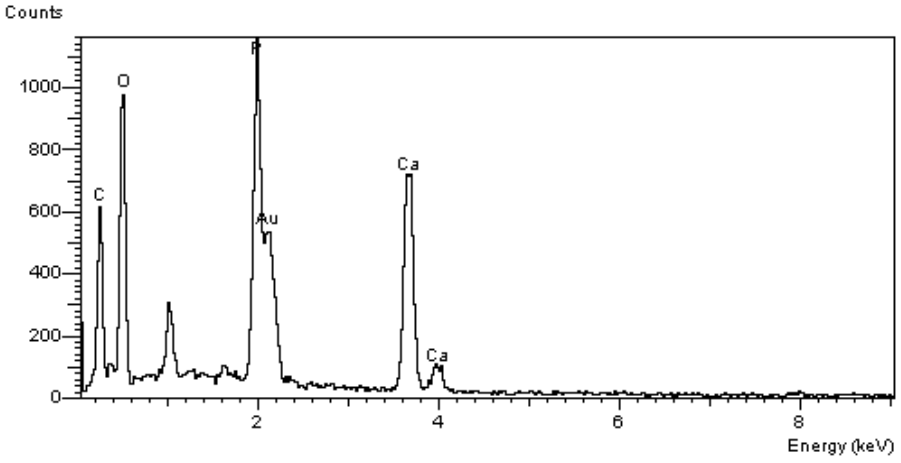

Figure 4.24 EDS spectrum of SEM image from figure 4.23 (circle area).

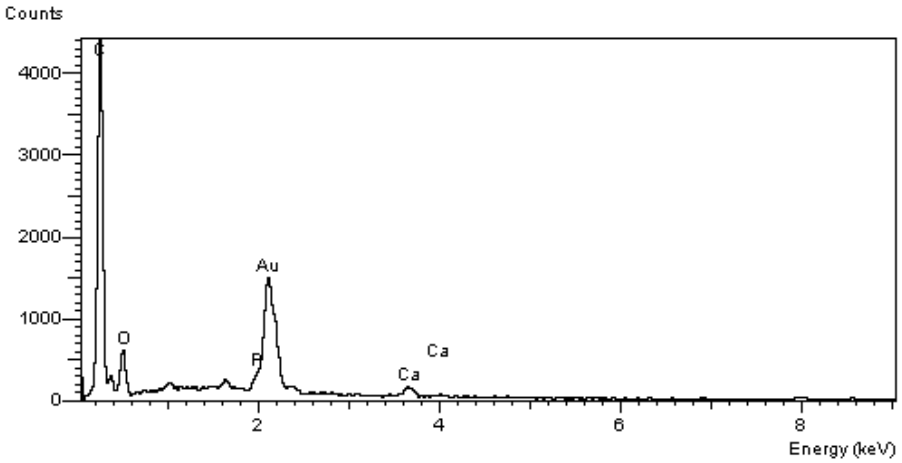

Figure 4.25 EDS spectrum of SEM image from figure 4.23 (dashed circle area).

4.6 Verification of Hydroxyapatite Crystals by X-Ray Diffraction (XRD)

In order to identify the Calcium crystalline phases, on day 42, tissue-engineered bone was dried and prepared for the x-ray diffraction analysis. The diffraction peaks were verified relative to the standard of hydroxyapatite crystals by referring to JCPDS files (reference number 74-0565).

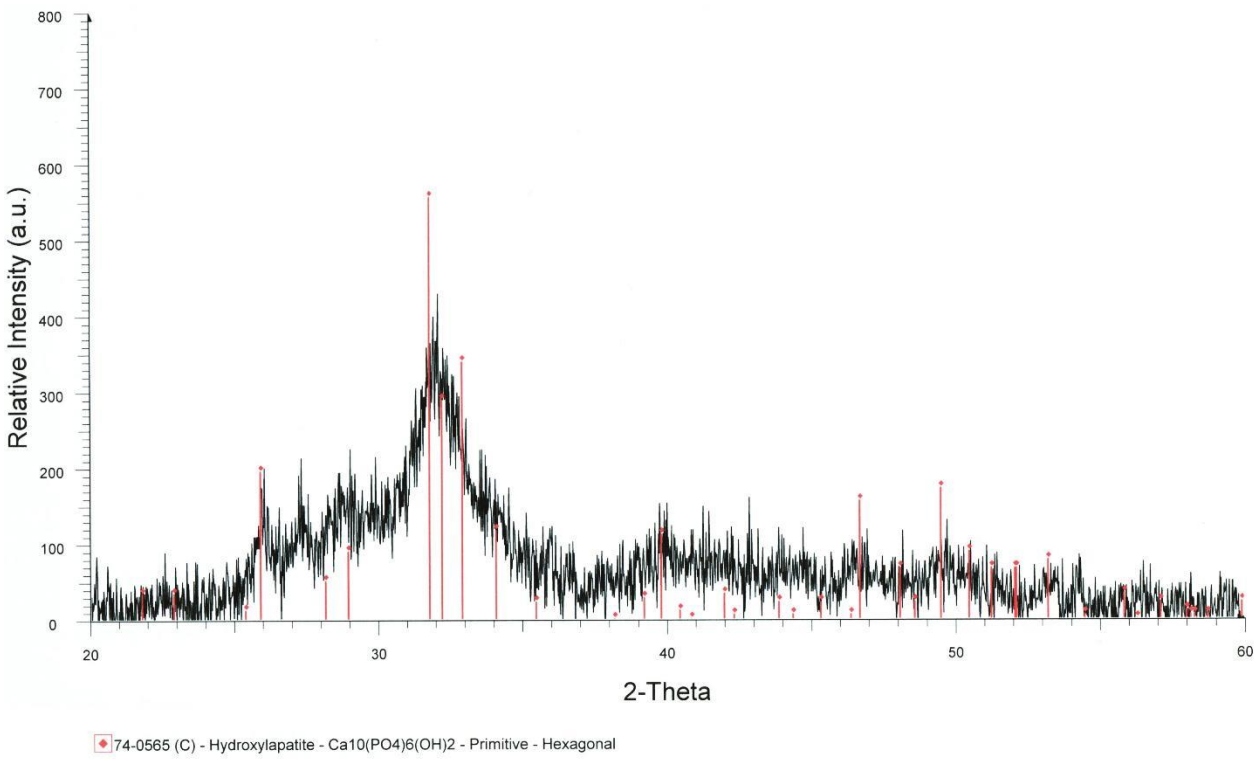

Figure 4.26 X- ray diffraction patterns for the stimulated construct compared with the hydroxyapatite standard peaks from the JCPDS file.

From figure 4.26, X-ray diffraction of tissue-engineered bone revealed characteristic peaks corresponding to the hydroxyapatite standard file. The broad diffraction peaks for hydroxyapatite were indicative of nano-sized Calcium crystallites, similar to that measured for human bone mineral.

CHAPTER 5 CONCLUSIONS

5.1 Conclusions

Many types of intervention such as physical or biochemical stimulation have been studied and shown a potential to promote in vitro calcification of tissue-engineered bone. Optimization of stimulation conditions is important in order to achieve successful promotion of the calcification. However, it is time-consuming work with repetition of examinations in every possible condition. Moreover, since only destructive measurement methods are available currently for three-dimensional osteoblastic calcification, an enormous number of samples have to be prepared. A non-destructive optical monitoring device was therefore fabricated to evaluate calcification of tissue-engineered bone in vitro. This device was calibrated with hydroxyapatite-deposited scaffolds, and the calibration results correlated with Kubelka–Munk's equation with a high correlation coefficient (r^2) of regression curves, suggesting the reliability of the optical monitoring device. The results not only give a more time- and work-saving investigation but also suggest the effectiveness of this device for long term monitoring. This device could contribute not only to the advance of bone tissue engineering applications, but also to basic research in orthopedic technology.

A mechanical stimulator was fabricated for encouraging the calcification response of the bone cells. This stimulator using a piezoelectric actuator can makes it possible to produce any physiological strain profile with a high speed frequency for stimulated tissue-engineered bone in vitro. This device produced a mechanical strain to the construct for induced fluid flow inside the tissue-engineered bone. Fluid shear stress which occurred from fluid flow is a signal to activate the osteogenesis process of bone cells. In this study, in vitro osteogenic stimulation was tested by applying the sinusoidal loading frequencies at 0.5 – 2.5 Hz for 42 days to a tissue-engineered bone. A non-destructive optical monitoring device showed that sinusoidal loading frequencies at 1.5 – 2.0 Hz provided the best stimulated condition for increasing the degree of calcification of the construct over the culture period. From the results, it was concluded that the sinusoidal loading frequency could function as a potent enhancer of the bone formation process in vitro, suggesting the usefulness of mechanical loading in bone tissue engineering applications.

5.2 Recommendations

The height of a basketball or volleyball player is very high because the impact force during their high jumping. Therefore, a jumping strain waveform with impact loading is an interesting strain profile to stimulate tissue-engineered bone.

Mesenchymal stem cells (MSCs) should be used in future experiments because MSCs have a higher potential of cell differentiation and calcification than the MC3T3-E1 cell line.

Other stimulations such as light, electromagnetic or electrical, can combine with this mechanical stimulator for a more successful calcification response.

REFERENCES

1. Bilezikian, J.P., Raisz, L.G., and Martin, T.J., 2008, **Principles of Bone Biology**, 3rd, Academic Press/Elsevier, San Diego, Calif.

2. Currey, J.D., 2002, **Bones : Structure and Mechanics**, Princeton University Press, Princeton, NJ.

3. Weiss, L., 1988, **Cell and Tissue Biology : A Textbook of Histology**, 6th, Urban & Schwarzenberg, Baltimore.

4. Cowin, S.C., 2001, **Bone Mechanics Handbook**, 2nd, CRC Press, Boca Raton, FL.

5. Miller, M.D. and Hart, J.A., 2008, **Review of Orthopaedics**, 5th, Saunders / Elsevier, Philadelphia, PA.

6. Hall, B.K., 1990, **Bone**, Telford Press, Caldwell, N.J.

7. Bourne, G.H., 1971, **The Biochemistry and Physiology of Bone**, 2d, Academic Press, New York.

8. Lowenstam, H.A. and Weiner, S., 1989, **On Biomineralization**, Oxford University Press, New York.

9. Riggs, B.L., 1993, **Prevention and Treatment of Osteoporosis : An International Symposium Held During the Xiith European Congress of Rheumatology,** Budapest, Hungary, 1991, Hogrefe & Huber, Seattle.

10. Organization., W.H., 1994, Assessment of Fracture Risk and Its Application to Screening for Postmenopausal Osteoporosis. **WHO Technical Report Series**, Geneva, Vol. 843.

11. Cooper, C. and Woolf, A.D., 2006, **Osteoporosis : Best Practice & Research Compendium**, Elsevier, Edinburgh ; New York.

12. Black, A.J., Sandison, R., and Reid, D., 2009, **Osteoporosis : The Facts**, Oxford University Press, Oxford ; New York.

13. Wise, D.L., 2000, **Biomaterials Engineering and Devices**, Humana Press, Totowa, NJ.

14. Rose, F.R.A.J. and Oreffo, R.O.C., 2002, "Bone Tissue Engineering: Hope Vs Hype", **Biochemical and Biophysical Research Communications**, Vol. 292, No. 1, pp. 1-7.

15. Laurencin, C.T. and American Academy of Orthopaedic Surgeons., 2003, **Bone Graft Substitutes**, ASTM International, W. Conshohocken, PA.

16. Petite, H., Viateau, V., Bensaid, W., Meunier, A., de Pollak, C., Bourguignon, M., Oudina, K., Sedel, L., and Guillemin, G., 2000, "Tissue-Engineered Bone Regeneration", **Nat Biotechnol**, Vol. 18, No. 9, pp. 959-963.

17. An, H.S. and Jenis, L.G., 2006, **Complications of Spine Surgery : Treatment and Prevention**, Lippincott Williams & Wilkins, Philadelphia.

18. Lieberman, J.R. and Friedlaender, G.E., 2005, **Bone Regeneration and Repair : Biology and Clinical Applications**, Humana Press, Totowa, N.J.

19. Hollinger, J.O., 2005, **Bone Tissue Engineering**, CRC Press, Boca Raton.

20. Legard, V. and Schluter, R.m., 2010, **Bone Regeneration : Growth Factors, Augmentation Procedures and Tissue Engineering Applications**, Nova Science Publishers, New York.

21. Fisher, J.P., 2006, **Tissue Engineering**, Springer : Aegean Conferences, New York, N.Y.

22. Martini, F., Timmons, M.J., and Tallitsch, R.B., 2012, **Human Anatomy**, 7th, Pearson Benjamin Cummings, Boston.

23. McKinley, M.P. and O'Loughlin, V.D., 2012, **Human Anatomy**, 3rd, McGraw-Hill, New York.

24. Shier, D., Butler, J., and Lewis, R., 2012, **Hole's Human Anatomy & Physiology**, Thirteenth, McGraw-Hill Companies, Inc., New York.

25. Greco, G.N., 2008, **Tissue Engineering Research Trends**, Nova Science Publishers, New York.

26. Suga, S., Nakahara, H., Nihon Gakujutsu Kaigi., and Kanagawa Academy of Science and Technology., 1991, **Mechanisms and Phylogeny of Mineralization in Biological Systems**, Springer-Verlag, Tokyo New York.

27. Caplan, A.I. and Goldberg, V.M., 2004, **Orthopedic Tissue Engineering : Basic Science and Practices**, Marcel Dekker ; Momenta, New York London.

28. Prockop, D.J., Phinney, D.G., and Bunnell, B.A., 2008, **Mesenchymal Stem Cells : Methods and Protocols**, Humana Press, Totowa, NJ.

29. Karsdal, M.A., Larsen, L., Engsig, M.T., Lou, H., Ferreras, M., Lochter, A., Delaisse, J.M., and Foged, N.T., 2002, "Matrix Metalloproteinase-Dependent Activation of Latent Transforming Growth Factor-Beta Controls the Conversion of Osteoblasts into Osteocytes by Blocking Osteoblast Apoptosis", **J Biol Chem**, Vol. 277, No. 46, pp. 44061-44067.

30. Basu, B., Katti, D., and Kumar, A., 2009, **Advanced Biomaterials : Fundamentals, Processing, and Applications**, John Wiley & Sons ; The American Ceramic Society, Hoboken, N.J. Westerville, Ohio.

31. Tanaka, S.M., Sun, H.B., Roeder, R.K., Burr, D.B., Turner, C.H., and Yokota, H., 2005, "Osteoblast Responses One Hour after Load-Induced Fluid Flow in a Three-Dimensional Porous Matrix", **Calcif Tissue Int**, Vol. 76, No. 4, pp. 261-271.

32. Takahashi, Y., Yamamoto, M., and Tabata, Y., 2005, "Osteogenic Differentiation of Mesenchymal Stem Cells in Biodegradable Sponges Composed of Gelatin and Beta-Tricalcium Phosphate", **Biomaterials**, Vol. 26, No. 17, pp. 3587-3596,

33. Sudo, H., Kodama, H.A., Amagai, Y., Yamamoto, S., and Kasai, S., 1983, "In Vitro Differentiation and Calcification in a New Clonal Osteogenic Cell Line Derived from Newborn Mouse Calvaria", **J Cell Biol**, Vol. 96, No. 1, pp. 191-198.

34. Antolli, P.G. and Liu, Z., 2011, **Bioreactors : Design, Properties, and Applications**, Nova Science Publishers, Hauppauge, N.Y.

35. Alleman, B.C. and Leeson, A., 1999, **Bioreactor and Ex Situ Biological Treatment Technologies**, Battelle Press, Columbus.

36. Rubin, C.T. and Lanyon, L.E., 1982, "Limb Mechanics as a Function of Speed and Gait: A Study of Functional Strains in the Radius and Tibia of Horse and Dog", **J Exp Biol**, Vol. 101, No., pp. 187-211.

37. Rubin, C.T. and Lanyon, L.E., 1984, "Regulation of Bone Formation by Applied Dynamic Loads", **J Bone Joint Surg Am**, Vol. 66, No. 3, pp. 397-402.

38. Rubin, C.T. and Lanyon, L.E., 1985, "Regulation of Bone Mass by Mechanical Strain Magnitude", **Calcif Tissue Int**, Vol. 37, No. 4, pp. 411-417.

39. Turner, C.H., Forwood, M.R., Rho, J.Y., and Yoshikawa, T., 1994, "Mechanical Loading Thresholds for Lamellar and Woven Bone Formation", **J Bone Miner Res**, Vol. 9, No. 1, pp. 87-97.

40. Lanyon, L.E. and Rubin, C.T., 1984, "Static Vs Dynamic Loads as an Influence on Bone Remodelling", **J Biomech**, Vol. 17, No. 12, pp. 897-905,

41. Turner, C.H., 1998, "Three Rules for Bone Adaptation to Mechanical Stimuli", **Bone**, Vol. 23, No. 5, pp. 399-407.

42. Claes, L.E. and Heigele, C.A., 1999, "Magnitudes of Local Stress and Strain Along Bony Surfaces Predict the Course and Type of Fracture Healing", **J Biomech**, Vol. 32, No. 3, pp. 255-266.

43. Tanaka, S.M., Li, J., Duncan, R.L., Yokota, H., Burr, D.B., and Turner, C.H., 2003, "Effects of Broad Frequency Vibration on Cultured Osteoblasts", **J Biomech**, Vol. 36, No. 1, pp. 73-80,

44. Ballas, R.G., 2007, **Piezoelectric Multilayer Beam Bending Actuators : Static and Dynamic Behavior and Aspects of Sensor Integration**, Springer, Berlin ; New York.

45. Carpi, F. and Smela, E., 2009, **Biomedical Applications of Electroactive Polymer Actuators**, John Wiley & Sons, Chichester, West Sussex.

46. Choi, S.-B. and Han, Y.-M., 2010, **Piezoelectric Actuators : Control Applications of Smart Materials**, CRC Press, Boca Raton, FL.

47. Galassi, C., 2000, **Piezoelectric Materials : Advances in Science, Technology, and Applications**, Kluwer Academic Publishers, Dordrecht ; Boston.

48. Nelson, W.G., 2010, **Piezoelectric Materials : Structure, Properties, and Applications**, Nova Science Publishers, New York.

49. Tanaka, S.M., 1999, "A New Mechanical Stimulator for Cultured Bone Cells Using Piezoelectric Actuator", **J Biomech**, Vol. 32, No. 4, pp. 427-430,

50. Christy, A.A., Ozaki, Y., and Gregoriou, V.G., 2001, **Modern Fourier Transform Infrared Spectroscopy**, Elsevier, Amsterdam ; New York.

51. Malley, D.F., PDK Projects Inc., and Winnipeg (Man.), 2000, **Evaluating the Use of near-Infrared Spectroscopy for the Analysis of Biosolids Constituents**, Water Environment Research Foundation, Alexandria, VA.

52. Barth, A. and Haris, P.I., 2009, **Biological and Biomedical Infrared Spectroscopy**, IOS Press, Amsterdam ; Washington, DC.

53. Shigeo. M. TANAKA, M.K., Ken-ich YAMAKOSHI, 2008, "Non-Destructive Optical Monitoring for Calcification of Tissue-Engineered Bone in Vitro", **Journal of Biomechanical Science and Engineering**, Vol. 3, No. 3, pp. 332-342.

54. Dawson, J.A., Davis, P.G., O'Donnell, C.P., Kamlin, C.O., and Morley, C.J., 2007, "Pulse Oximetry for Monitoring Infants in the Delivery Room: A Review", **Arch Dis Child Fetal Neonatal Ed**, Vol. 92, No. 1, pp. F4-7.

55. Maruo, K., Oota, T., Tsurugi, M., Nakagawa, T., Arimoto, H., Hayakawa, M., Tamura, M., Ozaki, Y., and Yamada, Y., 2006, "Noninvasive near-Infrared Blood Glucose Monitoring Using a Calibration Model Built by a Numerical Simulation Method: Trial Application to Patients in an Intensive Care Unit", **Appl Spectrosc**, Vol. 60, No. 12, pp. 1423-1431.

56. Tanaka, G., Sawada, Y., and Yamakoshi, K., 2000, "Beat-by-Beat Double-Normalized Pulse Volume Derived Photoplethysmographically as a New Quantitative Index of Finger Vascular Tone in Humans", **Eur J Appl Physiol**, Vol. 81, No. 1-2, pp. 148-154.

57. Ugryumova, N., Matcher, S.J., and Attenburrow, D.P., 2004, "Measurement of Bone Mineral Density Via Light Scattering", **Phys Med Biol**, Vol. 49, No. 3, pp. 469-483.

APPENDIX A

STANDARD CURVES

A.1 Calcium Content Standard Curve

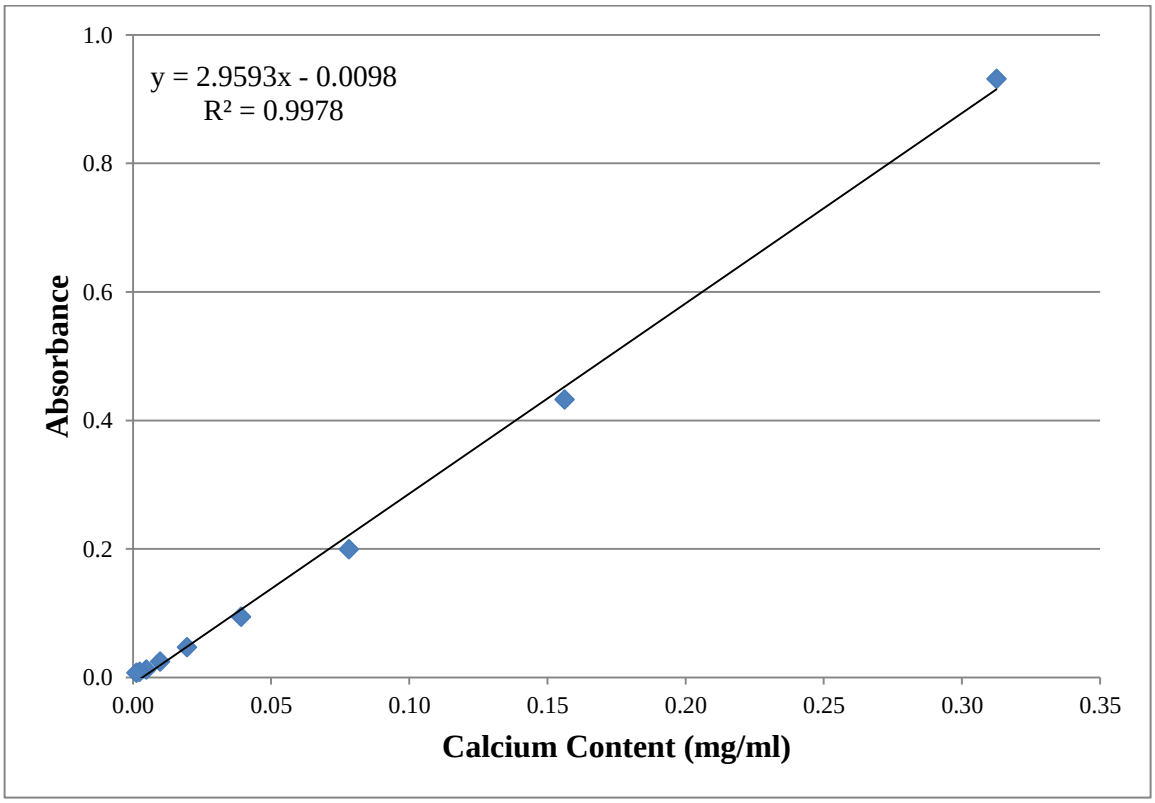

Figure A.1 Calcium content standard curve

A.2 DNA Standard Curve

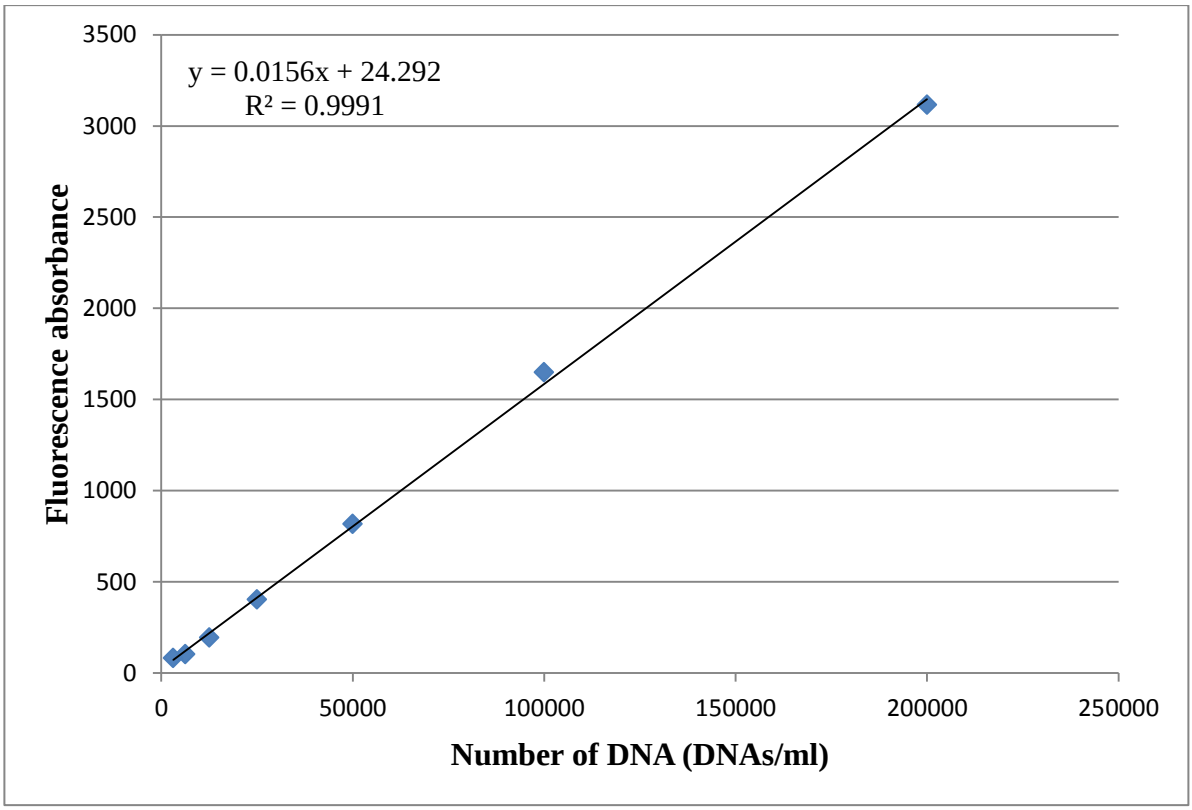

Figure A.2 DNA standard curve

APPENDIX B

NON-DESTRUCTIVE OPTICAL MONITORING DEVICE DRAWINGS

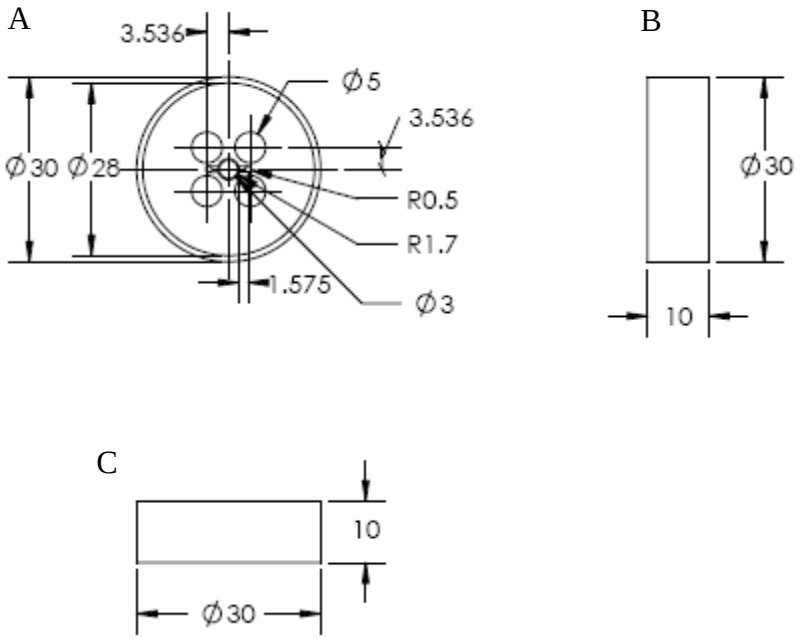

Figure B.1 An acrylic holder drawing in mm scale, (A) top view, (B) side view and (C) front view.

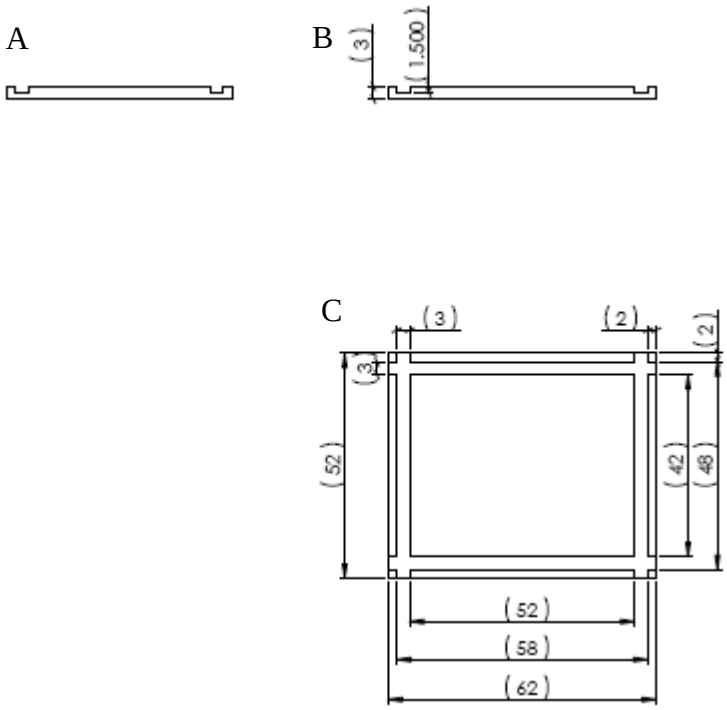

Figure B.2 An acrylic box no.1 drawing in mm scale, (A) side view, (B) front view and (C) top view.

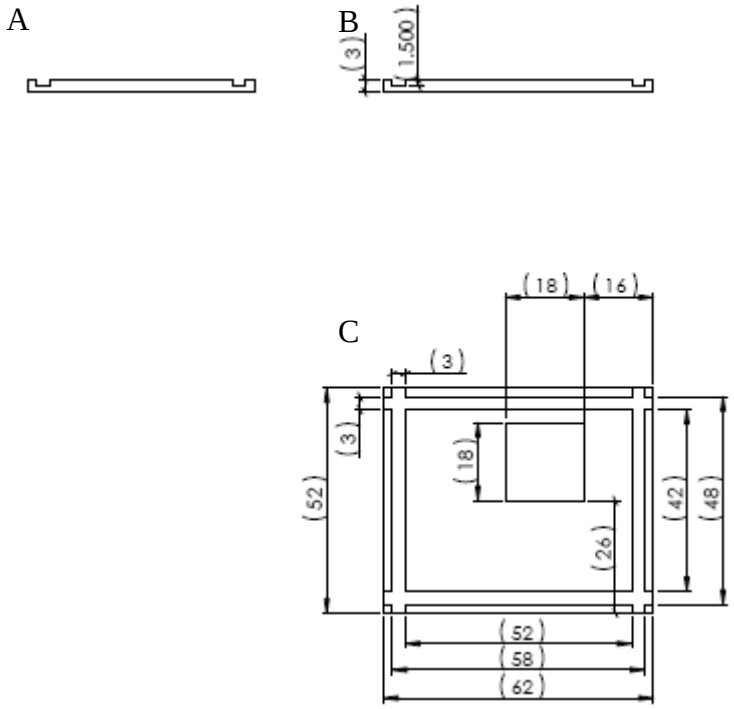

Figure B.3 An acrylic box no.2 drawing in mm scale, (A) side view, (B) front view and (C) top view.

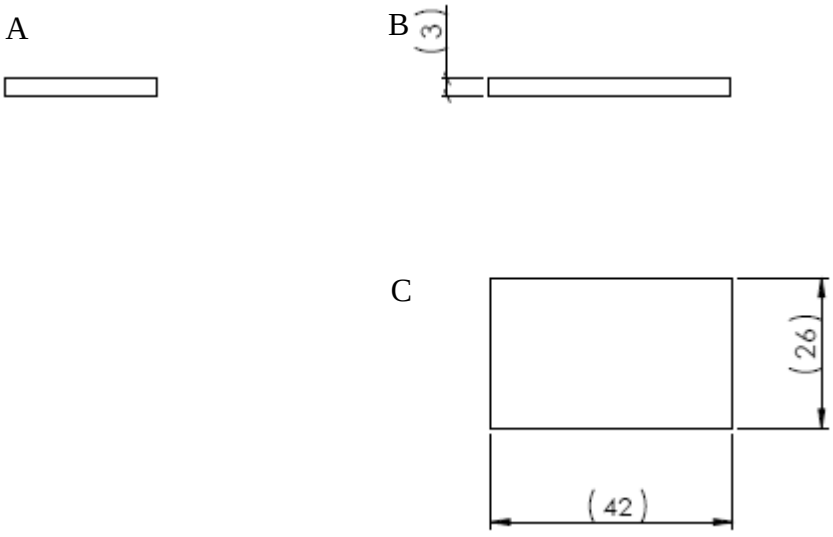

Figure B.4 An acrylic box no.3 drawing in mm scale, (A) side view, (B) front view and (C) top view.

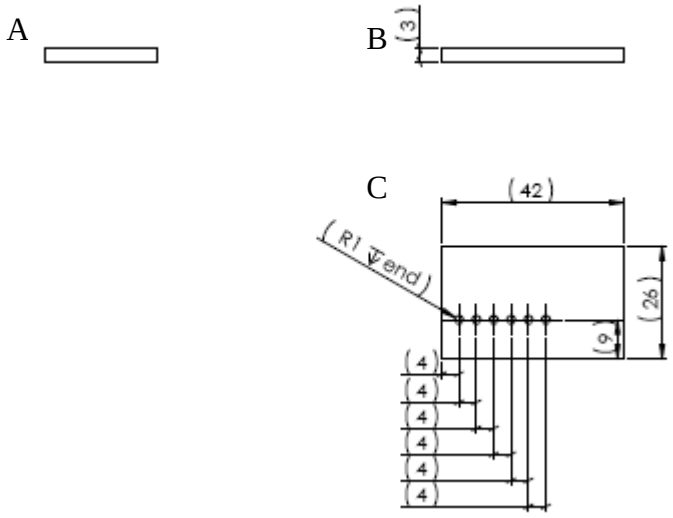

Figure B.5 An acrylic box no.4 drawing in mm scale, (A) side view, (B) front view and (C) top view.

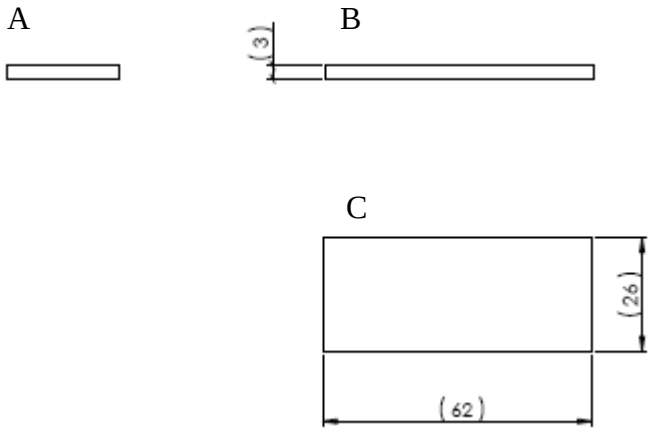

Figure B.6 An acrylic box no.5 drawing in mm scale, (A) side view, (B) front view and (C) top view.

APPENDIX C

MECHANICAL STIMULATOR DRAWINGS

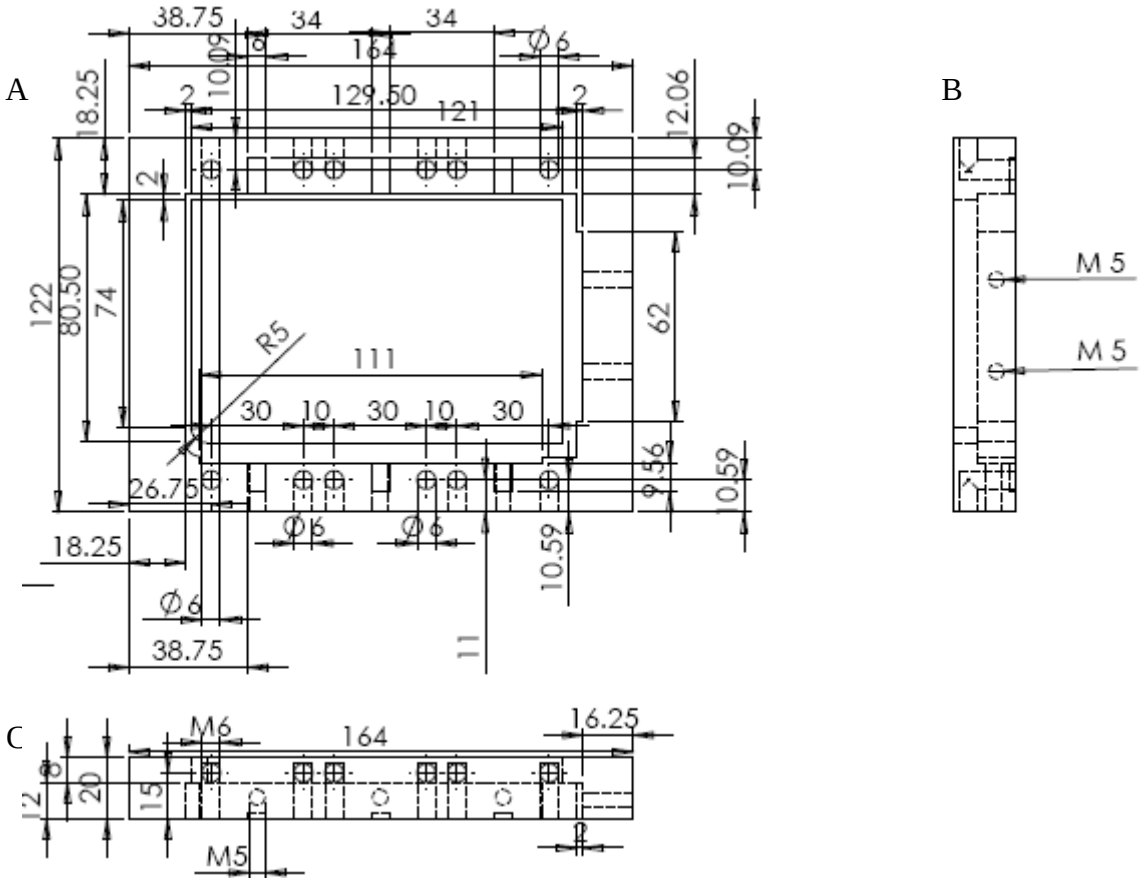

Figure C.1 An Aluminum base drawing in mm scale, (A) top view, (B) side view and (C) front view.

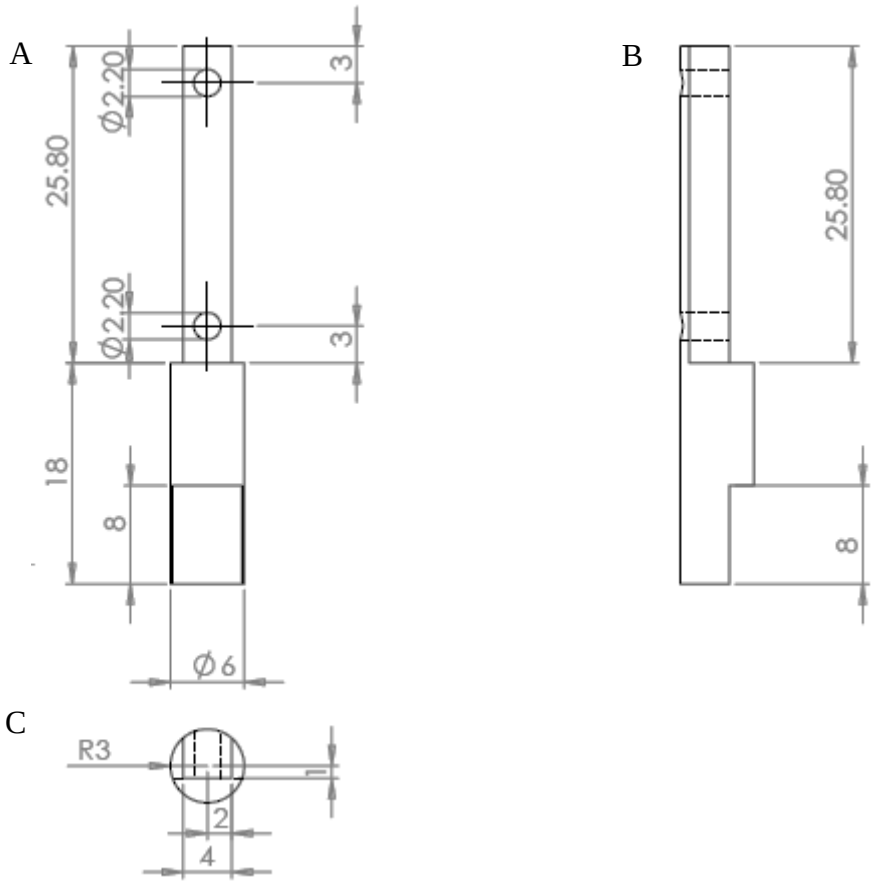

Figure C.2 An Aluminum pole drawing in mm scale, (A) front view, (B) side view and (C) top view.

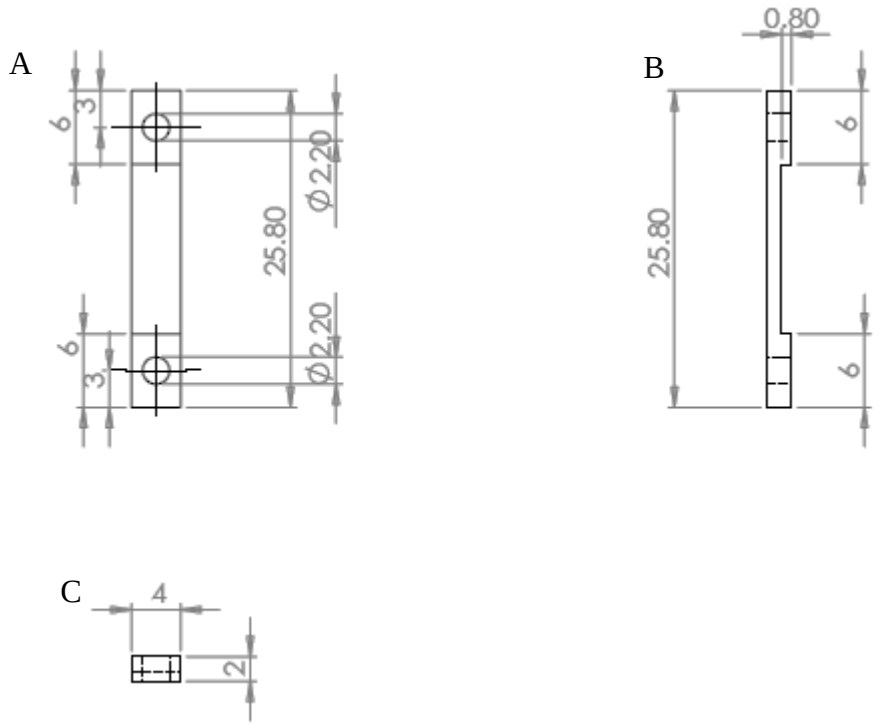

Figure C.3 An Aluminum locked pole drawing in mm scale, (A) front view, (B) side view and (C) top view.

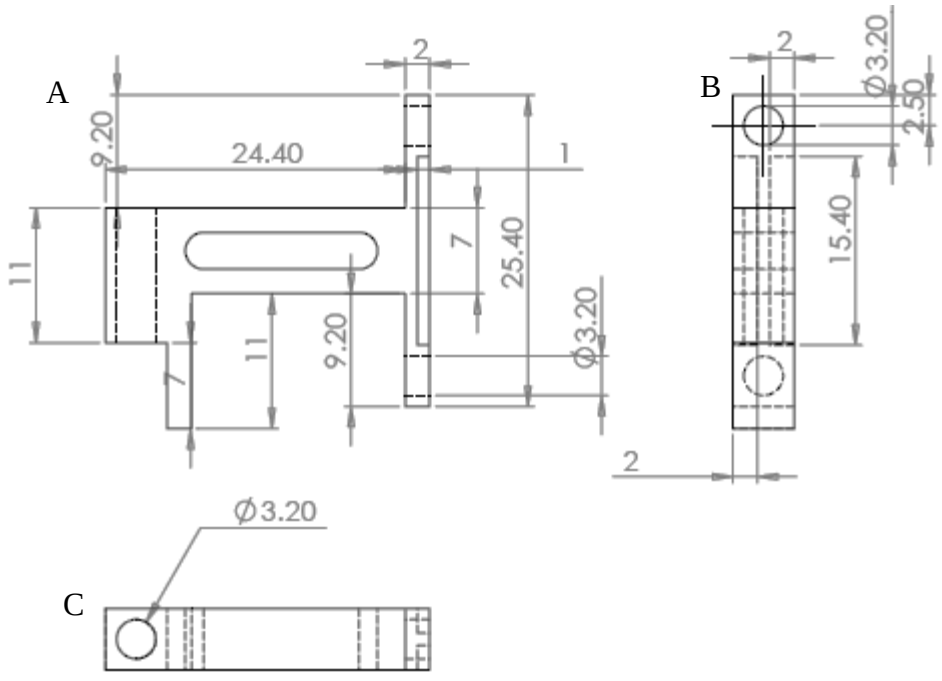

Figure C.4 An acrylic moving plunger no.1 drawing in mm scale, (A) front view, (B) side view and (C) top view.

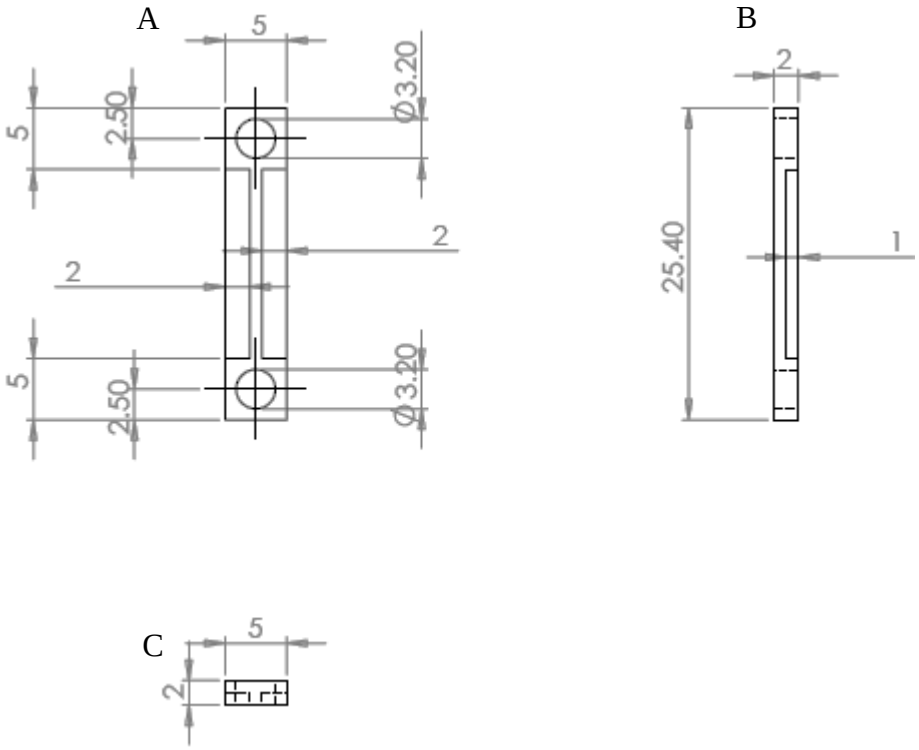

Figure C.5 An acrylic fixed moving plunger with piezoelectric actuator drawing in mm scale, (A) front view, (B) side view and (C) top view.

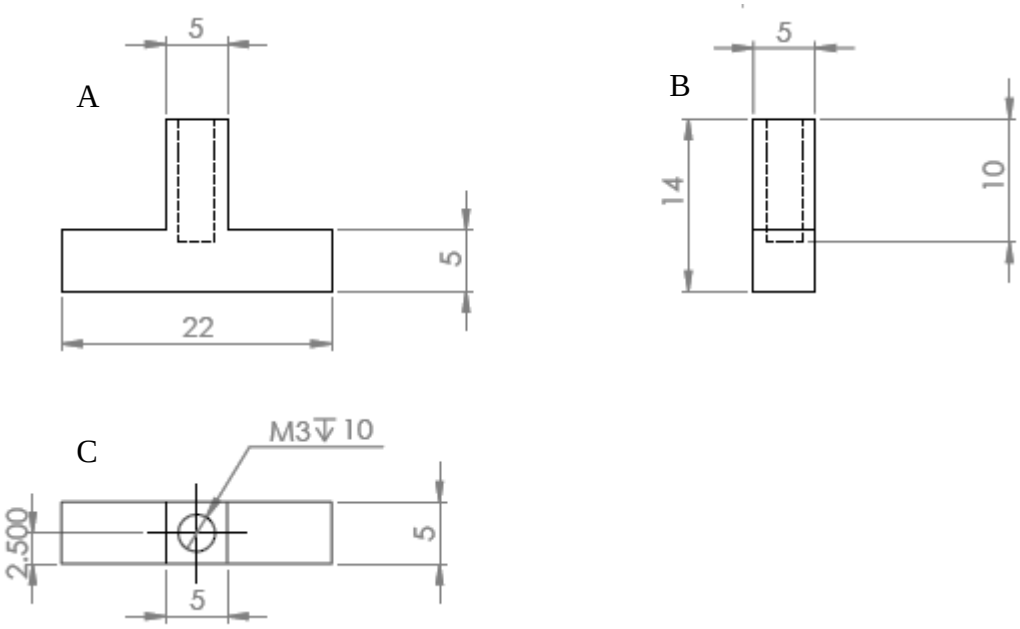

Figure C.6 An acrylic moving plunger no. 2 drawing in mm scale, (A) front view, (B) side view and (C) top view.

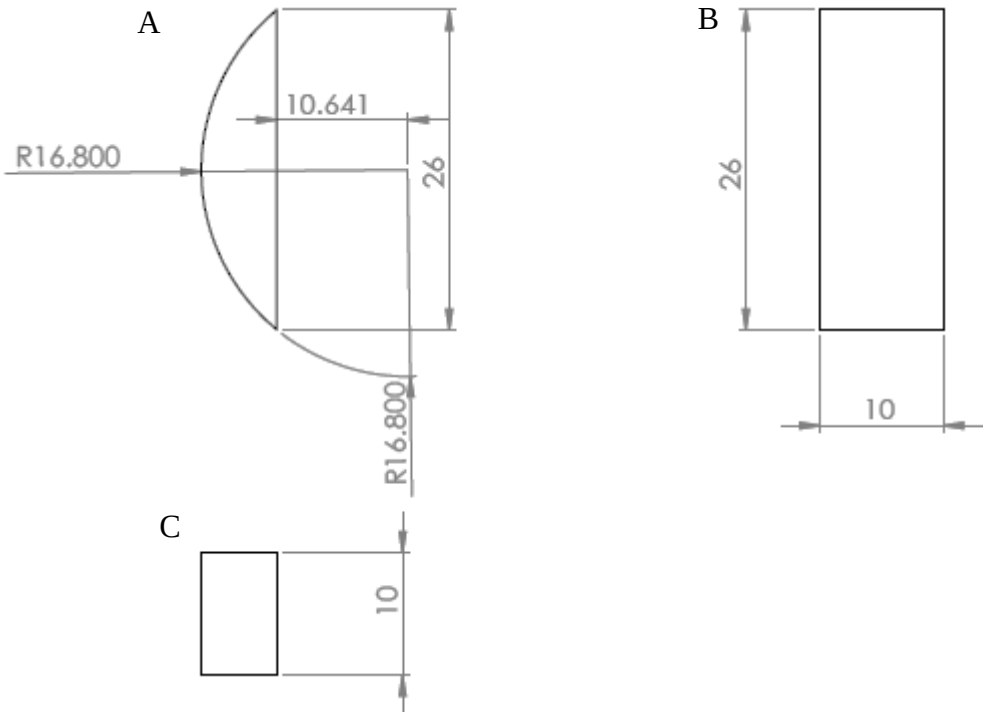

Figure C.7 An acrylic fixed plunger drawing in mm scale, (A) top view, (B) side view and (C) front view.

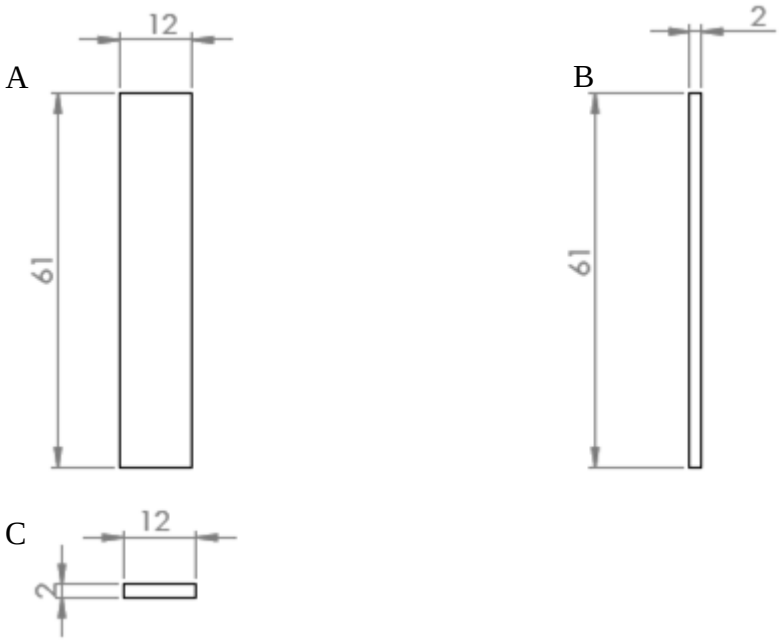

Figure C.8 An acrylic locked 6-well plate no.1 drawing in mm scale, (A) front view, (B) side view and (C) top view.

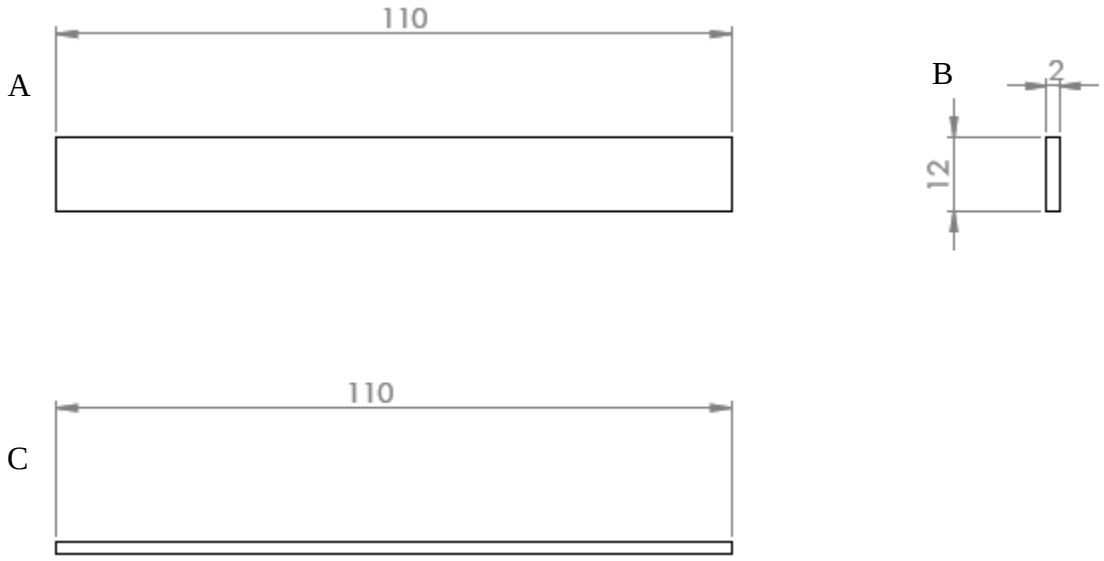

Figure C.9 An acrylic locked 6-well plate no.2 drawing in mm scale, (A) front view, (B) side view and (C) top view.

APPENDIX D

MECHANICAL STIMULATION WAVEFORMS

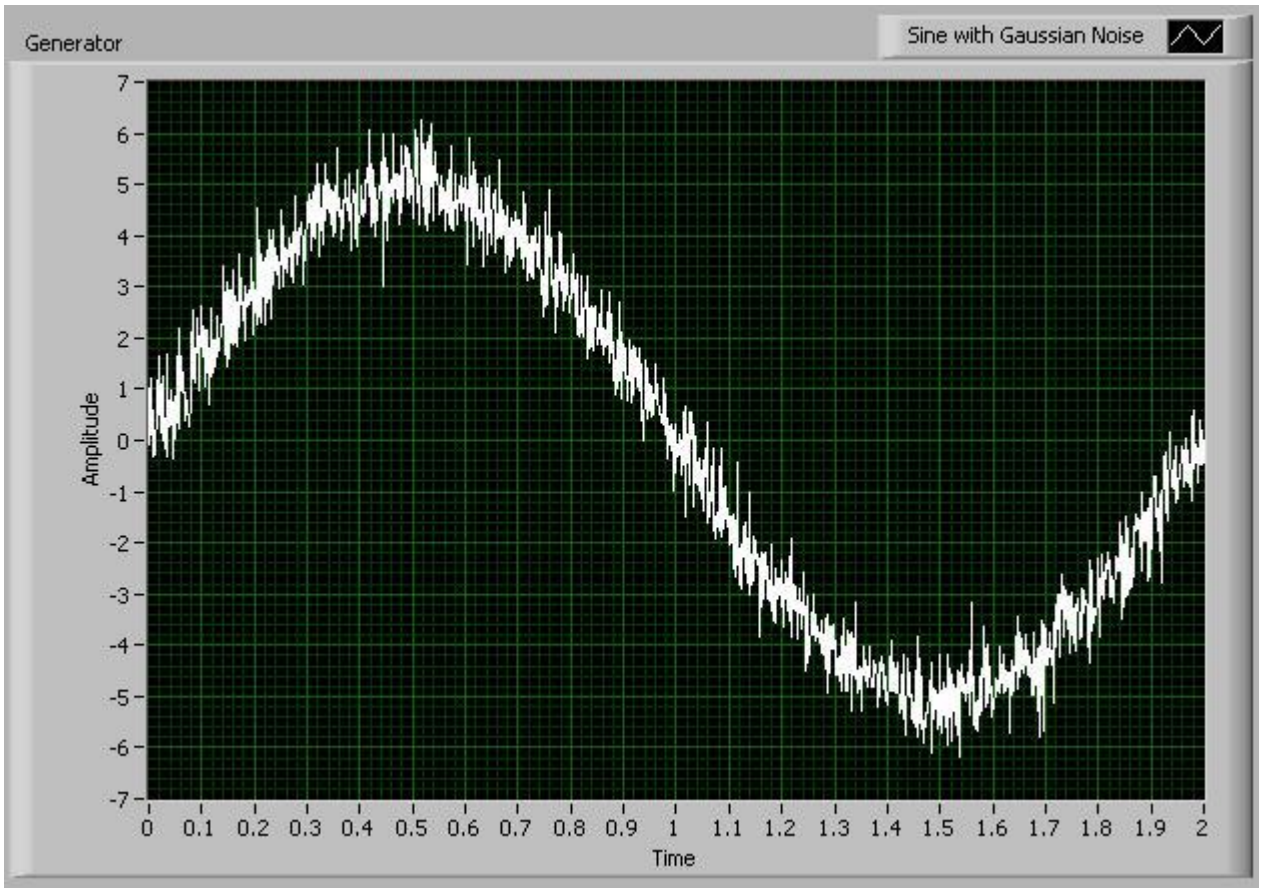

Figure D.1 Sinusoidal waveform at 0.5 Hz with amplitude peak to peak of 10 V with vibration (Gaussian quasi-white noise with a standard deviation of 0.5 V deformation and frequency components up to 50 Hz)

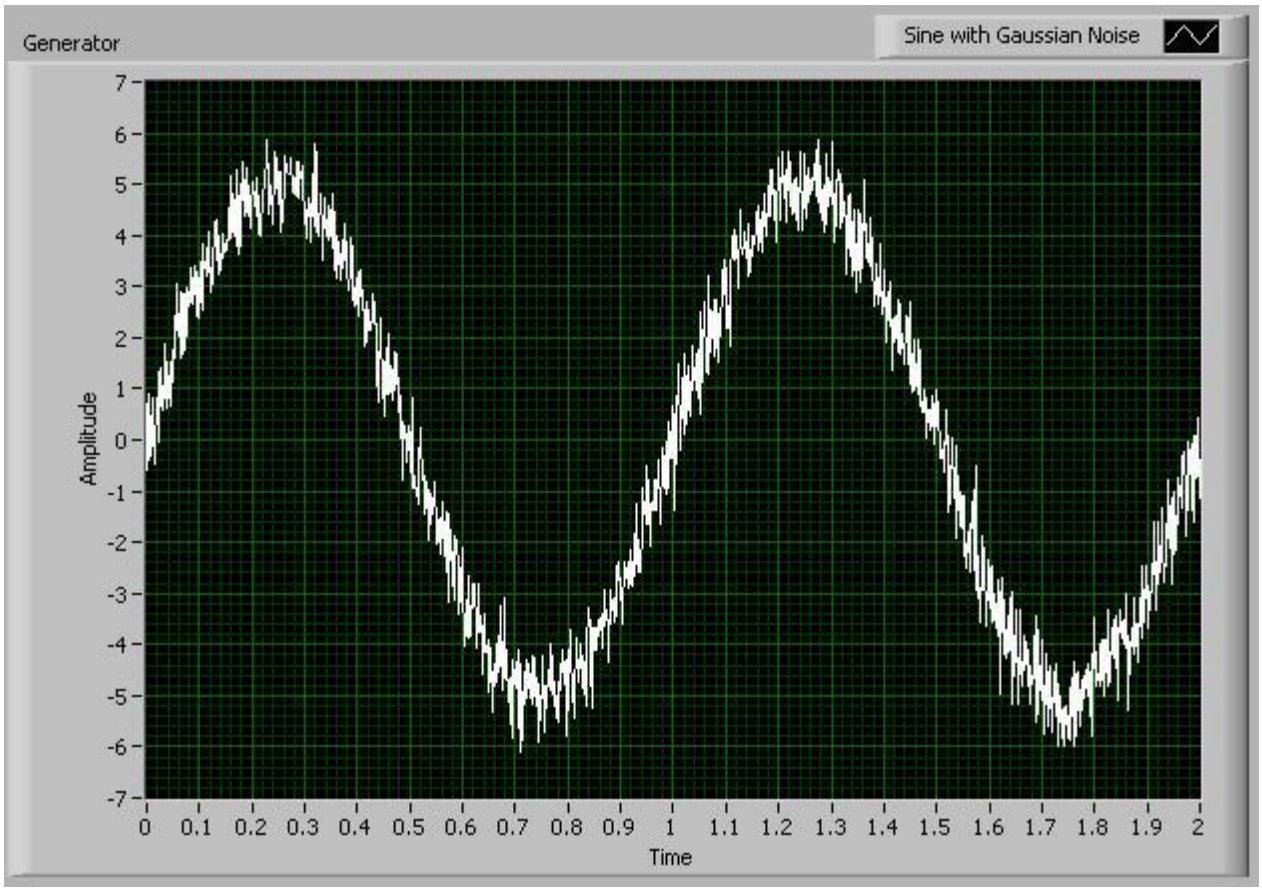

Figure D.2 Sinusoidal waveform at 1.0 Hz with amplitude peak to peak of 10 V with vibration (Gaussian quasi-white noise with a standard deviation of 0.5 V deformation and frequency components up to 50 Hz)

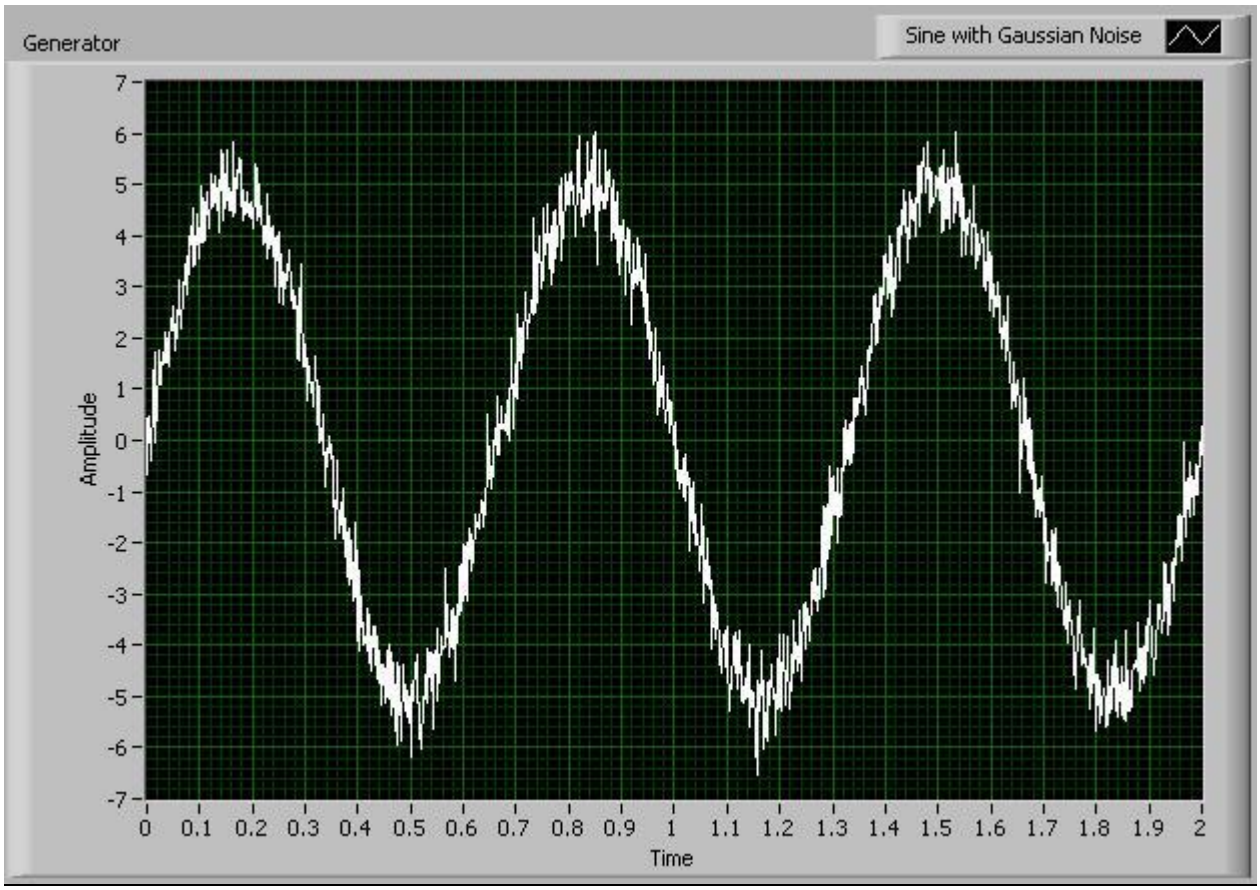

Figure D.3 Sinusoidal waveform at 1.5 Hz with amplitude peak to peak of 10 V with vibration (Gaussian quasi-white noise with a standard deviation of 0.5 V deformation and frequency components up to 50 Hz)

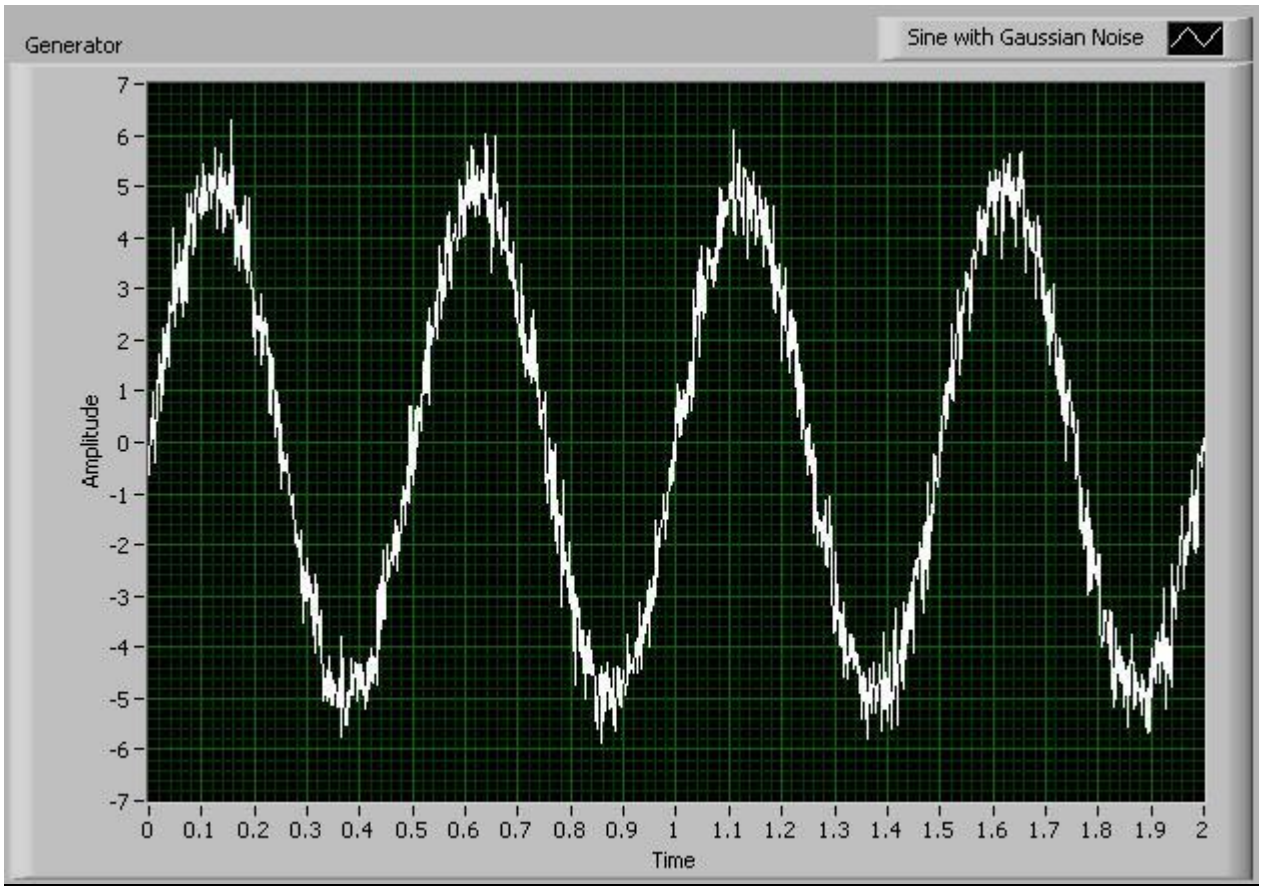

Figure D.4 Sinusoidal waveform at 2.0 Hz with amplitude peak to peak of 10 V with vibration (Gaussian quasi-white noise with a standard deviation of 0.5 V deformation and frequency components up to 50 Hz)

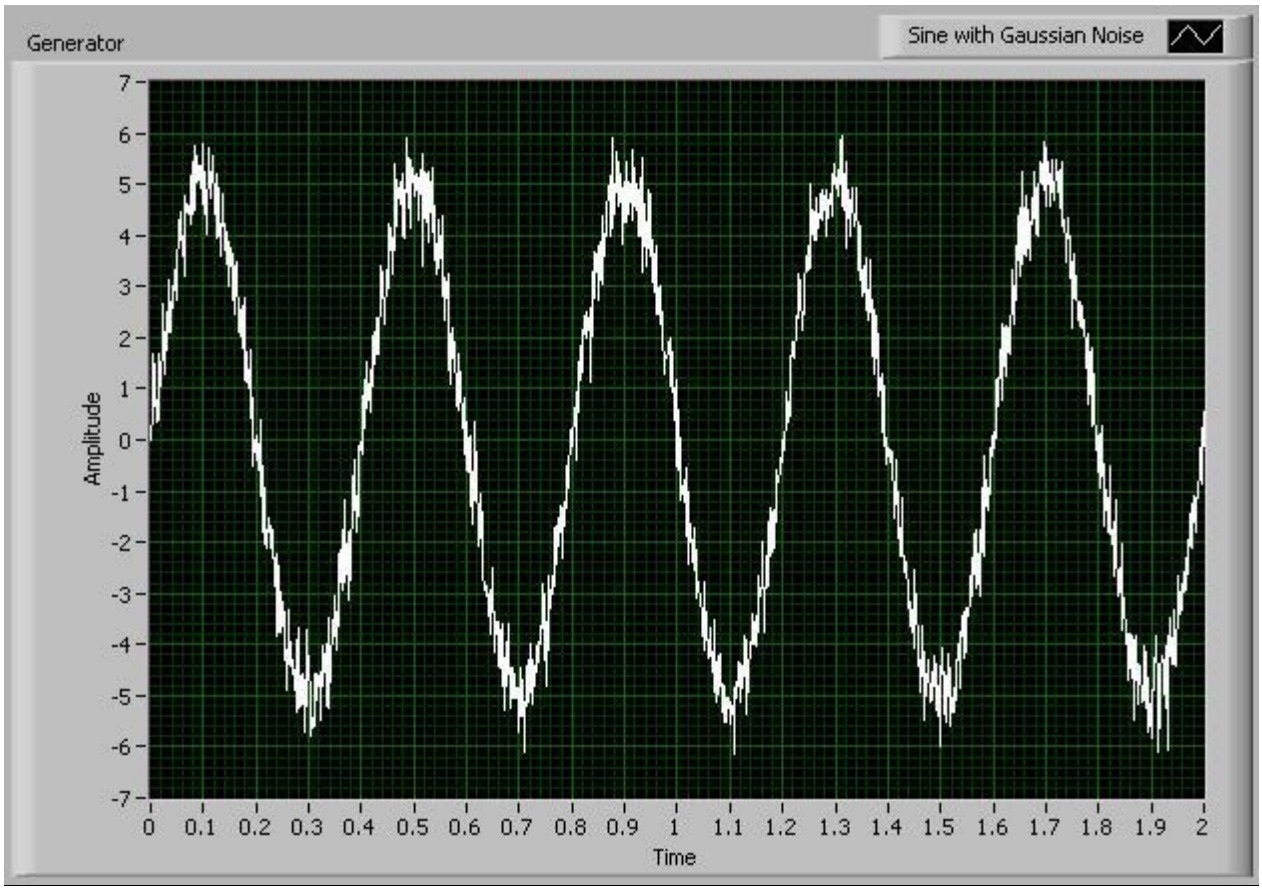

Figure D.5 Sinusoidal waveform at 2.5 Hz with amplitude peak to peak of 10 V with vibration (Gaussian quasi-white noise with a standard deviation of 0.5 V deformation and frequency components up to 50 Hz)

APPENDIX E

THE I_0 – I SLOPE OF TISSUE-ENGINEERED BONES MEASURING BY THE OPTICAL MONITORING DEVICE

Table E.1 The $I_0 - I$ slope of stimulated constructs at 0.5 – 1.5 Hz

		The slope of $I_0 - I$								
Condition		**0.5 Hz**			**1.0 Hz**			**1.5 Hz**		
Samples		**1**	**2**	**3**	**1**	**2**	**3**	**1**	**2**	**3**
Days	**0**	0.1816	0.1801	0.1779	0.1752	0.1863	0.1789	0.1851	0.1790	0.1784
	1	0.1805	0.1847	0.1769	0.1782	0.1837	0.1770	0.1828	0.1786	0.1772
	2	0.1837	0.1807	0.1812	0.1786	0.1861	0.1789	0.1897	0.1814	0.1791
	3	0.1813	0.1807	0.1799	0.1791	0.1849	0.1796	0.1840	0.1820	0.1802
	4	0.1808	0.1810	0.1816	0.1803	0.1840	0.1811	0.1836	0.1810	0.1755
	5	0.1826	0.1796	0.1830	0.1804	0.1853	0.1804	0.1862	0.1824	0.1766
	6	0.1843	0.1810	0.1814	0.1809	0.1845	0.1800	0.1866	0.1850	0.1772
	7	0.1846	0.1805	0.1830	0.1824	0.1835	0.1809	0.1865	0.1855	0.1781
	8	0.1856	0.1824	0.1836	0.1829	0.1865	0.1849	0.1913	0.1863	0.1785
	9	0.1876	0.1844	0.1846	0.1864	0.1898	0.1860	0.1909	0.1876	0.1789
	10	0.1868	0.1828	0.1841	0.1863	0.1894	0.1868	0.1929	0.1908	0.1804
	11	0.1878	0.1843	0.1858	0.1869	0.1878	0.1860	0.1905	0.1848	0.1825
	12	0.1869	0.1853	0.1860	0.1882	0.1876	0.1848	0.1894	0.1851	0.1836
	13	0.1889	0.1853	0.1861	0.1906	0.1877	0.1870	0.1932	0.1876	0.1839
	14	0.1896	0.1860	0.1860	0.1921	0.1854	0.1863	0.1939	0.1879	0.1861
	15	0.1896	0.1862	0.1875	0.1921	0.1881	0.1866	0.1948	0.1882	0.1868
	16	0.1910	0.1878	0.1868	0.1960	0.1886	0.1859	0.1971	0.1904	0.1891
	17	0.1928	0.1887	0.1888	0.1949	0.1907	0.1875	0.2022	0.1932	0.1905
	18	0.1923	0.1883	0.1891	0.1971	0.1901	0.1874	0.2051	0.1919	0.1926
	19	0.1931	0.1902	0.1879	0.1971	0.1884	0.1876	0.2065	0.1930	0.1895
	20	0.1937	0.1900	0.1912	0.1963	0.1903	0.1883	0.2048	0.1962	0.1910
	21	0.1968	0.1933	0.1913	0.2001	0.1926	0.1908	0.2078	0.1980	0.1934
	22	0.1960	0.1896	0.1918	0.2006	0.1930	0.1903	0.2132	0.2005	0.1904
	23	0.1966	0.1922	0.1922	0.2013	0.1973	0.1920	0.2135	0.2037	0.1961
	24	0.1978	0.1943	0.1940	0.2032	0.1980	0.1959	0.2177	0.2064	0.2017
	25	0.1969	0.1913	0.1949	0.2048	0.1997	0.1964	0.2249	0.2041	0.1998
	26	0.1973	0.1934	0.1951	0.2053	0.1979	0.1956	0.2206	0.2035	0.1963
	27	0.1980	0.1955	0.1969	0.2054	0.2018	0.1998	0.2208	0.2079	0.1993

Table E.1 The $I_0 – I$ slope of stimulated constructs at 0.5 – 1.5 Hz (continued)

		The slope of $I_0 – I$								
Condition		**0.5 Hz**			**1.0 Hz**			**1.5 Hz**		
Samples		**1**	**2**	**3**	**1**	**2**	**3**	**1**	**2**	**3**
Days	**28**	0.1991	0.1958	0.1978	0.2054	0.2027	0.1986	0.2292	0.2045	0.2030
	29	0.1979	0.1957	0.1992	0.2059	0.2050	0.2002	0.2401	0.2094	0.2044
	30	0.1983	0.1970	0.2002	0.2094	0.2026	0.2008	0.2479	0.2042	0.2065
	31	0.2007	0.1986	0.2012	0.2114	0.2082	0.2020	0.2566	0.2102	0.2037
	32	0.1992	0.1969	0.2022	0.2109	0.2080	0.2034	0.2540	0.2084	0.2087
	33	0.2031	0.2002	0.2012	0.2139	0.2121	0.2054	0.2493	0.2091	0.2079
	34	0.2031	0.2009	0.2047	0.2199	0.2168	0.2040	0.2593	0.2119	0.2141
	35	0.2032	0.2011	0.2081	0.2191	0.2190	0.2090	0.2628	0.2107	0.2167
	36	0.2069	0.2035	0.2082	0.2240	0.2233	0.2108	0.2623	0.2118	0.2157
	37	0.2097	0.2071	0.2108	0.2211	0.2205	0.2104	0.2668	0.2128	0.2189
	38	0.2134	0.2091	0.2124	0.2232	0.2205	0.2061	0.2702	0.2158	0.2154
	39	0.2158	0.2089	0.2144	0.2326	0.2202	0.2086	0.2734	0.2283	0.2349
	40	0.2166	0.2102	0.2190	0.2319	0.2268	0.2221	0.2732	0.2305	0.2392
	41	0.2196	0.2133	0.2189	0.2379	0.2264	0.2244	0.2743	0.2360	0.2362
	42	0.2208	0.2144	0.2160	0.2415	0.2280	0.2206	0.2716	0.2397	0.2369

Table E.2 The $I_0 - I$ slope of stimulated constructs at 2.0 – 2.5 Hz and controlled constructs

Condition		**2.0 Hz**			**2.5 Hz**			**Control**		
Samples		**1**	**2**	**3**	**1**	**2**	**3**	**1**	**2**	**3**
Days	**0**	0.1803	0.1755	0.1747	0.1783	0.1812	0.1711	0.1759	0.1744	0.1801
	1	0.1856	0.1786	0.1801	0.1819	0.1855	0.1761	0.1800	0.1781	0.1786
	2	0.1830	0.1759	0.1789	0.1809	0.1802	0.1769	0.1791	0.1770	0.1809
	3	0.1860	0.1775	0.1804	0.1828	0.1817	0.1775	0.1834	0.1795	0.1822
	4	0.1873	0.1774	0.1811	0.1818	0.1826	0.1781	0.1809	0.1797	0.1832
	5	0.1801	0.1796	0.1809	0.1821	0.1818	0.1802	0.1809	0.1800	0.1820
	6	0.1816	0.1804	0.1817	0.1814	0.1864	0.1790	0.1809	0.1809	0.1817
	7	0.1823	0.1799	0.1832	0.1822	0.1833	0.1804	0.1812	0.1803	0.1830
	8	0.1859	0.1833	0.1814	0.1843	0.1846	0.1792	0.1786	0.1808	0.1822
	9	0.1902	0.1836	0.1814	0.1852	0.1858	0.1811	0.1829	0.1811	0.1824
	10	0.1894	0.1832	0.1815	0.1849	0.1854	0.1813	0.1814	0.1823	0.1833
	11	0.1932	0.1866	0.1828	0.1866	0.1861	0.1821	0.1822	0.1824	0.1828
	12	0.1921	0.1875	0.1820	0.1869	0.1853	0.1839	0.1842	0.1818	0.1823
	13	0.1929	0.1830	0.1794	0.1870	0.1870	0.1838	0.1836	0.1818	0.1839
	14	0.1952	0.1876	0.1807	0.1862	0.1866	0.1857	0.1856	0.1832	0.1834
	15	0.1954	0.1873	0.1829	0.1868	0.1873	0.1863	0.1847	0.1810	0.1828
	16	0.1964	0.1904	0.1834	0.1873	0.1880	0.1865	0.1863	0.1821	0.1836
	17	0.2003	0.1897	0.1815	0.1884	0.1900	0.1869	0.1851	0.1845	0.1825
	18	0.2023	0.1903	0.1851	0.1893	0.1921	0.1888	0.1857	0.1832	0.1839
	19	0.2022	0.1906	0.1888	0.1895	0.1908	0.1886	0.1858	0.1851	0.1856
	20	0.2012	0.1900	0.1871	0.1904	0.1908	0.1888	0.1864	0.1837	0.1850
	21	0.2027	0.1923	0.1914	0.1905	0.1921	0.1884	0.1852	0.1858	0.1867
	22	0.2116	0.1896	0.1935	0.1927	0.1939	0.1907	0.1851	0.1856	0.1856
	23	0.2163	0.1949	0.1913	0.1940	0.1949	0.1912	0.1864	0.1832	0.1850
	24	0.2123	0.1964	0.1937	0.1913	0.1916	0.1932	0.1858	0.1854	0.1853
	25	0.2152	0.1985	0.1930	0.1931	0.1925	0.1934	0.1876	0.1861	0.1868
	26	0.2226	0.1977	0.1934	0.1948	0.1948	0.1945	0.1872	0.1866	0.1862
	27	0.2285	0.1976	0.1978	0.1948	0.1957	0.1956	0.1884	0.1858	0.1865

Table E.2 The I_0 – I slope of stimulated constructs at 2.0 – 2.5 Hz and controlled constructs (continued)

Condition		**2.0 Hz**			**2.5 Hz**			**Control**		
Samples		**1**	**2**	**3**	**1**	**2**	**3**	**1**	**2**	**3**
Days	**28**	0.2324	0.1996	0.1969	0.1974	0.1983	0.1979	0.1880	0.1877	0.1886
	29	0.2315	0.2012	0.1999	0.1973	0.1967	0.1972	0.1893	0.1892	0.1877
	30	0.2416	0.1989	0.2064	0.2008	0.2002	0.2009	0.1903	0.1898	0.1914
	31	0.2479	0.2030	0.2027	0.2016	0.2000	0.2021	0.1906	0.1881	0.1890
	32	0.2526	0.2018	0.2113	0.2003	0.2005	0.2055	0.1898	0.1906	0.1919
	33	0.2580	0.2123	0.2139	0.2024	0.2019	0.2039	0.1911	0.1907	0.1919
	34	0.2632	0.2194	0.2231	0.2024	0.2050	0.2049	0.1918	0.1914	0.1923
	35	0.2590	0.2303	0.2155	0.2102	0.2059	0.2057	0.1902	0.1938	0.1902
	36	0.2642	0.2309	0.2208	0.2062	0.2096	0.2095	0.1921	0.1880	0.1911
	37	0.2658	0.2286	0.2143	0.2151	0.2126	0.2098	0.1939	0.1918	0.1912
	38	0.2692	0.2261	0.2233	0.2170	0.2152	0.2123	0.1905	0.1925	0.1932
	39	0.2660	0.2345	0.2266	0.2170	0.2196	0.2149	0.1929	0.1926	0.1938
	40	0.2703	0.2320	0.2388	0.2199	0.2212	0.2149	0.1913	0.1899	0.1925
	41	0.2756	0.2391	0.2442	0.2231	0.2206	0.2198	0.1917	0.1927	0.1900
	42	0.2774	0.2406	0.2440	0.2199	0.2182	0.2147	0.1923	0.1932	0.1922

CURRICULUM VITAE

NAME	Mr. Chaiyong Koaykul
DATE OF BIRTH	16 August 1987
EDUCATIONAL RECORD	
HIGH SCHOOL	Bangkok Christian Collage, 2005
BACHELOR'S DEGREE	Bachelor of Engineering (Mechanical Engineering) King Mongkut's University of Technology Thonburi, 2009
MASTER'S DEGREE	Master of Engineering (Biological Engineering) King Mongkut's University of Technology Thonburi, 2012
SCHOLARSHIP	KMUTT Diamond Scholarship in Research Field, Academic Year 2010
	KMUTT Diamond Scholarship in Leadership Field, Academic Year 2007 – 2009
	KMUTT Diamond Scholarship in Academic Outstanding Field, Academic Year 2005 – 2007
PUBLICATIONS	Koaykul, C., Khantachawana, A., Viravaidya-Pasuwat, K. and Tanaka, SM., 2011, "Effect of Sinusoidal Loading Frequencies on Calcification of Tissue-Engineered Bone In Vitro", **World conference on regenerative medicine (WRM)**, November, 2-4, Germany.
	Koaykul, C., Rattanarojjanathom, P., Keawtatip, P. and Khantachawana, A., 2009, "The Fabrication of Titanium-Niobium Alloy Having Pseudoelastic Properties for Artificial Bone", **The 23rd Conference of the Mechanical Engineering Network of Thailand (ME-NETT23)**, November, 4 – 7, Thailand.